Pontifícia Universidade Católica
do Rio de Janeiro

Erika Imada Barcelos

Coupling Machine Learning and Mesoscale Modeling to study the flow of semi-dense and dense suspensions

Tese de Doutorado

Thesis presented to the Programa de Pós–graduação em Engenharia Mecânica, do Departamento de Engenharia Mecânica da PUC-Rio in partial fulfillment of the requirements for the degree of Doutor em Engenharia Mecânica.

Advisor : Prof. Mônica Feijó Naccache
Co-advisor: Prof. João Manuel Luis Lopes Maia

Rio de Janeiro
January 2022

Erika Imada Barcelos

Coupling Machine Learning and Mesoscale Modeling to study the flow of semi-dense and dense suspensions

Thesis presented to the Programa de Pós–graduação em Engenharia Mecânica da PUC-Rio in partial fulfillment of the requirements for the degree of Doutor em Engenharia Mecânica. Approved by the Examination Committee:

Prof. Mônica Feijó Naccache
Advisor
Departamento de Engenharia Mecânica – PUC-Rio

Prof. João Manuel Luis Lopes Maia
MACRO/CWRU

Prof. Paulo Roberto de Souza Mendes
PUC-Rio

Prof. Ricardo Jorge Espanhol Andrade
Mackenzie

Prof. Gary E. Wnek
CWRU

Prof. Michael-Jon A. Hore
CWRU

Prof. Daniel J. Lacks
CWRU

Rio de Janeiro, January 31st, 2022

Erika Imada Barcelos

Graduated in Chemical Engineering at Universidade Federal de Santa Catarina

Bibliographic data

Imada Barcelos,Erika

Coupling Machine Learning and Mesoscale Modeling to study the flow of semi-dense and dense suspensions / Erika Imada Barcelos; advisor: Mônica Feijó Naccache; co-advisor: João Manuel Luis Lopes Maia. – 2022.

92 f: il. color. ; 30 cm

Tese (doutorado) - Pontifícia Universidade Católica do Rio de Janeiro, Departamento de Engenharia Mecânica, 2022.

Inclui bibliografia

1. Dinâmica Dissipativa de Partículas. 2. Aprendizado de Máquina. 3. Suspensõess. I. Naccache, Mônica. II. Luis Lopes Maia, João Manuel . III. Pontifícia Universidade Católica do Rio de Janeiro. Departamento de Engenharia Mecânica. IV. Título.

CDD: 004

To my parents, for their unconditional love and support throughout these years

Acknowledgments

Acknowledging all the people that crossed my journey and help me to conclude this chapter of my life would be a challenge. There are so many people, including friends and family, that have support me throughout all these years that I could not cite everyone here.

First of all, I would like to thank God for providing me this amazing life full of opportunities and wonderful supportive friends and family.

Secondly, I would like to thank my family. Everything I have accomplished in my life would no be possible if I did not have such a supportive, caring and understanding family. Thanks for always be there for me and to support every single decision I have made in my life.

This dual PhD would not be possible without my advisors Prof. João Maia from Case Western Reserve University and Prof. Mônica Naccache from PUC-Rio. I am very grateful, first of all, for making this program possible and secondly for being my advisors. Thanks for guiding me throughout this past five years and for giving me the flexibility and intellectual support to perform my research.

This work would not be the same without Dr. Shaghayegh Khani. Thanks for your friendship and for being side by side with me all these years, for all the guidance and discussions and specially for all the help with coding. I had no programming or molecular modelling background before joining the PhD and your help and support was essential and very important not only in the beginning of the research, but also during all these years.

I would like to leave a special thanks to my friends and group colleagues Felipe and Lucivan. We worked close all these past 5 years and your moral support, your friendship and company in all the bad and good moments made this journey much more enjoyable.

Luiz is another program colleague and friend that I would like to thanks. You thought me everything I know about matlab and showed me the importance of insert in our routine programming and scripts to optimize the data treatments and analytical procedures. Thanks for helping me not only with coding but also for the DPD discussions.

A very special colleague that became a close friend and that I could not forget is Fellipe Carvalho. The time we shared in Cleveland was very special and your help me with the code, in writing scripts and adapting your algorithm for me to use in my system was essential for the success of this research.

I would like to thank my very supporting group at Case, in special to my computational colleagues Sunsheng, Saeed and Brandy. Having you as part of the group was so exciting and so enriching, I could not have asked for better

group mates. Also, thanks to the experimental colleagues Dana, Vivek, Tyler and Moulin for all the enjoyable moments together.

I could not forget my Brazilian friends that became my family in the US, in special to Alana, Claudio, Bela, Carol, Gustavo and Gabriela. You made my stay in Cleveland so pleasant and happy. A more than special thanks to my friends that become my big sisters Irlaine, Jucara and my roommate Marte, you will always be a very important part of my life.

A special thanks to the GREO group at PUC-Rio. We did not spend a lot of time together but it was enough to make very good friends. Thank you Priscilla for always attend my lab needs and providing me the resources I needed for my project. A very a special thanks to Lorena, Angela and Gustavo for being such a good friends and office partners. A would also like to thank, in special, Eliana for helping me with my internship.

I would also like to thank HPC at CWRU for the computational resources and NSF grant NSFCBET 1703919 and CAPES for the finance support.

Finally, I would like to acknowledge everyone that I did not cite specifically in this document but that helped me in some way to accomplish the goals I had for this project.

This study was financed in part by the Coordenação de Aperfeiçoamento de Pessoal de Nível Superior - Brasil (CAPES) - Finance Code 001.

Abstract

Imada Barcelos,Erika; Naccache, Mônica (Advisor); Luis Lopes Maia, João Manuel (Co-Advisor). **Coupling Machine Learning and Mesoscale Modeling to study the flow of semi-dense and dense suspensions**. Rio de Janeiro, 2022. 92p. Tese de Doutorado – Departamento de Engenharia Mecânica, Pontifícia Universidade Católica do Rio de Janeiro.

Suspensions correspond to a class of materials vastly used in a large set of applications and industries. Due to its extreme versatility, they have been the focus of numerous studies over the past decades. Suspensions are also very flexible and can display different rheological properties and macroscopic responses depending on the choice of parameters used as input in the system. More specifically, the rheological response of suspensions is intimately associated to the microstructural arrangement of the particles composing the medium and external factors, such as how strongly they are confined and particle rigidity. In the present study, the effect of particle rigidity, confinement and flow rate on the microstructure of highly concentrated suspensions is studied using Core-Modified Dissipative Particle Dynamics. Preceding this main study, two other steps were necessary to guarantee a reliable and realistic simulation system, which consisted, essentially, on performing parametric studies to understand and estimate the appropriate values for wall-particle interaction parameters.

The present work address parametric studies performed to assist the input parameters choice to prevent particle penetration in a wall-bounded system. Initially a simpler system, composed of solvent and walls, is built and the interaction parameters and wall densities were adjusted. Following, the interactions are set for suspensions. In the latter case multiple parameters play a role in penetration and the traditional way to investigate these effects would be exhaustive and time consuming. Hence, we choose to use a Machine Learning approach to perform this study. Once the parameters were adjusted, the study of confinement could be carried out. The main goal of this study was to understand how the microstructure of concentrated suspensions is affected by flow rate, particle rigidity and confinement. It was found that very soft particles always form a giant cluster regardless the confinement ratio; the difference being on how packed the particles are. In the rigid case, a stronger confinement leads the formation of larger clusters. The final

study addresses a machine learning study carried out to predict the rheology of unconfined suspensions. The main contribution of this work is that it was possible to understand and adjust simulation parameters and develop a computational domain that enables to systematically study confinement effects on suspensions.

Keywords

Dissipative Particle Dynamics; Machine Learning; Suspensions.

Resumo

Imada Barcelos,Erika; Naccache, Mônica; Luis Lopes Maia, João Manuel . **Interligando aprendizado de máquina e simulação em meso-escala para estudar o escoamento em suspensões semi-densas e densas**. Rio de Janeiro, 2022. 92p. Tese de Doutorado – Departamento de Engenharia Mecânica, Pontifícia Universidade Católica do Rio de Janeiro.

Suspensões correspondem a uma classe de materiais amplamente utilizada em uma grande variedade de aplicações e indústrias. Devido à sua extrema versatilidade, elas têm sido foco de inúmeros estudos nas últimas décadas. Suspensões também são muito flexíveis e podem apresentar diferentes propriedades reológicas e respostas macroscópicas dependendo da escolha dos parâmetros usados como entrada no sistema. Mais especificamente, a resposta reológica de suspensões está intimamente associada ao arranjo microestrutural das partículas que compõem o meio e a fatores externos, como o quão confinadas elas se encontram e a rigidez das partículas. No presente estudo, o efeito da rigidez, confinamento e vazão na microestrutura de suspensões altamente concentradas é avaliado usando Dinâmica Dissipativa de Partículas com Núcleo Modificado. Precedento este estudo principal, foram necessárias outras duas etapas para garantir um sistema de simulação confiável e representativo, que consistiu, essencialmente, na realização de estudos paramétricos para compreender e estimar os valores adequados para os parâmetros de interacção parede-partícula.

O presente trabalho aborda estudos paramétricos realizados para auxiliar na escolha dos parâmetros de entrada para evitar a penetração de partículas em um sistema delimitado por paredes. Inicialmente um sistema mais simples, composto por solvente e paredes é construído e os parâmetros de interação e densidades de parede foram ajustados. Em seguida as interações são definidas para suspensões. Neste último caso, vários parâmetros desempenham um papel na penetração e a maneira tradicional de investigar esses efeitos seria exaustiva e demorada. Por isso, optamos por usar uma abordagem de Machine Learning para realizar este estudo. Uma vez ajustados os parâmetros, o estudo de confinamento pôde ser realizado. O objetivo principal deste estudo foi entender como a microestrutura de suspensões concentradas é afetada pela vazão, rigidez das partículas e confinamento. Verificou-se que partículas

muito flexíveis sempre formam um aglomerado gigante independente da razão de confinamento; a diferença está em quão compactadas são as partículas. No caso de partículas rígidas, um confinamento mais forte leva à formação de aglomerados maiores. O estudo final aborda um estudo de aprendizado de máquina realizado para prever a reologia de suspensões não confinadas. Com este trabalho foi possível entender e ajustar parâmetros de simulação e desenvolver um domínio computacional que permite estudar sistematicamente efeitos do confinamento em suspensões.

Palavras-chave

Dinâmica Dissipativa de Partículas; Aprendizado de Máquina; Suspensões.

Table of contents

List of figures

List of tables

1
Introduction

Suspensions are probably one of the most popular and studied system in the soft matter community. Due to its versatility and flexibility, they are, still, in the core development on many academic and industrial research. The vast range of potential applications is possible due to the rich variety of physical properties and macroscopic responses that can be obtained by tuning different parameters at flow and particle level.

A particular property of central importance in suspensions applications is its flow and deformation behavior. Typically, when one wants to study different materials and flow properties a systematic study must be carried out, giving a special attention to the intrinsic particle parameters at play. A particular important feature that needs to be taken into account is particle concentration, which is intimately connect to the hydrodynamic interactions and particles microstructure arrangements (MEWIS; WAGNER, 2011).

At very low particle concentration the particles do not see one another and the motion induced by a particle does not influence its distant neighbors. Random motion, in this case, drives the motion in system. As concentration increases, a second particle starts feeling the presence of its close neighbors and the flow around them is affected; at his point hydrodynamic interactions become non-negligible. If concentration raises even more multi-body hydrodynamic interactions start taking place and understanding and studying those systems become more challenging; the rheology becomes strongly affected by the microstructure (MEWIS; WAGNER, 2011). Innumerous works have addressed the rheology and microstructure of suspensions at different flow conditions and particle concentration (BIAN et al., 2014; RAMASWAMY et al., 2017; JAMALI; YAMANOI; MAIA, 2013; JAMALI et al., 2015b; BOROMAND et al., 2018)

Size ratio difference (MAI-DUY; PHAN-THIEN; KHOO, 2015; JAMALI; YAMANOI; MAIA, 2013), particle rigidity (JAMALI et al., 2015b; KUMAR; Henríquez Rivera; GRAHAM, 2014; MEHRABADI; KU; AIDUN, 2016), shape (KUMAR; Henríquez Rivera; GRAHAM, 2014; MEHRABADI; KU; AIDUN, 2016; BROWN et al., 2011), polydispersity (RAMASWAMY et al., 2017) and confinement (GALLIER et al., 2016; BIAN et al., 2014; PEYLA; VERDIER, 2011; RAMASWAMY et al., 2017) are also proven factors that might influence particle migration and fluid macroscopic properties.

Particle rigidity, in particular, has been proven in experimental and computational works to affect the rheology of suspensions as previously reported by (JAMALI; YAMANOI; MAIA, 2013; JAMALI et al., 2015b; COULOMB et al., 2017). Thermodynamic, diffusion behavior and structure of suspensions made of soft particles can differs significantly of the rigid ones as observed experimentally by (ECKERT; RICHTERING, 2008). Most of the available literature relies on the effect of rigidity in bulk and low concentration conditions(CHEN, 2014; KILIMNIK; MAO; ALEXEEV, 2011). When concentration and confinement are introduced additional physical effects become non negligible.

In addition to particle rigidity, confinement is also a very relevant topic since many real world suspensions applications are confined by physical restrictions. Although studies investigating confinement effects date from a long time ago, there is still room for further investigation in the field, specially when walls are present in highly concentrated soft suspensions. Walls can enhance difference rheological and flow behavior that divers from bulk systems as verified experimentally (ERAL et al., 2009; LYON; LEAL, 1998b; **??**; RAMASWAMY et al., 2017), and in numeric works (BIAN et al., 2014; PEYLA; VERDIER, 2011; GALLIER et al., 2016; GROSS; KRÜGER; VARNIK, 2014; DOYEUX et al., 2016; KOMNIK; HARTING; HERRMANN, 2004).

Particularly in highly concentrated confined suspensions studies, a numerical approach is usually preferred due to the complexity in setting an experimental setup. Computer simulations, in this case, represent an alternative approach to target those systems. Different numerical methods can be used as reviewed in (Van Der Sman, 2009). A particle-based method that has gained considerable attention in the past decades and has been successfully used to model complex fluids confined in walls geometries is mesoscale is Dissipative Particle Dynamics.

Modelling geometrical constraints imposed by walls in DPD dates from earlier 1995 (KONG et al., 1994), just a few years after the method was first introduced. Since then, many studies targeting wall slip, density fluctuations and unwanted layering effects have been published (PIVKIN; KARNIADAKIS, 2006; PIVKIN; KARNIADAKIS, 2005; WILLEMSEN; HOEFSLOOT; IEDEMA, 2000; MEHBOUDI; SAIDI, 2014; LITVINOV et al., 2010). Many of them were able to eliminate those spurious effects by using modifications and improvements of the traditional approach. These methods, however, are in its majority focused on solvent systems merely, without any incorporation of particles. An exception is the work published in (DARIAS et al., 2003) in which colloidal particles were modeled in a confined geometry using DPD. In that particular study the walls were not modeled using the traditional wall-frozen procedure, instead, only bounce back boundary conditions were applied at the wall to prevent particle penetration. The colloidal particles were modelled as neutrally buoyant particles interacting by soft repulsion potentials.

Later on, some works modelling the colloidal particles using a freezing approach(CHATTERJEE; WU, 2008; BOEK et al., 1997) as well explained in (BOEK et al., 1997) were published. Following this methodology, DPD particles are aggregated after a collision and have their momenta redistributed and subsequently move as single entity. That methodology enables the representation of solid object with desirable shapes and sizes (BOEK; COVENEY; LEKKERKERKER, 1996; BOEK et al., 1997), however modelling completely smooth surfaces is a challenge. Another alternative approach to model suspensions was introduced recently by (PHAN-THIEN; MAI-DUY; KHOO, 2014) and was posteriorly used by (MAI-DUY; PHAN-THIEN; KHOO, 2015) which considers a spring model to represent the colloidal particles. In this approach, a few DPD particles are connected though very stiff springs to reference some sites, which will, in a subsequent step, move as a rigid body.

To overcome the constraints associated to the lower surface definition arising from the freezing-related procedures, single particle models considering the colloidal particles as individual entities have been proposed. In some cases, DPD forces are modified to account for particle-particle interactions (PRYAMITSYN; GANESAN, 2005; PAN; CASWELL; KARNIADAKIS, 2010). Another possibility relies on the usage of pairwise colloidal forces between the particles, as proposed initially by (WHITTLE; TRAVIS, 2010) in a model named Core-Modified Dissipative Particle Dynamics CM-DPD. Following this methodology, the colloidal particles are represented as a smooth and repulsive hard core having attached a dissipative coat. In this model the repulsive nature is provided by the core force and hydrodynamic interactions are accounted by a a short-range lubrication potential.

Since its first introduction, Core-Modified DPD has been successfully employed to model suspensions at different flow strengths and different volume fractions (JAMALI; YAMANOI; MAIA, 2013; BOROMAND et al., 2018; JAMALI; BRADY, 2019; JAMALI et al., 2015b). Nevertheless, as far as we are aware, a systematic study on the combined effects of confinement, particle rigidity, high volume fraction and flow rate in suspensions using CM-DPD has not been addressed yet. The main study of this thesis addresses flow rate, particle rigidity and confinement effects on the microstructure of suspensions that are investigated in detail in systems at different concentrations, focusing on the semi-dense and dense regimes. Before this main study, two other additional studies were performed to guarantee a reliable simulation domain which were based on setting up the appropriate interactions of the computational domain. In Chapter 2 a brief literature review of the topic in study will be introduced. In Chapter 3 the computational method as well as the Machine Learning model applied are described. In Chapter 4 the results of all the studies are presented followed by some conclusions and suggestions for potential future works.

2
Previous Work

2.1
Colloids

Since Thomas Graham official definition of the term "colloids", and particularly from 1861, when a systematic study on colloidal particles was performed, a large number of research studies comprising those systems have been carried out. (DHONT, 1996). Nowadays, colloids preserve its popularity mostly due to its extremely vast range of potential applications. They are present in many aspects of everyone's routine life, in products such as food,cosmetics, pharmaceuticals, chemicals, paints, oil and gas, etc.

The term 'colloids' refers to the dispersed phase in a mixture of two components. According to the particle size in a colloidal mixture it can be classified in three different categories. In a solution, the size of the suspending particle is smaller than 1nm, these particles do not scatter light and for this reason the mixture is transparent and therefore, particles cannot be distinguished one another visually. The second category is the colloidal dispersion, where the particles suspending size has a maximum size of 1 μm. It is popularly defined as a heterogeneous mixture and although the size is smaller than in suspensions, they are still small enough to do not settle and remain suspended. Suspensions are the third type of colloidal mixture in which the particles' size is greater than 1 μm. In many cases, suspensions are treated as colloidal dispersion, and in literature many times the terms are interchangeable (MEWIS J.; WAGNER,).

The physics of suspensions is highly dependent on some parameters at the particle level, as for instance, volume fraction, shape and size of the particles. Among them, the concentration of particles in the system is a key factor in determining the rheological behavior of suspensions, and depending on the load of particles in the system different behaviors can be observed. Suspensions classification according to the concentration will be later addressed in this Chapter.

A topic of high importance in suspensions world is the governing forces and interaction potential between the particles.

2.1.1
Colloidal Forces

In general terms, the forces present in a colloidal system at a macroscopic and microscopic level can be divided in: external forces (such as electrical, gravitational and centrifugal forces), contact forces(found, for example in pastes and granular medium (COUSSOT; ANCEY, 1999; Van Der Sman, 2009)), hydrodynamic force and colloidal forces. The latter is significantly important when the particle diameter is smaller than 1 μm and some examples of it are depletion, electrostatic, Brownian forces, Van der Walls and structural forces (Van Der Sman, 2009; RUSSEL, 1980).

Herein we are focusing on colloidal forces. Among them, electrostatic interactions, observed when charged species are present, are the strongest ones and are able to induce different surface properties. Van der Waals interactions are composed of three components: a dipole-dipole force, dipole-induced and dispersion(London) forces. The latter has the most important contribution due to its universal nature and it arises from quantum mechanics of the species present in the system. They are essentially long-range forces and can be attractive or repulsive (MYERS, 1999). Depletion forces is an attractive force resultant from when particles are not able to access the space separating them. Brownian forces arise from the random thermal collision between the particles. It is governed by diffusion and can be represented as:

$$F^B = k_B T/a \tag{2-1}$$

Where k_B is the Boltzmann constant, T the temperature and a the particle radius. The presence of Brownian motion induces a stress that can be reduced according to the characteristic of the system, for example, bigger particles induce a weaker stress. Furthermore, Brownian motion acts smoothing gradients in particle concentration, helping particles in a more concentrated region move towards lower concentration zones(MEWIS J.; WAGNER,).

Hydrodynamic interactions arise from particles interactions promoted by the fluid presence. It is originated from a disturbance in the flow induced by the existing particles which are affected by the neighboring particles. They can be divided into short and long-range hydrodynamics forces. A clear explanation of the hydrodynamic interactions origin is given by (DHONT, 1996): A particle that is moving in a certain velocity induces the flow motion, which in turn propagates through the solvent until it encounters another particle, affecting their motion. That interaction is determined by the velocities and positions of these particles (as shown in Figure 2.1) and can be described by the Navies Stokes equation.

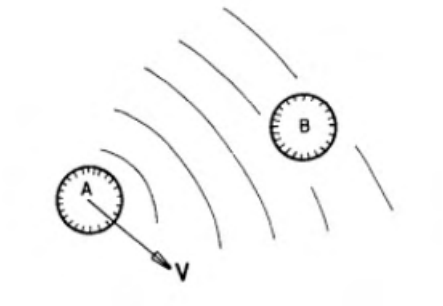

Figure 2.1: Flow disturbance by particle A in particle B through the solvent (DHONT, 1996)

2.1.2 Concentration

It is primordial to divide suspensions into separate groups when it comes to concentration to fully understand their physics and rheological behavior. In a very dilute suspension the system can be observed as a simple viscous

fluid while for a concentrated suspension the material approaches a granular material behavior. In fact, above a certain volume fraction, called maximum packing factor, the suspensions can no longer flow. In general therms, one can classify suspensions in dilute, semi-dilute and concentrated regimes.

In dilute system the particles do not see one another and the eventual collision between them can be neglected. Although there are a few particles, the flow is still disturbed by their presence, and as a consequence, the energy dissipation increases and the viscosity raises. This energy addition can be calculated by the classic Einstein equation (MEWIS J.; WAGNER,):

$$\eta = \eta_m(1 + 2/5\phi) \tag{2-2}$$

η_m is the medium viscosity and ϕ is the concentration. As shown in the equation, the contribution of the particles to the viscosity is linear with concentration. As the particle load increases, the semi-dilute regime, characterized by a volume fraction above 0.1, is reached. In this case, the presence of a second particle is felt by the first one, i.e. there is a local disturbance and the flow around them and the energy dissipation is strongly altered. Viscosity for that particular case can be described as a Taylor expansion of Einstein equation, as shown in equation 2-3:

$$\eta = \eta_m(1 + 2/5\phi) + c_2\phi^2 + c_3\phi^3 + ... \tag{2-3}$$

c2 is a coefficient that depends on the type of flow and it governs the interactions. The other coefficients accounts for many-body interactions and their calculation is not trivial.

When the concentration increases, some major challenges arise. At high load of particles the volume fraction is high enough for short-range interactions become important. Multi-body hydrodynamic interactions take place and its calculation is extremely hard. In effect, at this point, hydrodynamic interactions become predominant and affect strongly the suspension behavior.

Many challenges emerge from the many-body interactions affecting hydrodynamic interactions. The first of them in related to lubrication forces, which correspond to the short-range hydrodynamic contribution from interactions and it is resultant of the viscous force acting between two nearly touching spheres separated by an interstitial fluid. That force goes to zero when the surfaces gets too close and computations at this point become intensive. Selecting a model that can capture these effects is extremely important and crucial for an accurate suspensions characterization (MEWIS J.; WAGNER,).

Apart from lubrication forces, the long-range character of the hydrodynamic interactions is also another issue that has to be addressed and that poses difficulty. The high concentration of particles may lead to a non convergence of the sum of interactions, and a screen in the interactions can take place (BRADY; BOSSIS, 1988).

Most of these difficulties are nowadays addresses specially with the support of computational models, such as Stokesian Dynamics (BRADY; BOSSIS, 1988) that can addressed both long and short-range hydrodynamic interactions. Some other popular computational methods will be introduced later in this Chapter.

As mentioned previously, some factors are known to alter the behavior and structure of suspensions, such as particle shape, size distribution and the

presence of physical constraints. Some of these issues will be later addressed. When it comes to the research and development of suspensions, a key aspect in the characterization of those systems is the rheological properties associated.

2.2 Rheology

Rheology is the field of study focused primarily on understanding the phenomena involved in the flow of matter, which is extremely important in materials characterization and engineering applications since the rheology of a given system relates to its macroscopic structural properties. The rheology of suspensions has a crucial importance in the research and development of new materials and in improving and adjusting the material characteristics based on a desirable application. In pure fluids, the Newton's law that correlates the flow kinematics and stresses is satisfied according to the equation:

$$\tau_{xy} = \mu \frac{dv_x}{dy} = \mu \dot{\gamma}_{xy} \tag{2-4}$$

Where τ_{xy} represents the xy component of the stress tensor, μ the viscosity and $\dot{\gamma}_{xy}$ the shear rate. The fluids in which this equations holds are called Newtonian Fluids. In the majority of suspensions, a non-Newtonian behavior is seen, i.e. the stress is not proportional to the strain and viscosity varies non-linearly with the shear rate. Two non-Newtonian behaviors very often observed in suspensions is shear-thinning and shear-thickening. In the former case, the suspension viscosity decreases as the applied shear rate increases, mostly due to the formation of particle layering that reduces the energy dissipation and therefore the viscosity. In the latter case the opposite behavior is seen. As the flow rate becomes stronger, particle aggregation and cluster formation start taking place, that will retard the flow and increase the energy dissipation, consequently the system viscosity. Figure 2.2 illustrates these transitions. In both cases, the non-linear nature of the relation stress/shear rate requires a modification of Newton's law. A common expression that generalizes the stress-shear rate relation is given by the power law expression(2-5)

$$\sigma = k\dot{\gamma}^n \tag{2-5}$$

n is known as power law index. σ represents the stress and $\dot{\gamma}$ the shear rate. When $n < 1$ a shear-thinning behavior can be identified and shear-thickening is seen for any $n > 1$. The fluid behavior is commonly dependent on many flow and particle properties, such as the flow rate, particle concentration, polydispersity, shape of particles, size, etc. An example of a study in which a shear-thickening behavior preceded by shear-thinning regime is observed in Figure 2.3. It shows the relative viscosity variations at different volume fractions for increasing flow rates. η_r corresponds to the relative viscosity with respect to the solvent.

Suspensions at high concentration can display an abrupt increase in the viscosity if a force sufficiently large enough is applied; that transition is known as discontinuous shear-thickening DST. Many works in the literature have reported discontinuous shear-thickening (MARI et al., 2015; SETO et al., 2013; LIN et al., 2015; BROWN; JAEGER, 2012; FERNANDEZ et al., 2013),in the majority of them, a requirement to observe such transition is the presence of

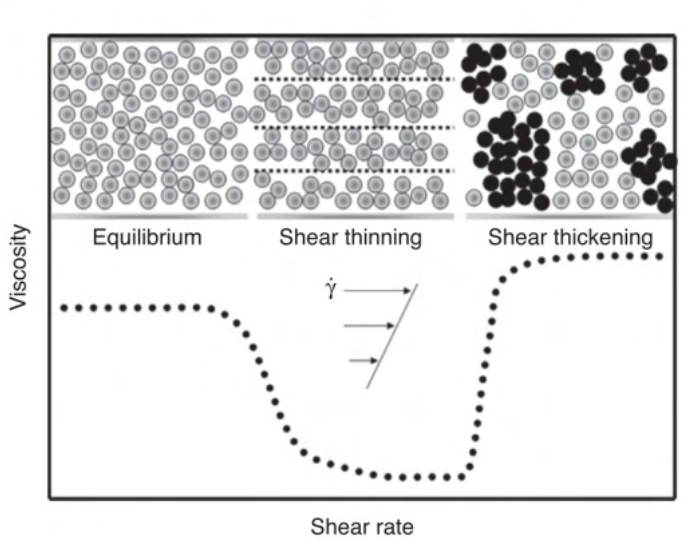

Figure 2.2: Schematic representation of the correlation viscosity and microstructure for different shear regimes, ranging from equilibrium to Shear-Thickening(MEWIS J.; WAGNER,)

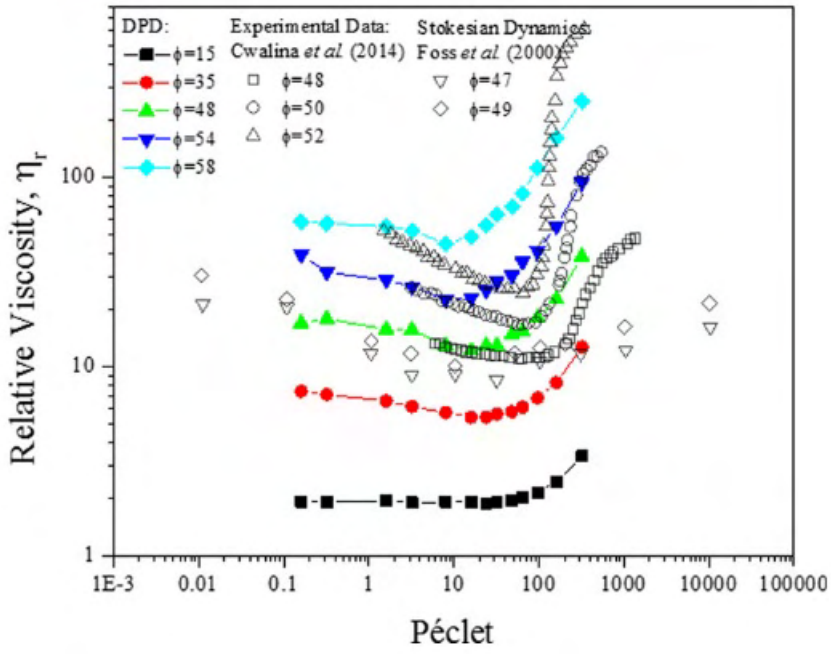

Figure 2.3: Evolution of the viscosity of suspensions at different volume fraction with the applied shear rate represented in terms of the Peclet number. (JAMALI et al., 2015b)

frictional forces. However some more recent work has shown that DSC can be reached even when only hydrodynamics is used (JAMALI; BRADY, 2019). As illustrated in Figure 2.4, a clear transition from Continuous shear-thickening to Discontinuous-shear thickening is observed at volume fraction 0.52 and surface covered from 0.25; in this case, no frictional forces are applied.

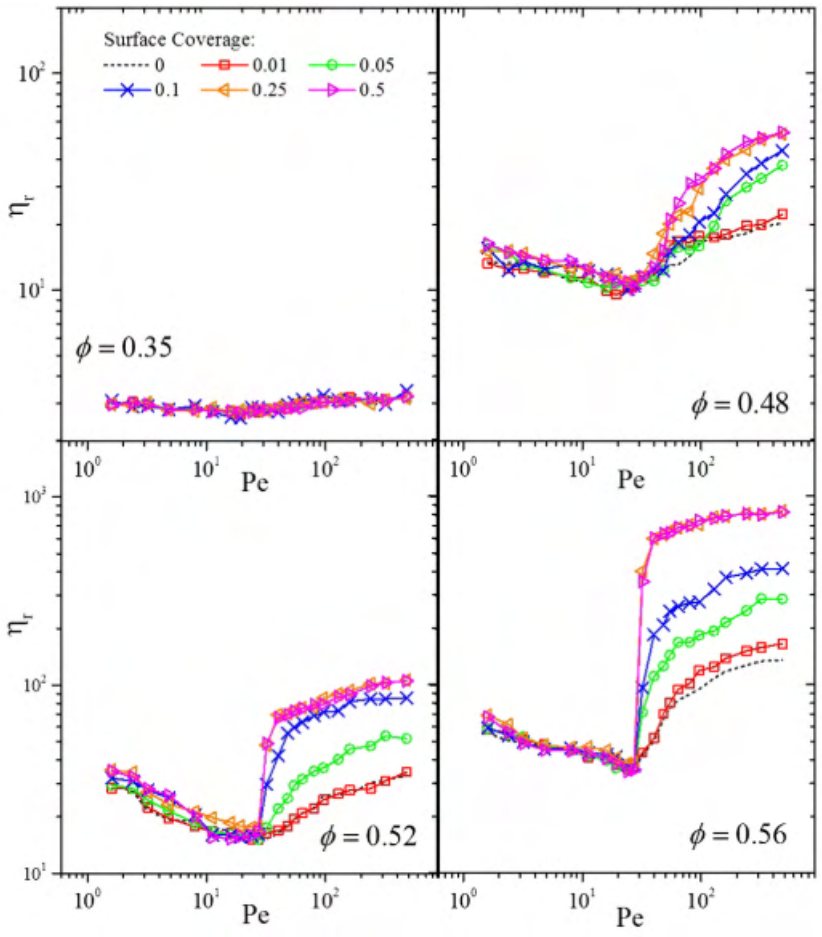

Figure 2.4: Viscosity changes at increasing Pe and different surface coverage. (JAMALI; BRADY, 2019)

2.3 Confinement

Many suspensions works focus on fluid bulk properties, however, in real applications materials are limited in space by physical constraints. Because of that, research of fluids under confinement remains as a large and important area of study. With the development and advancement of new experimental tools and computational resources, the research of confined geometries has became a topic increasingly explored.

Confinement is a multi-scale field of study encompassing different length and time scales due to the diversity of the components in the system such as colloidal particle size, solvent size and dimensions of the channels. Simulation methods are an interesting alternative over traditional experimental research to study a particular phenomenon present within a specific time and length scale. Depending on the choice of the method different information can be obtained from the systems in study.

Several studies targeting confinement effects on suspensions are reported in the literature. Confinement is a relatively rich and well explored area. For example, in a study from around 20 years ago (NOTT; BRADY, 1994), Stokesian dynamics simulations were performed to investigate confinement effect in systems where the ratio between the channel height and the particle diame-

ter (y/d) as well as volume fraction were varied. They observed that in order for suspensions to present a constant pressure perpendicular to the flow, the particles need to migrate towards the center of the channel leading to an inhomogeneous distribution of the particle velocity and formation of clusters, which are broken when short-range repulsive forces are included. Those migration effects increase with the volume fraction. From the same date as (NOTT; BRADY, 1994), (KOH; HOOKHAM; LEAL, 1994) proposed an experimental study in order to investigate suspensions flow in a rectangular channel and reached a similar conclusion. A blunt in the velocity profile in the middle of the channel was seen in the flow of concentrated suspensions. The inhomogeneity increases as volume fraction and the ratio particle size/confinement gap of the channel raises.

A common and relatively well established suspensions behavior observed in many experimental and numerical works (YEO; MAXEY, 2010b; GALLIER et al., 2016) is particle ordering induced by the presence of walls. (YEO; MAXEY, 2010a), for example, reported and extensive work investigating the ordering structure evolution of suspensions at different gap ratios for a range of volume fractions. They separated the study in three regions according to the dominant microstructure in place, which they called wall, buffer and core zones. Depending on the volume fraction a strong layering at the wall is seen, following by a region that is similar to an homogeneous unbounded shear flow (core region). The buffer phase presented characteristics from the other two regions, displaying asymmetry in the microstructure.

In a following work (YEO; MAXEY, 2010b), the same group investigated ordering transition at different volume fractions and channel heights and concluded that both volume fraction and the channel gap influence the ordering mechanism. One of their conclusion was that for VF = 0.48 and ratios h/a (h representing the channel height and a the particle radius) above 40 a disordered phase is much bigger than the ordered one, approaching a bulk behavior. In stronger confinement conditions($h/a < 10$) the commensurability of the particles with the free space determines the ordering of the system. For intermediate gaps, ($h/a < 15$) an hexagonal structure was seen. Those transitions are dependent on the volume fraction. For VF=0.6, for example, a structural transition from triangular to rectangular was observed. Most importantly, the flow behavior is a consequence of the non-linear relationships between the gaps and the volume fraction.

More recently, (BIAN et al., 2014) in 2014 studied confinement in suspensions using Smoothed Particle Hydrodynamics (SPH). Simulations were performed for channel gaps from 8 to 256 and particle concentration of 0.589. They observed that confinement changes the hydrodynamic interactions between particles and that a percolating network at the onset of hydrodynamic shear-thickening is seen at strong confinement conditions. Slip at the wall was observed and increasing confinement gaps and the volume fraction resulted in a stronger suspension viscosity and formation of larger clusters, as observed in Figure 2.5. σ^* illustrates the critical shear stress, which is the minimum stress where shear stress emerges.

(GALLIER et al., 2016) and co-workers in 2016 studied the wall effects in the rheology and velocity of suspensions with gap ratios of 20 for volume

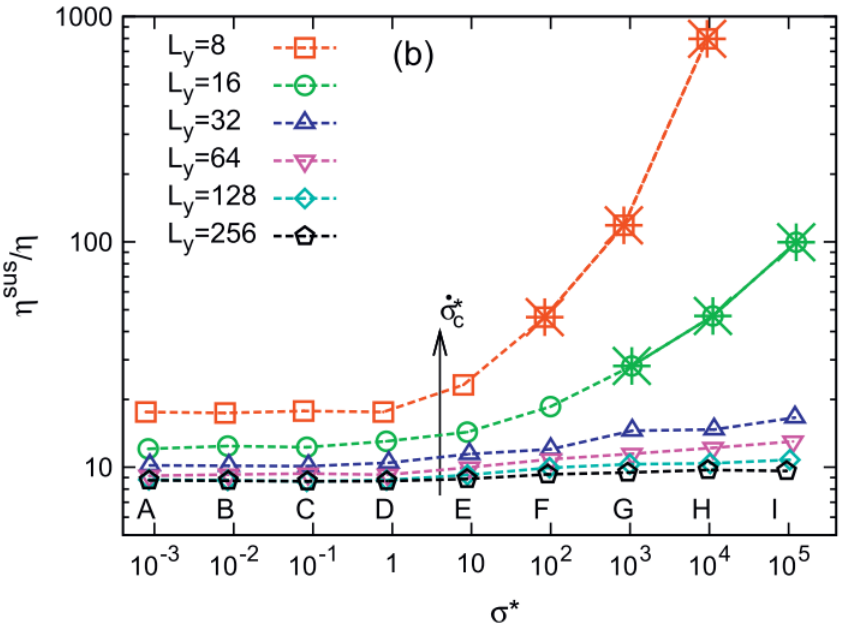

Figure 2.5: Suspensions viscosity as a function of the critical shear stress for volume fraction of 0.589. (BIAN et al., 2014)

fractions ranging from 0.1 to 0.5. They noted the presence of an hexagonal structure whose thickness was dependent on the volume fraction. They also observed that ordering has not a significant impact on the viscosity and second normal stress difference. The first normal stress is, however, greatly affected and that confinement can lead to positives N1.

In 2017, (RAMASWAMY et al., 2017) proposed a systematic study combining experiments and simulations to track rheological changes and microstructure of suspensions at different confinement ratios and volume fractions. They divided viscosity changes in three categories according to the confinement ratio. The first one they called moderate confinement, for $15>h/2a>6$ (where a is the particle radius and h the channel height), characterized by a strong particle layering. For $3< h/2a<6$, corresponding to a strong confinement region, fluctuations in viscosity are due to the formation of a bucket structure. The third phase is in extreme confinement conditions, when $h/2a < 3$. In this case, a sharp increase in the viscosity was reported. Those observations were only evidenced for volume fraction of 0.52. If volume fraction was reduced, layering and bucked structure were no longer seen.

All these works reported so far target stiff particles, however the particle rigidity is an important parameter that can affect fluid behavior and particle ordering. In the case of soft and deformable particles, in addition to the disturbance in the motion promoted by the particles, one also need to account for the deformation effects and the perturbations in the hydrodynamic interactions due to particle deformation.

2.4
Deformable Particles

Deformable particles are an interesting topic of study and have been investigated in many works. (PAKULA, 1991) for example, studying dense colloidal suspensions observed different dynamic structural states of particles when density and particle stiffness were tuned. (COULLIETTE; POZRIKIDIS, 1998) and co-workers observed in their work that deformable particles in a cylindrical tube tend to migrate towards the center of the channel after a period of deformation. That migration is mainly driven by a deformation-induced lift.

Another interesting study was proposed by (HSU; CHEN, 2010), in which volume fraction, gap and flow rate were investigated in a system composed of deformable particles. A migration of particles towards the center was seen due to the asymmetry in the hydrodynamic interactions caused by the particles deformability at the wall vicinity. At high volume fraction, particles can pack in the center of the channel.

On the confinement front, particle rigidity is also highlighted in some works. In (KILIMNIK; MAO; ALEXEEV, 2011), cross-migration of deformable particles was studied in a pressure-driven flow. The authors found that particles equilibrium position depends on several factor such as channel height, Reynolds number and elasticity. However, in general, softer particles tend to reach equilibrium positions at the channel mid-plane. In other words, the lift force responsible for particle displacement is enhanced by deformability.

(CHEN, 2014) published a work aiming to understand the effects of deformation and inertia of soft particles in both shear and Poiseuille flows. According to the authors, migration is driven by shear forces, inertial stresses and elastic contraction. In the case of Poiseuille flow they concluded that the particles concentrate in the channel mid-plane and that the effect is stronger as deformability and shear rate increases. That migration depends on particle inertia and deformability, while for hard particles, migration does not depend on the shear rate. In the latter case the steady state position that the particles adopt is weakly dependent on Reynolds.

Recently, in 2016, (MEHRABADI; KU; AIDUN, 2016) investigated the effect of particle rigidity among other factors in margination (particle migration towards the walls). They concluded that stronger margination is lead by particles that are smaller and less deformable.

Although many experimental studies of both rigid and soft particles can be found in the literature, the majority of works employ simulations techniques to explore and characterize those systems. That is true especially for concentrated and highly confined suspensions, where there exists important equipment's limitations that can pose a challenge to those studies.

2.5
Computational methods

Several computational approaches for modeling suspensions can be found in the literature. The development of such techniques is motivated by the increase and improvement of computational power and resources which enables

the study of systems that were a challenge before, as for example, suspensions at strong confinement conditions.

There are some studies that explore comparisons between the techniques and highlight some important parameters in the design of a system according to the desirable time and length scales.

(PADDING; LOUIS, 2006) introduces some key dimensionless numbers describing the physics of suspensions that should be accounted for before selecting a computational method. Although the authors focus on stochastic rotation dynamics methods SRD, some important insights about other simulations techniques are described. Most importantly, they summarize the main dimensionless numbers, showed in Figure 2.6, responsible for the governing physical process in each system - the table has been adapter for this work. Those are extremely important in the choice of the most suitable technique to be employed in order to describe correctly the physics of the system of interest.

Schimidt	collisional momentum transport/kinetic	$Sc = \frac{v}{D_f}$
Reynolds	inertial forces/viscous forces	$Re = \frac{v_s a}{v}$
Peclet	convecctive transport/diffusive	$Pe = \frac{v_s a}{D_{col}}$

Figure 2.6: Main dimensionless number governing the physics of suspensions. Adapted from (PADDING; LOUIS, 2006)

(Van Der Sman, 2009) in a more recent study also presents some numerical methods for suspensions modeling and classify them according to the physics and dimensionless number. In general terms, the physics of suspensions is described by Reynolds, Stokes and Peclet numbers. A choice for a specific computational method depends specially on the Re_p and Pe. Figure 2.7 summarizes their proposed methods based on the dimensionless numbers for each system.

More recently (BOLINTINEANU et al., 2014) published a review about some of the off-lattices and particle-based methods, those were: fast lubrication dynamics (Bybee, 2009), multi-particle collision dynamics (MPCD) (GOMPPER et al., 2008) and Dissipative Particle Dynamics (HOOGERBRUGGE; KOELMAN, 1992; GROOT; WARREN, 1997). Each one them have their own particularities and advantages/limitations.

A very powerful technique that has been broadly used to model suspensions is Stokesian Dynamics SD. SD accounts for high-order terms in the hydrodynamics interactions making the technique one of the most appropriate to target multi body hydrodynamics. However, it is limited to particles moving very slowly (that are in the Stokes regime), brings some difficulties in setting the boundary conditions and mostly spherical particles can be represented (Van Der Sman, 2009). In addition, a high computational cost makes it difficult to study long-time diffusion(BOLINTINEANU et al., 2014).

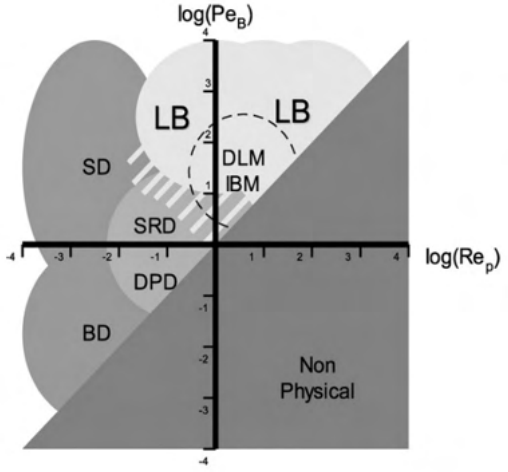

Figure 2.7: Simulations methods mapped according to the dimensionless Particle Reynolds and Peclet. LB stands for Lattice Boltzmann, DPD Dissipative Partice Dynamics, SD Stokesian Dynamics, BD Brownian Dynamics, SRD Multi-Particle Collision Dynamics, DLM distributed, Lagrangian multiplier, IBM - Immersed Boundary Method.

Brownian Dynamics is another pretty popular simulation technique used to model suspensions.The main limitation of the method is that long-range hydrodynamic interactions and momentum transport are ignored in the traditional approach(PADDING; LOUIS, 2006). Lattice-based methods, such as lattice Boltzmann have became pretty popular due to its implementation simplicity and versatility to work with Peclet numbers above 1 (Van Der Sman, 2009). A limitation of the method is when dealing with a system having more than one length scale. (PADDING; LOUIS, 2006)

An innovative method that accounts for both hydrodynamic and Brownian interactions, conserves the momentum locally and globally, translates the correct hydrodynamics due to the presence of a thermostat and employs soft potentials, which enable the usage of larger time steps, is called Dissipative Particle Dynamics (HOOGERBRUGGE; KOELMAN, 1992; GROOT; WARREN, 1997).

Dissipative Particle Dynamics is an off-lattice simulation method extensively used to model systems in the mesoscale such as suspensions, polymers, surfactants, blends, etc.

Inspired by Molecular Dynamics, in DPD the Newton equation of motion is solved for pairwise interacting particles. Each one of these particles is represented by several atoms using the coarse-graining technique, which consists of a clustering approach to reach higher time and length scales. DPD introduces some advantages compared to other mesoscales simulation techniques: the introduction of soft potentials, allowing to reach higher time scales, shorter equilibration time and the presence of a thermostat that preserves momentum. DPD will be latter described in more details in this document.

2.6
Modelling walls with DPD

DPD has also been successfully employed to model different mesoscale systems such as polymers (LIU et al., 2016; ZHAO et al., 2014; YAMANOI; POZO; MAIA, 2011; KHANI et al., 2015) suspensions (JAMALI; YAMANOI; MAIA, 2013; JAMALI et al., 2015b; BOROMAND et al., 2018), surfactants (GINZBURG et al., 2011; ANDERSON et al., 2018), nanocomposites (CUDJOE et al., 2017), gels(BOROMAND; JAMALI; MAIA, 2017) and Janus particles (PAIVA et al., 2019; PAIVA et al., 2020a; PAIVA et al., 2020b).

A remaining challenge in DPD is imposing the correct boundary condition when physical boundaries are present. Since the interactions between DPD particles are soft the free particles in the system may penetrate the wall. A very popular strategy to prevent particle penetration is artificially increase the wall density and/or the repulsion exerted by the walls to the solvent particles. However, a consequence of that break in the forces balance is density oscillation and layering (MEHBOUDI; SAIDI, 2014; KOMNIK; HARTING; HERRMANN, 2004).

The most classic approach to model walls is by frozen DPD particles at the edges of the simulation domain. The particles are fixed and not allowed to move, however they are free to interact with the solvent particles free in the system. Imposing the correct boundary condition at the wall is closely related to the model's ability to prevent particles to penetrate the wall while the formation of a depletion layer is controlled.

Several numerical studies for wall models using DPD can be found in the literature (WILLEMSEN; HOEFSLOOT; IEDEMA, 2000; LI et al., 2018; BOROMAND; JAMALI; MAIA, 2015; FEDOSOV; PIVKIN; KARNIADAKIS, 2008a; PIVKIN; KARNIADAKIS, 2005). The earliest ones model the wall as a single layer of DPD particles and to keep them away from the wall its density is artificially increased, as for example in (KONG et al., 1994). In that study, although particles did not penetrate the wall, large density fluctuations at the wall vicinity were observed.

From the nineties on, numerous studies targeting the development of models, able to simultaneously avoid wall penetration while reducing density fluctuations and promoting no-slip boundary conditions have been proposed. One of the initial ones was introduced by Pivkin and co-authors (PIVKIN; KARNIADAKIS, 2005). In their work, wall particles were shifted and the force field around the wall was corrected to estimate an ideal conservative force of the wall particles. The authors were able to reach non-slip boundary condition, however some density fluctuations at the wall proximity were detected.

Posteriorly, the same group (PIVKIN; KARNIADAKIS, 2006) introduced a new method to reduce density fluctuations based on a new modification of the force field around the wall in order to reach the desirable density. Using the same approach, they also adjusted the temperature at the wall by correcting the dissipative coefficient and successfully managed to reach an uniform density profile. More recently, some new studies targeting the creation wall-models with arbitrary shaped geometries have been published (LI et al., 2018; ZHANG; SHANGGUAN; WANG, 2018).

Apart from theoretical works, DPD wall-models have been broadly explored in the field of nanofluids (KASITEROPOULOU; KARAKASIDIS; LIAKOPOULOS, 2011; GUBBIOTTI; CHINAPPI; CASCIOLA, 2019; GOONEIE; HUFENUS, 2019; SMIATEK; SCHMID, 2011; ABU-NADA, 2017). The study of these models is motivated by the increasing development of nano-bases systems, which require a fundamental understanding of the flow phenomena that is distinct from the bulk behavior. For example, nanoconfined fluids can depict additional surface forces, phase transitions (CUMMINGS et al., 2010) and layering effects(NOORIAN; TOGHRAIE; AZIMIAN, 2014; BECKER; MUGELE, 2005).

A crucial step in the development of a successful study in confined geometries evolves the creation of a wall model capable of reproducing, as accurately as possible, the physical phenomena observed in real physical systems. The occurrence of density oscillations and layering at the wall vicinity, for example, are physically important and proven to happen, as observed in many studies (MEHBOUDI; SAIDI, 2014; KOMNIK; HARTING; HERRMANN, 2004; NOORIAN; TOGHRAIE; AZIMIAN, 2014; PERRET et al., 2010). Therefore, a better understanding of the factors and parameters that influence those phenomena is essential in the establishment of more accurate wall models.

Increasing wall density or/and the repulsion between wall and solvent particles are the most common approaches to prevent nonphysical effects. In a real systems, particle penetration inside the wall is not possible and we need to use artificial methods to achieve a non penetration condition. We are aware that those artifacts are synthetically induced and could not be directly applied in real physical systems.

2.7
Modeling Suspensions with DPD

Posterior to its first introduction, DPD has been used for modeling dispersed systems, as in suspensions and polymer solutions. The first report of DPD usage to model suspensions dates from one year after its initial introduction by (SCHLIJPER; HOOGERBRUGGE; MANKE, 1995; KOELMAN; HOOGERBRUGGE, 1993). In the work of (KOELMAN; HOOGERBRUGGE, 1993), more specifically, suspensions of hard spheres in a steady shear flow were modeled using DPD and their proposed approach is still used nowadays. It consists of a freezing procedure of the fluid particles in order to represent solid objects. Those particles move and the propagation steps are modified in a way that after a collision the momenta of particles composing the solid object are redistributed and they move together as a single unit. Figure 2.8 illustrates a snapshot obtained by the simulations using this approach (KOELMAN; HOOGERBRUGGE, 1993).

A few years later, (BOEK; COVENEY; LEKKERKERKER, 1996; BOEK et al., 1997) employed the same technique to study the rheology of suspensions at different shapes (rods, disks and spheres) at 30% of concentration. More recently, in 2008 (CHATTERJEE; WU, 2008), a comparative study between experiments and simulations using the same technique was carried out and a good comparison between the two approaches was obtained.

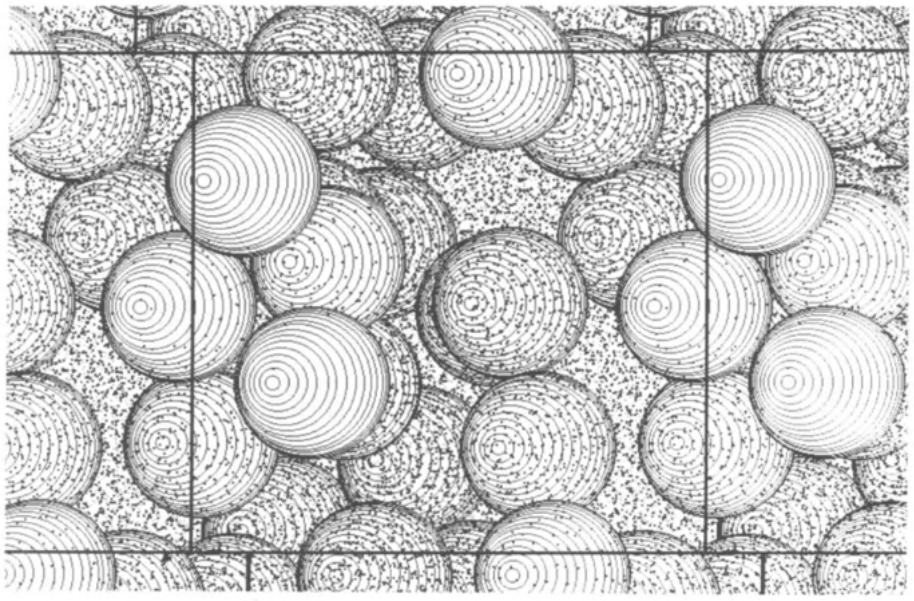

Figure 2.8: Snapshot of colloidal particles obtained by (KOELMAN; HOOGERBRUGGE, 1993). Spheres are concentrated at 30%. Dots represent fluid particles comprising colloidal particles (bigger spheres) .

The freezing approach main advantage is that modeling suspensions is not only limited to spherical objects, arbitrary shapes can also be represented. The downside of the technique is the lower surface definition of the particles, density oscillations and maintaining temperature is difficult. Some alternatives have been proposed to overcome those constraints, such as the usage of stiff spring forces between DPD particles to represent solid objects as first reported by (PHAN-THIEN; MAI-DUY; KHOO, 2014) and later used by (MAI-DUY; PHAN-THIEN; KHOO, 2015).

To overcome the constraints associated to a lower surface definition arising from the freezing-related procedures, single particle models considering the particles as single entities have been proposed. In this case, DPD particles are represented as a hard objects and the forces are modified to account for particle-particle interactions (PRYAMITSYN; GANESAN, 2005).

Another possibility relies on the usage of pairwise colloidal forces between the particles, as proposed initially by (WHITTLE; TRAVIS, 2010) in a model named Core-Modified Dissipative Particle Dynamics CM-DPD. Following this methodology, the colloidal particles are represented as a smooth and repulsive hard core having attached a dissipative shell that is included to reproduce suspensions in a more realistic way. In this model the repulsive nature is provided by the core force and hydrodynamic interactions are accounted by a a short-range lubrication potential.

2.8
Challenges in modeling Walls in Suspensions

As a mesoscale particle-based method, Dissipative Particle Dynamics has been extremely successful in the modeling soft matter and has successfully captured physics of complex fluids(PAIVA et al., 2019; JAMALI; YAMANOI;

MAIA, 2013; JAMALI et al., 2015b; WANG; JAMALI; BRADY, 2020; KHANI et al., 2015; BOROMAND; JAMALI; MAIA, 2015; BOROMAND; JAMALI; MAIA, 2017).

By utilizing soft potentials, DPD has shown extremely versatility and flexibility in the modeling of different soft matter systems including but not limited to polymers (SCHLIJPER; HOOGERBRUGGE; MANKE, 1995; SPENLEY, 2000; LAHMAR; ROUSSEAU, 2007; NARDAI; ZIFFERER, 2009; ZHAO et al., 2014; KHANI et al., 2015; PAIVA et al., 2019; PAIVA et al., 2020a), gels (YONG et al., 2013; BISWAS et al., 2017; BOROMAND; JAMALI; MAIA, 2017), suspensions(JAMALI; YAMANOI; MAIA, 2013; JAMALI et al., 2015b; BOROMAND et al., 2018; WANG; JAMALI; BRADY, 2020) and walls (REVENGA et al., 1998; PIVKIN; KARNIADAKIS, 2005; PIVKIN; KARNIADAKIS, 2006; FEDOSOV; PIVKIN; KARNIADAKIS, 2008b; MEHBOUDI; SAIDI, 2014). In most industrial, biomedical, pharmaceutical applications and many biological systems such as blood flow, fluid is flown through a confined geometry. DPD despite its advantages could be associated with artifacts when modelling wall-bounded systems. This matter has been a subject of study and many solutions have been developed for parametrizing DPD to avoid numerical artifacts(PIVKIN; KARNIADAKIS, 2005; PIVKIN; KARNIADAKIS, 2006; MEHBOUDI; SAIDI, 2014; FEDOSOV; PIVKIN; KARNIADAKIS, 2008b; LI et al., 2018; BARCELOS et al., 2021). Different boundary conditions have been proposed for realistic modeling of fluid motion in between the walls (**??**ZHANG; SHANGGUAN; WANG, 2018; LI et al., 2018; RANJITH; PATNAIK; VEDANTAM, 2013; VISSER; HOEFSLOOT; IEDEMA, 2005). However, traditionally, the walls are made out of frozen particles which are still free to interact with the fluid particles. This approach is associated with challenges which are mainly due to the soft inter-particle interactions. Penetration of fluid particles in the walls is inevitable and avoiding penetration and controlling density fluctuations in the vicinity of the walls is an extremely difficult task which requires extensive theoretical and parametric studies.

Preventing wall penetration in DPD-based walls was first addressed nearly three decades ago by (KONG et al., 1994). Posterior to this initial study, Pivkin and co-workers proposed a series of relevant studies targeting the nonphysical phenomena taking place at the wall (PIVKIN; KARNIADAKIS, 2005; PIVKIN; KARNIADAKIS, 2006; FEDOSOV; PIVKIN; KARNIADAKIS, 2008b). In those studies, several alternative strategies were introduced, including testing different boundary conditions, modifying wall forces, controlling density fluctuations and evaluating different wall densities and repulsion interactions. Posterior to these works, some theoretical and parametric studies have explored quantitatively repulsion at the wall (BARCELOS et al., 2021). Additionally, walls adopting different geometries have also been addressed in the past years (LI et al., 2018; ZHANG; SHANGGUAN; WANG, 2018).Previously, we explored (BARCELOS et al., 2021) the effect of fluid-wall interactions and wall density on controlling wall penetration and density fluctuations as these two parameters have been shown to have the most impact in determining a realistic physics-based simulation set up.

In the current study we expand upon our previous investigations of wall-

bounded flows and we would like to propose a model for simulating flow of colloidal suspensions in a confined geometry. For this purpose, we have employed the framework proposed by Whittle and Travis(WHITTLE; TRAVIS, 2010) named Core-Modified Dissipative Particle Dynamics CM-DPD, which represents colloidal particles with a rigid core and a soft hydrodynamic shell. This method has been evaluated and expanded by our group in multiple studies and has been found to be very advantageous and promising in capturing the full spectrum of suspension rheology with much lower computational cost compared to models based on standard DPD simulations.

Reports of DPD applied to complex fluids in wall geometries can be found in the literature (KONG et al., 1994; MALFREYT; TILDESLEY, 2000; FAN et al., 2003; FAN et al., 2006). In suspensions, however, the number of works is not as extensive, maybe because an additional complexity appears in setting the interactions since there are parameters at the particle level, such as rigidity and concentration, that may also play an unknown role in particle penetration. In other words, setting the wall-particle interactions might not be as trivial as in the case of pure solvent and wall system.

Adjusting colloid and solvent interactions in suspensions in a way that it prevents nonphysical effects is a key aspect in creating a successful simulating system for studying fluid properties. Since there are other parameters, in addition to wall repulsion, which play a role in the interactions a systematic study about the individual and collective effect of those variables is essential to a better understanding of the problem and to the creation of a more reliable system.

Understanding the extension to which particle parameters and flow properties impact particle migration and wall penetration in DPD-based suspensions has not been addressed yet even though it is essential in the establishment of a geometry that can be posteriorly used to study the physical properties of a system. Adjusting colloidal and solvent interactions to avoid penetration is a key aspect in creating a successful simulating geometry for a reproducible study.

Exploring the essential relationships and associations between the parameters affecting penetration is a challenge in two aspects. First, there might exist interactions between the parameters that influence the response variable, thus, not only individual effects must be taken into account but also possible interactions between them. Secondly, particle penetration potentially varies in a non-linear way depending on the levels of the parameters adopted. Therefore, developing a strategy to quantify penetration would be an extremely complex task.

Due to the vast variety of data and the great number of machine learning algorithms, today it is possible to solve an enormous range of problems. Therefore, Machine Learning algorithms can be used as a powerful tool for understanding correlations between different parameters and hidden patterns withing data through statistical analysis and decoupling of combined effect. Machine Learning, in a time efficient manner, provides a systematic understanding of individual effects and combined responses especially in cases when the response variable depends in an unknown and complex way on the original variables. There has been a plethora of interest in using Machine Learning

in material science for making fast predictions about materials' behavior [refs]. ML has also been combined with DPD simulations for modelling different fluid properties(INOKUCHI et al., 2018; CHEN; YONG, 2019; INOKUCHI; OKAMOTO; ARAI, 2020; ZHAO et al., 2021; WANG; OUYANG; WANG, 2021a).

2.9 Machine Learning

Machine learning ML corresponds to a sub-field of Artificial Intelligence consisting of a series of algorithms that are able to learn from data, find patterns and make future predictions (MITCHELL, 1997). The basic idea behind ML and data driven approaches is that instead of explicitly programming a computer to perform specific tasks one can show examples and let the computer work on its own to discover information and find patterns and insights in the data. There are a very large number of choices of algorithms available depending on the type of problem and data. Tabular data is one of the most traditional and highly used type of data in ML. Many engineering applications involves this type of data such as time series and in predictions of materials properties and functionalities. ML can also be used in text and image data, which are advanced applications that are responsible for many of the smart services we have access today such as instantaneous translations, speech recognition, image recognition etc. Figure 2.9 displays the most used models categorized by the type of learning problem.

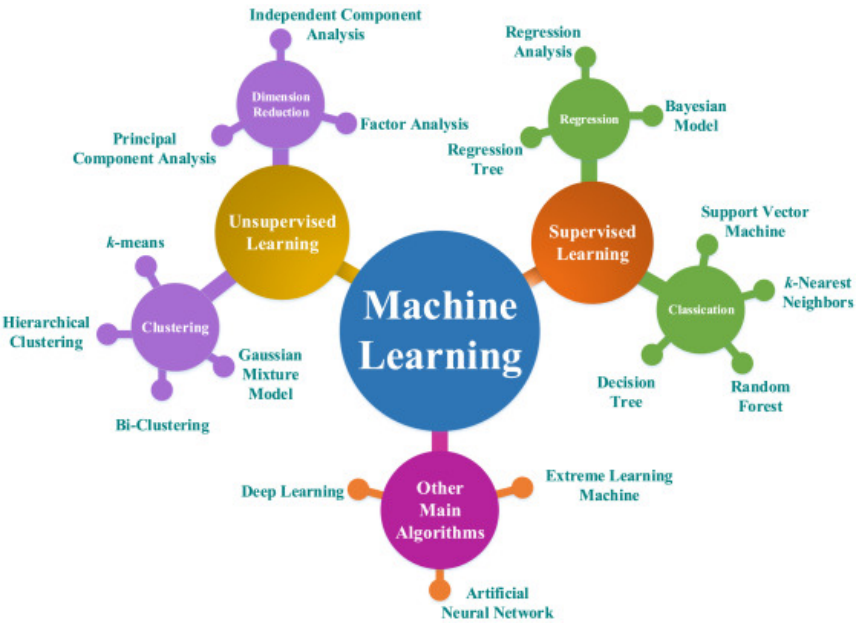

Figure 2.9: Some popular ML models (GAO et al., 2020)

In general terms, there are two main types of problems: supervised and unsupervised learning. In the former case, the model is trained under supervision, meaning that a label is provided for the algorithm to use to evaluate its performance. In unsupervised problems, on the other hand, no

label is given and the model is free to work on is own to discovery information - the goal is, therefore, to find patterns and structure in the data. In supervised learning tasks, on the other hand, the objective is to make predictions from an input set of data. On can categorize supervised algorithms in two main classes of models:

a) Parametric: Parametric models are the ones that the learning function mapping inputs to outputs is learnt by the algorithm and is expressed as a mathematical expression in which the coefficients are adjusted as more data in fed in the model. In short, the way it works is that initially the model receives inputs and makes random predictions. These predictions are subsequently compared to the true values using a loss function. The goal of the training process is to minimize the error in the loss function, i.e. the difference between predictions and true values. Traditionally, that can be done by using least squares method or more optimal techniques such as gradient descent. Those methods goals are to find the minimum of the loss function. When that happens, the model becomes accurate and performant in terms of making right predictions. Some common parametric models are: linear regression, logistic regression and multi-layer perceptron.

b) Non-parametric: Non parametric models do not make assumptions between the mapping function between the problem input and outputs, which give them some additional flexibility for learning any functional form of the data. They are particularly good when there are a lot of data available and no prior knowledge about it. Because of their extra learning flexibility, these model usually present higher performances, especially for non-linear data. As a drawback they can overfit easily and are slower compared to parametric models. Some examples of non-parametric models are: K-Nearest neighbors, support vector machines and decision trees.

There are many studies that used DPD combined with machine learning models in the literature and it has been proven to be a successful approach to complement computational studies. (INOKUCHI et al., 2018) for instance, used machine learning to predict viscosity and dispersion in a surfactant solution. Two years later, the same group (INOKUCHI; OKAMOTO; ARAI, 2020) compared different regression models ability to predict phase transition ordering and temperature of a liquid crystal. (CHEN; YONG, 2019) employed two supervised learning problems to build a microstructure phase diagram based on the particle concentration and radius. More recently,(WANG; OUYANG; WANG, 2021b) in a very interesting work used ML to perform lubrication corrections in suspensions. These works used conventional data-driven approaches, where the learning process occurs as the algorithm is fed with more data. The challenge, and many times limitation of ML, is that gathering the necessary data for the model to be able to learn is not always possible, specially in experimental studies. To overcome this, physics-based deep learning models can be used and have been gaining a lot of attention lately. In these approaches, some previous knowledge of the physics of the system is included when designing the architecture of the neural net and as a result,the number of necessary data for the model to learn is significantly reduced (RAISSI; PERDIKARIS; KARNIADAKIS, 2019; MAHMOUDABADBOZCHELOU et al., 2021; MURALIDHAR et al., 2019).

2.9.1
Predictive Modeling

Machine learning consists of data-driven approaches to support the decision-making process in a recurrent problem. Basically, a model can learn and understand how to solve complex problems from data reflecting past experiences [42]. Essentially, an input matrix containing the features and their associated values is fed in a pre-determined machine learning algorithm and the model will make predictions from it. To compute how accurate the predictions are a performance metric is used, in which the differences between true values and predictions are computed. At first the predictive power will be poor and the outputs will be the result of a random guess, but as the model keeps receiving new data it starts learning from it and eventually it will improve the output prediction.

Depending on the problem to be solved and the type of data different ML approaches can be used. Supervised learning, which corresponds to the class of algorithms with the goal of making predictions, can be classified into two tasks according to desired predicted output. In classification tasks, the algorithm predicts a categorical variable from the independent variables while in regression tasks the response is a continuous value. Several ML models can be applied to a specific problem and the choice of the most appropriate one depends, essentially, on the type of data and type of problem.

Decision learning tree is one of the Machine Learning algorithms that enables developing predictive models via data observation. Herein, we train a Random Forest (RF), which is a learning method that is mostly used for classification and regression constituted of ensembles of decision trees. RF are used to predict solvent and wall penetration value from a collection of input parameters. A detailed description of the method is given in following.

2.9.2
Random Forests

Random forests RF, introduced in 1995 (HO, 1995) and extended in 2001 by (BREIMAN, 2001) is a very popular machine learning model able to solve regression and classification problems. As an ensemble method, RF combine decisions trees that work as weak learners and return predictions based on the average results returned by the individual trees. The fundamental concept is that these uncorrelated trees when combined will most frequently outperform the individual components and will yield more accurate predictions.

RF are essentially a modification of the bagging technique (BREIMAN, 1996), which is particularly useful in reducing the model variance and therefore, it is very effective in preventing overfitting. The overall idea behind bagging is that by combining multiple and uncorrelated predictors a more stable and assertive prediction can be obtained. Bagging is often used in decision trees, that are considered high variance algorithms.Figure 2.10 presents a schematic representation of a Random Forest

Decision trees are the constituents of RF. The fundamental idea behind them is that if a model can learn certain rules from the training data it will be able to make predictions on new and unseen data. In short, they are built

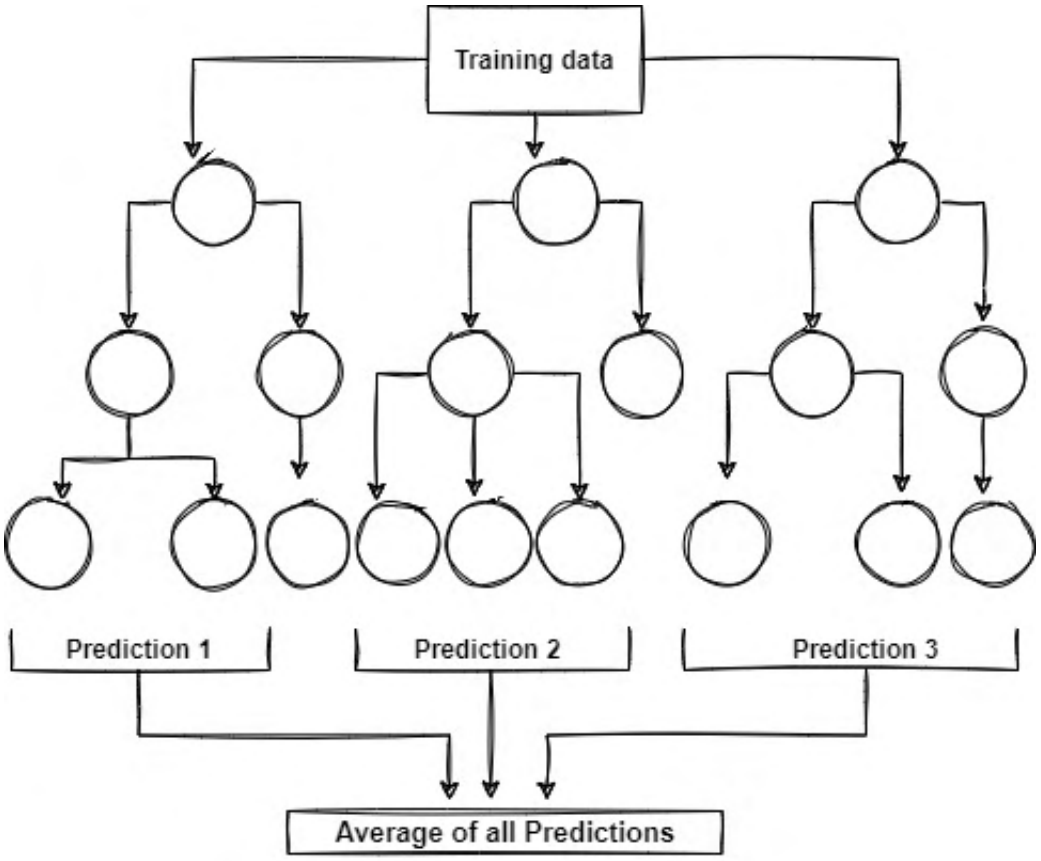

Figure 2.10: Scheme of a Random Forest

from the root node, corresponding to the attribute that best separates the observations. From the root nodes the tree is split in smaller subsets (nodes) until it reaches a decision node. An important step in building a decision tree is selecting the attribute to be used in the root node as well as in the branches. A random selection would yield bad accuracy results, thus, a common criterion for splitting the trees is the Gini index and Entropy.

The most used performance metrics to evaluate how accurate the model predictions are, which, in regression, means how close the predictions made by the model are compared to the simulated results are mean squared error MSE, root mean squared error RMSE and R^2.

3
Proposal

3.1
Dissipative Particle Dynamics

Dissipative Particle Dynamics (HOOGERBRUGGE; KOELMAN, 1992) is a particle-based simulation approach popularly employed to model complex fluids. One of the main advantages of DPD is the flexibility and versatility in modeling a large variety of structures. DPD particles in its essence are not actual real particles, but points in the space having an interaction range defined as r_c, representing the maximum distance in which particle interactions are active and it is commonly set to r_c =1. DPD was first introduced by Hoogerbrugge and Koelman (HOOGERBRUGGE; KOELMAN, 1992) and has posteriorly received major contributions from works of Groot and Warren (GROOT; WARREN, 1997). As a particle-based method, in DPD the entire simulation domain is filled by homogeneous particles, representing the solvent, that are momentum carriers. In DPD the local linear and angular momentum is preserved and navie-stokes hydrodynamics is reproduced. Those particles interact by short-range soft potentials according to the Newton equation of motion:

$$F_i = \sum_{i \neq j} F_{ij}^C + F_{ij}^D + F_{ij}^R \tag{3-1}$$

The interactions are pairwise and the range in which these forces are active is determined by the cut-off distance r_c, commonly set as 1. The interaction is maximum when the particles are completely overlapped and vanishes when then distance between the centers is beyond one. Figure 3.1 introduces a schematic representation of DPD interactions.

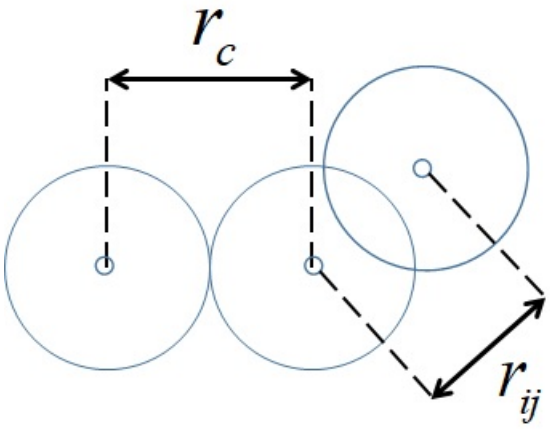

Figure 3.1: Schematic representation of DPD particles. Interaction is active as long as the center-to-center distance is smaller than $1r_c$

.

In DPD the forces are symmetric and composed of three components. The first one is a conservative force F_{ij}^{C}, which is a soft repulsion potential that accounts for the interactions of the particles and governs the thermodynamics of the system. The values adopted for a_{ij} are mapped to the fluid compressibility and it is set as 25 for water(GROOT; WARREN, 1997). The conservative force expression is given by:

$$\mathbf{F_{ij}^{C}} = a_{ij} w_{ij}^{C}(r_{ij}) \mathbf{e_{ij}} \tag{3-2}$$

Where a_{ij} gives the repulsion potential coefficient between the particles i and j, r_{ij} =$|\mathbf{r_i}|$ and $|\mathbf{r_{ij}}| = |\mathbf{r_i}| - |\mathbf{r_j}|$, is the distance between the particles, the unit vector $\mathbf{e_{ij}}$ is represented by $\mathbf{e_{ij}}$=$\mathbf{r_{ij}}/r_{ij}$ and $w_{ij}^{C}$is the weight function.

Groot and Warren (GROOT; WARREN, 1997), in their pioneer work in DPD, employed an equation of state to map the repulsion parameters to the compressibility of different systems. In order to keep the water compressibility, the repulsion parameter between DPD particles have to be set at a=$25k_BT$ when system density ρ_s is constant at 3.

The second contribution comes from the random force which is associated to the thermal energy added to the system and represents the Brownian motion. The energy added by the random force F_{ij}^{R} is removed by the Dissipative force F_{ij}^{D}, which acts as a heat sink, dissipating the energy. Combined, the random and dissipative force act as a thermostat, keeping the temperature of the system constant.

$$\mathbf{F_{ij}^{R}} = \sigma_{ij} \omega_{ij}^{R}(r_{ij}) \theta_{ij} \mathbf{e_{ij}} \tag{3-3}$$

$$\mathbf{F_{ij}^{D}} = -\gamma_{ij} \omega_{ij}^{D}(r_{ij}) (\mathbf{e_{ij}} \cdot \mathbf{v_{ij}}) \mathbf{e_{ij}} \tag{3-4}$$

γ_{ij} and σ_{ij} are respectively, the dissipative and random coefficients, $\mathbf{v_{ij}}$ is the relative velocity of the pair of particles i and j $\mathbf{v_{ij}} = \mathbf{v_i} - \mathbf{v_j}$ and θ_{ij} represent the white noise with Gaussian distribution .

The weight functions frequently take the form: $w_{ij}^{C} = 1/r_C$, $w_D = w_R^2 = (1 - r/r_C)^2$ and 0 for any $r_{ij} > r_c$.

Random and dissipative forces are related one another by the fluctuation-dissipation theorem, which assures that the momentum is conserved and hydrodynamic is preserved. To achieve that, the relation between the random and dissipative coefficients as well as the weight functions must obey the following expressions(ESPANOL; WARREN, 1995):

$$\omega^{D}(r_{ij}) = \left[\omega^{R}(r_{ij})\right]^2 \tag{3-5}$$

$$\sigma_{ij}^2 = 2\gamma_{ij} k_B T \tag{3-6}$$

In DPD the force and velocities calculations are updated at discrete time steps. To integrate and solve DPD equations of motion and advance the particles position and velocity a modified velocity Verlet algorithm (GROOT; WARREN, 1997) is used. In the traditional Velocity Verlet algorithm the forces depend on particles' position and not on their velocity, as it is the case for DPD. For this reason, a modified velocity Verlet algorithm has to be employed. Modified velocity Verlet has two steps: in part I the particles velocities and position are updated and the new forces are calculated and in part II, the velocities are corrected using the updated forces.

DPD can be mapped into real physical units as proposed by (GROOT; RABONE, 2001). Using a system composed of a phospolipide(phosphatidylethanolamine (PE)), a surfactant and water they represented the phospolipde molecule in terms of DPD beads, each bead having 3 carbons. By calculating the volume of each bead they were able to determine the size of the interaction radius, r_c as 6.4633 Å . Based on that, other properties units were derived. (GHOUFI; MALFREYT, 2012), for example, introduce a table correlating DPD main parameters to real physical units as represented in Figure (3.2)

DPD	DPD → real units		physical units
parameter	value		value
bead	1	N_m	3 H_2O
r_c	1	$(\rho N_m V)^{1/3}$	8.52 Å
ρ	6.88	$\rho N_m M/N_a r_c^3$	997 kg m^3
γ	12.4	$\gamma kBT/r_c^2$	70.6 mN m^{-1}
p	0.1	pk_BT/r_c^3	0.67 MPa
a	50	ak_BT/r_c	2.41×10^{-10} J m^{-1}
α	0.101	α/r_c^4	5.32×10^{-38} m^4

Figure 3.2: r_c, ρ, γ, p and a are, respectively, the cutoff radius, density, surface tension, pressure and energy. M is the water molecular weight and V the volume. k_B is the Boltzmann's constant, N_A the number of Avogadro and N_m represents the number of water molecules in a bead.(GHOUFI; MALFREYT, 2012)

3.2
Core-Modified Dissipative Particle Dynamics

Initially introduced by White and Travis (WHITTLE; TRAVIS, 2010), CM-DPD has been used to model suspensions at different flow conditions and concentrations (JAMALI; YAMANOI; MAIA, 2013; JAMALI et al., 2015a; BOROMAND et al., 2018).

In this model, the fluid phase is represented as DPD particles that interact pairwise center-to-center through soft potentials, as traditional DPD. The colloidal particles, on the other hand, are represented by a spherical, repulsive and hard core particles having attached a soft shell. As opposite to DPD interactions, in CM-DPD the interactions are called semi-hard, given that they are not as hard as the one used in MD (JAMALI; YAMANOI; MAIA, 2013) neither as soft as DPD interactions. Furthermore, the interaction between two particles occurs surface-to-surface in contrast to the center-to-center interaction used in conventional DPD.

The interaction between DPD particles is maximum when they are completely overlapped and goes to zero at center-to-center distances beyond r_c. In the case of the interaction solvent/ colloidal particles, the force is active for any distance between the surface of the colloidal particle and the center of DPD particle, corresponding to r_c. That case can be visualized in Figure 3.3.

For a pair of colloidal particles, the DPD forces are no longer applied. Instead, a repulsive contact force F_{core} and a short-range hydrodynamic force

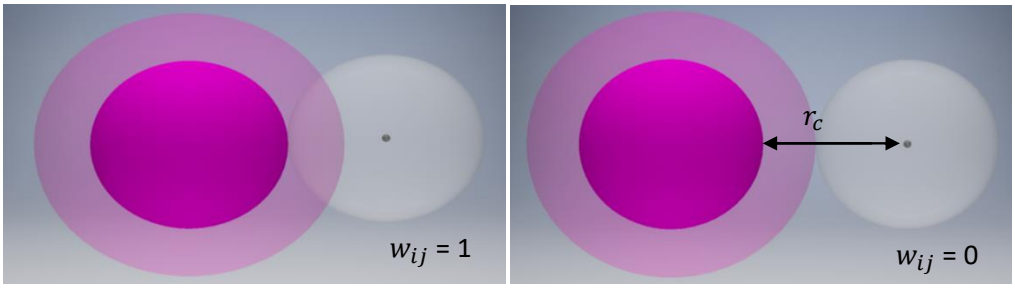

Figure 3.3: Interactions between solvent DPD Particles and colloidal particles. White spheres represent DPD particles and colloidal particles can be visualized in pink. In the left figure the repulsion is maximum and it decreases as the distance increases. The forces go to zero at any distance above r_c, represented in the right figure.

F_{Hydro}, representing a lubrication force, are used. The interaction between two colloidal forces is pairwise and surface-to-surface. Therefore, naturally, the center-to-center separation distance r_{ij} is replaced by a surface-to-surface distance h_{ij}. Since the interaction is semi-hard as previously stated, the model does not allow the overlap of the cores. The repulsion between them is maximum when the cores are in nearly contact and it vanishes for any distances above the equivalent to r_c. Figure 3.4 illustrates the maximum and minimum interaction between two colloidal particles.

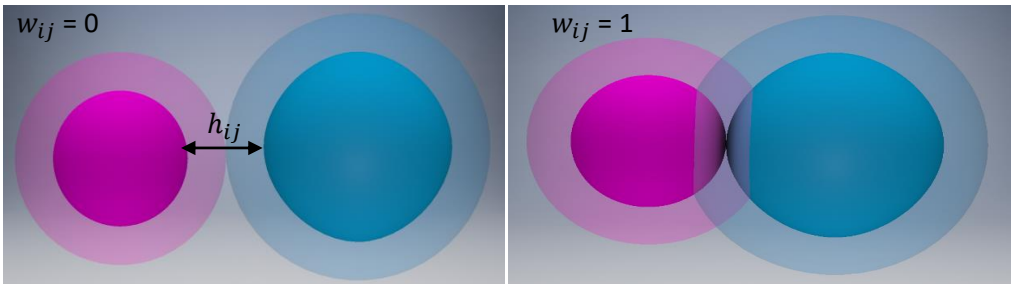

Figure 3.4: Interactions between colloidal Particles. The blue particle corresponds to a colloidal particle having $1.4r_c$ as radius and the pink particle has $1r_c$. On the right figure the repulsion is maximum and in the left image the interactions vanishes, for any $h_{ij} > r_c$. The cores thickness for the two types of particles is fixed at $0.5r_c$.

For a more comprehensive visualization, Figure 3.6 displays the simulation box with all the types of particles present. Any time a DPD/Solvent particle interacts with either wall, other DPD and colloidal particles the forces taking places are DPD forces. These forces are only replaced when the interaction is between two colloidal particles.

The core-force in the model is responsible for the rigid and repulsive nature of the colloidal particles and it is included to prevent particle overlapping, recurrent especially at high shear rates. This force is associated with surface roughness in real particles, Δ which would range around 10^{-3} of the colloidal

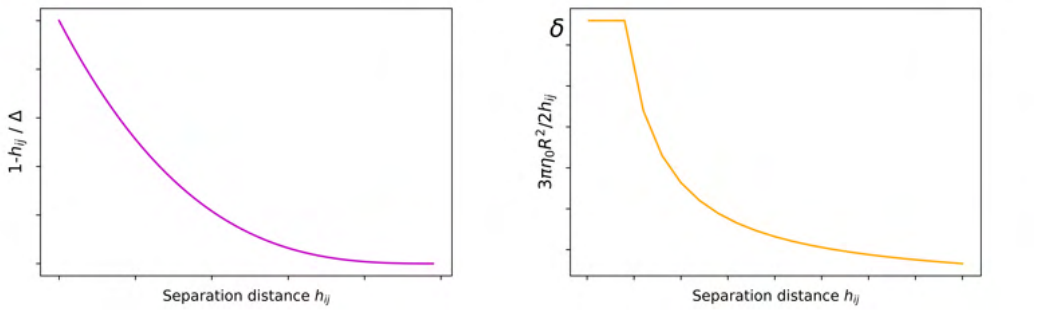

(a) Core force represented as a cubically decaying function between the separation distances.

(b) Hydrodynamic potential

Figure 3.5: Potential graphs of the colloidal forces used in the model. The y axis in the hydrodynamic potential represents the pair-drag term (SILBERT; MELROSE; BALL, 1997), $\triangle$ is the smallest separation distance between the cores and h_{ij} is the surface-to-surface distance.

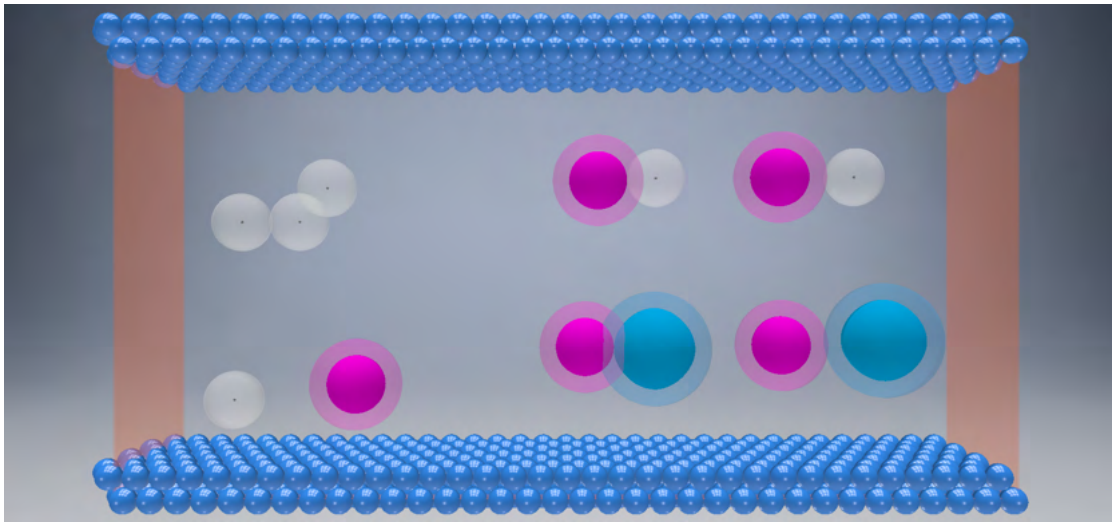

Figure 3.6: Simulation box.The top right white beads represent the interaction between two DPD particles. Top left shows the interaction colloid-solvent, bottom left represents colloid-colloid interactions and bottom left interactions with the wall.

radius. The force is maximum at surface-surface contact and it vanishes cubically at very low separation distances, as seen in the following expression:

$$F_{ij}^{Core} = \begin{cases} f^{Core}(1+h_{ij}), & h_{ij} \leq 0 \\ f^{Core}\left(1+\frac{h_{ij}}{\Delta}\right)^3, & < h_{ij} \leq \Delta \\ 0, & h_{ij} > \Delta \end{cases} \quad (3\text{-}7)$$

In addition to the Core Force, the model also accounts for a lubrication potential. When particles are at close proximity the solvent particles are expelled and that may originate a break down in the hydrodynamics. To avoid that, a lubrication potential is included to represent the short-range hydrodynamic interactions. The force is based on a pair drag term as proposed by (BALL; MELROSE, 1995). Because of the fact that at the surface-surface

contact the force is singular, a small gap δ is included in the equations to truncate the force. For any distances below δ the force is constant and maximum and it decreases as particles move away from another. Equation 3-8 describes the expression for the force and Figure 3.5 illustrates the core and hydrodynamic potentials decaying graphs for both hydrodynamic and core forces.

$$F_{ij}^{H} = -f_{ij}^{H}(\mathbf{v_{ij}} \cdot \mathbf{e_{ij}})\mathbf{e_{ij}} \tag{3-8}$$

$$f_{ij}^{H} \equiv \begin{cases} \frac{3\pi\eta_0 R^2}{2\delta} & h_{ij} < \delta \\ \frac{3\pi\eta_0 R^2}{2h_{ij}} & h_{ij} \geq \delta \end{cases} \tag{3-9}$$

3.3
Simulation Conditions

3.3.1
Modeling a Simple Confined Geometry : A Solvent Study

Our system is entirely represented by DPD particles. The solvent, as single DPD particles interacting pairwise center-to-center according to Newtons' equation of motion and the walls are built as frozen DPD particles at the edges of the simulation box. Our computational domain is $20.36r_c$ x $20.36r_c$ x $20.36r_c$ where $r_c = 1$. The density of the system is 3 and the number of solvent particles was determined as $d = mN_p/V_{box}$. m is the mass of the solvent particles, that for simplicity is assumed to be one, N_p is the total number of solvent particles and V_{box} is the volume of the simulation domain. Using that expression, in order to keep the density of the system at 3, 25325 solvent particles were used. The interactions between the particles are set in a way that it ensures the compressibility of the water and for that, it takes the value of 25 (GROOT; WARREN, 1997). K_bT=1 and the dissipative γ and random σ coefficients adopted are, respectively, 50 and 10 (BOROMAND; JAMALI; MAIA, 2015). The solvent-wall interactions(a_{ij}) in the conservative force range from 10 to 100 and four wall densities were tested $\rho_w = 3$, $\rho_w = 6$, $\rho_w = 9$, $\rho_w = 12$. In order to model an infinite microchannel in the x and z directions, periodic boundary conditions were employed. In addition, no bounce-back boundary condition in the y direction was used. The walls were placed at the boundaries of the simulation domain and were excluded of the force and velocity calculations along the y axis.

The walls are formed by a double layer of frozen DPD particles equally spaced positioned in the z and x directions inside the simulation domain. They cannot move, but they have the freedom to interact with the free solvent particles. In order to avoid an extra repulsion of the solvent particles from the boundaries, the wall particles were shifted one another in a distance in z and x adjusted according to the desirable wall density, similar to the method proposed by (PIVKIN; KARNIADAKIS, 2005). The distance between the wall particles in y is held fixed at $0.5r_c$, and to calculate wall penetration the box was divided in 40 layers, each layer having 0.5 r_c of thickness.

In addition to the distance, the number of wall particles was also adjusted to vary wall density, given by $\rho_w = mN_w/V_w$, where m is the mass, N_w is the

number of wall particles and V_w the wall volume. Initially, the solvent particles were randomly generated in the box and were let equilibrate for 100,000 time steps before the flow begins. A schematic representation of the wall structure and its main parameters are presented, respectively, in Figure 3.7a and 3.7b.

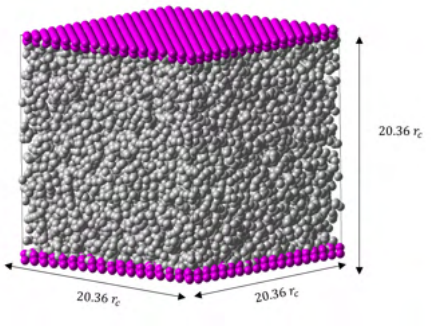

(a) Simulation box

σ	10
γ	50
ρ_f	3
ρ_w	3-12
$a_{fluid\text{-}fluid}$	25
$a_{wall\text{-}fluid}$	10-100
fluid particles	25,325
time step	0.01

(b) Main simulation parameters

Figure 3.7: Schematic of the simulation system and main parameters employed. Fluid DPD particles are represented in grey and wall particles in purple.

A code written in C++ is used to model the system. The simulations were sent to a cluster and took about 30 hours to reach 300,000 time steps. The time step used is $0.01\sqrt{\frac{mr_c^2}{k_BT}}$.

3.3.2
Predicting Particle Penetration in Suspensions: A machine Learning Study

The simulation box was built by placing the walls at the edges of the computational domain. The number of solvent DPD particles, colloids, and wall DPD particles were calculated to ensure a constant density in the entire system of $\rho_s = 3$. The box size used was regulated according to the desired confinement ratio. Once the y-direction was fixed, the other two dimensions were set in a way that the in all the cases the box volume remained practically unchanged. Periodic boundary conditions were applied in the x and z directions and no wall boundary condition was employed.

The wall design was inspired by the previous works (PIVKIN; KARNIADAKIS, 2005; PIVKIN; KARNIADAKIS, 2006), in which a double layer of symmetrically spaced DPD particles were frozen to represent it. These particles are not allowed to move neither interact among themselves, and therefore are excluded from the calculations. However, they are free to interact with the remaining particles in the system.

Colloidal particles were built as Core-Modified particles having a size ratio difference of 1.4 and masses calculated as $d_s\frac{4}{3}\pi R^3$, where d_s is the system density. A bimodal suspension was used and to achieve the desired global concentration the number of particles was calculated in a way that:

$$VF_{global} = VF_{type1} + VF_{type2} \tag{3-10}$$

given

$\text{VF}_{type1} = VF_{type2}$(3-11)$VF_{type1}$ and VF_{type2} are, respectively, the volume frac-

a_{ij}	**Body Force**	**Rigidity**	**y/D**	**VF**
25	0.1	100	5	0.08
50	1	1000	7.5	0.28
75	10	25,000	10	0.48
100			20	0.58

Table 3.1: Parameters with the respective levels adopted in the simulations. a_{ij} refers to the interactions between wall/DPD and wall/colloids. y/D represents the confinement ratio, y is the box width and D is DPD particle diameter. Rigidity is set by the strength of the core force f_{core} in colloid-colloid interactions.

tion of colloidal particle type 1 and type 2. The solvent assumes the water compressibility, and hence the a_{ij} between solvent DPD particles remained fixed at a_{ij}=25. For DPD-colloid interactions, the a_{ij} used was 100 (BOROMAND; JAMALI; MAIA, 2015). The dissipative γ and random σ coefficients adopted are 50 and 10 (BOROMAND; JAMALI; MAIA, 2015). It is important to emphasize that the a_{ij} that was varied, as shown in Table3.4, is the one between wall/solvent and wall/colloids. In this work, these two wall interactions varied by the same proportion. The time step used was $5x10^{-5}$(JAMALI; YAMANOI; MAIA, 2013) and the simulations ran for 500,000 time steps, prior to an equilibrium step of 100,000 time steps. Five input variables were used with varying levels, as showed in Table 3.1. Combining all of them resulted in the total of 558 simulations.

Wall penetration is calculated as:

$$Penetration = \frac{d_n}{d_{100\%}} \tag{3-12}$$

where

$$d_{n_{dpd}} = \frac{N_{dpd}}{V_{layer}} \tag{3-13}$$

$$d_{n_{col}} = \frac{N_{col}M_{col_1} + N_{col}M_{col_2}}{V_{layer}} \tag{3-14}$$

V_{layer} is the volume of the layer expressed as $V_{layer} = V_{box}/n_{layers}$ and n_{layer} is the number of layer in which the box is divided, being the first and last layer of the channel corresponding to the wall. $d_{100\%}$ corresponds to the layer density considering 100% of penetration. N_{dpd} is the number of DPD particles; for simplification, since the DPD mass is one, the mass term is not included in the equation. N_{col} is the number of colloids an M_{col} is the colloid mass. In order to compute penetration, the densities were calculated in the wall layers and penetration was calculated according to Eq. (3-12).

For predictive modeling, the data was randomly split in 80% for training and 20% for testing. The data was normalized to avoid scaling problems using MinMaxScaler class in sklearn library and log transformations were also applied to the output columns. The model performance was measured by calculating MAE, MSE and RMSE and R^2.

3.3.3
Effect of Particle Rigididy, Flow rate and Confinement in Concentrated Suspensions

The fluid phase as well as the walls are modelled as DPD particles, the later being created by freezing DPD particles at the edge of the simulation box. A double layer of particles is used not only to keep the force field more uniform, but also to prevent the excess of repulsion from the walls. Wall particles were uniformly spaced and distributed (PIVKIN; KARNIADAKIS, 2005) and their number and position were set according to the desirable wall density, in our case $\rho_w = 3$. Wall particles once frozen can not move, however we let them interact with the free particles in the system by means of the conservative force. The repulsion interaction between wall and solvent particles as well as wall and colloids was carefully chosen in a previous study in order to guarantee, simultaneously, impenetrability and the formation of low depletion zones(BARCELOS et al., 2021).

A bimodal suspension was used in all the simulations with particle radius of $1r_c$ and $1.4r_c$. The number of colloidal particles was selected to ensure the system density of around 3 and the box volume of approximately 24000, depending on the confinement ratio. The mass of the particles was calculated as $m = dV \rightarrow \frac{4\pi R^3}{3}$,volume fraction $\mathrm{VF} = \mathrm{V}_{colloid}/V_{box} \rightarrow \frac{N_{p1}4\pi R_1^3}{3V_{box}} + \frac{N_{p2}4\pi R_2^3}{3V_{box}}$. N_{p1} and N_{p2} and R_{p1} and R_{p2} being the number and radii of colloidal particles 1 and 2, respectively. The number of solvent, colloidal particles 1 and 2 was set according to the desirable volume fraction.

The confinement gaps were set as gap = y/d, in which d is the diameter of the particle and y is the box height (y dimension of the simulation domain). To reach different ratios, the box dimensions proportions were varied (keeping the approximate same total box volume). Varying the walls volume, one would expect a difference in the number of wall particles, which were adjusted to ensure $\rho_s = 3$ and a minimum box volume variation. The values of those simulation parameters are summarized in Table 3.2.

Table 3.2: Simulation Box dimensions for each confinement ratio

y/D	Simulation box dimensions
5	28x10x28
7.5	27x15x23
10	20x20x20
12.5	18x25x18
15	16.5x30x16.5
17.5	15x35x15
20	14x40x14

A uniform body force, corresponding to a pressure drop, is applied to the particles along the y-direction to generate a parabolic flow and periodic boundary conditions were used in z and x directions. In this work, no bounce-back boundary condition was not used at the wall, and to avoid wall penetration the wall-solvent and wall-colloidal particle were carefully chosen, according to one of our previous work. The interaction DPD-DPD is set at 25 and DPD-colloid at 100 (JAMALI; YAMANOI; MAIA, 2013; BOROMAND et al., 2018).

All the particles were randomly generated in the box and the system was let equilibrate for 100,000 time steps. Since we are not capturing contact and frictional effect, there is no need for a very low time step, hence we used it at $5x10^{-6}$. The simulations ran for 4 million timesteps, long enough to ensure that the microstructures was no longer changing. DPD parameters can be mapped in to real physical units as proposed in (GHOUFI; MALFREYT, 2012). Based on that work, (JAMALI et al., 2015b) correlated the contact modules of real particles to DPD units. An $f_{core}of100$ would correspond a contact modulus of a 100MPa, representing soft particles, and 25,000, equivalent to a contact modulus of 100GPa representing the most rigid particles. Table 3.3 illustrates the main parameters values used in the simulations.

Table 3.3: Parameters used in the simulations

Body Force	VF	Rigidity	Confinement
0.1	0.48	100	5
1	0.58	5,000	7.5
-	-	25,000	10
-	-	-	12.5
-	-	-	15
-	-	-	17.5
-	-	-	20

3.3.4 Predicting Viscosity and N1 in Suspensions using Machine Learning

In this section, a supervised learning approach was used to predict viscosity and first normal stress difference N1 in a bimodal suspension. As input, the proposed model takes the particle volume fraction, Peclet number and particle rigidity and as output it returns the viscosity and N1. The simulation system was built using Core-Modified DPD as previously introduced.

In this particular study, as opposite to the other studies in the thesis, walls are not included in the simulation domain. That means that the fluid properties are evaluated in bulk conditions. Lee-Edwards boundary conditions (LEES; EDWARDS, 1972) is applied in the simulation box as opposite to traditional periodic boundary conditions. Basically, in Lee-Edwards, particles that leave a boundary are introduced back in a displaced location of the box with its velocity modified as a linear function of the difference in velocity between the two plates (CHATTERJEE, 2007).

The viscosity in the system is calculated using the local stress tensor according to the Irving-Kirkhood (IRVING; KIRKWOOD, 1950) expression:

$$P = \frac{1}{V}\sum_{i=1}^{N} m_i(v_i - u(r_i)) \otimes (v_i - u(r_i)) + \sum_{j>1}^{N}\sum_{j=1}^{N-1} r_{ij} \otimes F_{ij}^{T} \qquad (3\text{-}15)$$

The above equation account for two main terms. The first one corresponds to the kinetics part of the stress tensor and the second one is relative to the contribution due to the particle interactions. The stress tensor is given by $S = -P$ and the shear viscosity can be calculated as the xy component:

$$\eta = \langle S_{xy}/\dot{\gamma} \rangle \tag{3-16}$$

The first normal stress difference is calculated as:

$$N_{11} = S_{11} - S_{22} \tag{3-17}$$

The dimensions of the simulation box are $25r_c$ x $25r_c$ x $25r_c$. The fluid phase is composed of traditional DPD particles while the colloidal particles are built as Core-Modified particles. A bimodal suspension with size ratio difference 1.4 is used and volume fraction, rigidity and flow rate are varied. To induce the flow, a shear rate is applied on the top and bottom edges of the simulation box and the flow strength is given by varying the magnitude of the shear rate. Particle volume fraction is calculated as VF = $V_{colloid}/V_{box}$ $\rightarrow \frac{N_{p1}4\pi R_1^3}{3V_{box}} + \frac{N_{p2}4\pi R_2^3}{3V_{box}}$. Index 1 and 2 refers, respectivley, to particle type 1 and 2.

Rigidity	**Volume Fraction**	**Peclet**
100	0.08	0.1
500	0.18	0.5
1000	0.28	1
5000	0.38	5
10000	0.48	10
25000	0.58	50
		100
		500
		1000

Table 3.4: Parameters used and values adopted for each variable

The interaction between the particles is 25 for fluid-fluid (DPD-DPD) and 100 for DPD-colloids(JAMALI; YAMANOI; MAIA, 2013). The time step used in the simulations was $5x10^{-6}$ and the simulations ran for 1 million time step, time long enough to ensure the system was in steady state.

The input data of the model, comprising the variables and the levels tested is described in Table 3.4. Combining all these parameters and levels resulted in a total of 324 simulations.

4
Results

4.1
Modeling a Simple Confined Geometry : A Solvent Study

4.1.1
Setting simulation parameters

When a pressure drop is imposed to an incompressible liquid in the laminar regime, a parabolic profile, i.e, simple Poiseuille flow is developed. In our simulations, a body force f_B, corresponding to a pressure drop, is imposed to all solvent particles to generate the parabolic profile. Figure 4.1 introduces the velocity profile developed when a body force of f_B= 0.01 is applied. In red it is presented the Poiseuille flow solution that fits pretty satisfactory our computational data. The simulation ran for 300,000 time steps, long enough to ensure a fully developed velocity profile.

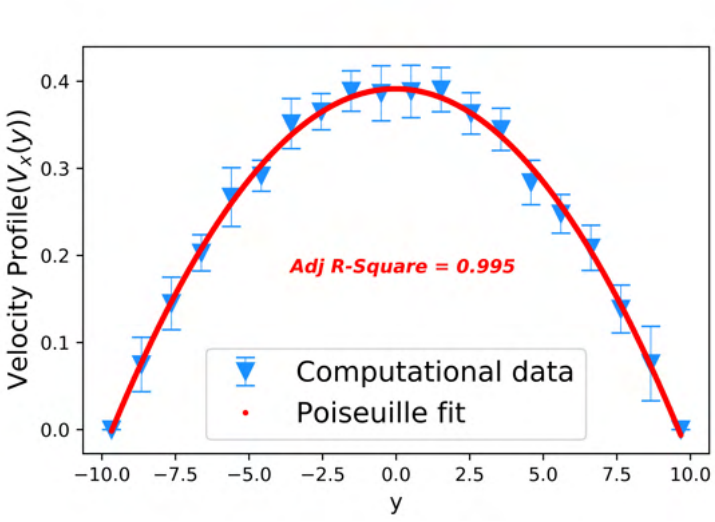

Figure 4.1: Fit of Poiseuille solution to the computational data. Interaction wall-solvent is a_{ij}=100 to ensure no-slip condition and wall impenetrability.

Next, it is important to define the body force f_B to be used in the simulations. The fluctuation-dissipation theorem behind the DPD thermostat ensures that the temperature of the system remain unaltered. The dissipative force depends on the relative velocity of the particles, as a consequence, at higher forces the random force might not be able to compensate the energy dissipated by the dissipative force. As a result, the temperature of the system might increase in a way that the fluctuation-dissipation theorem is no longer valid, which is undesirable. Figure 4.2 introduces the velocity profile for different body forces.

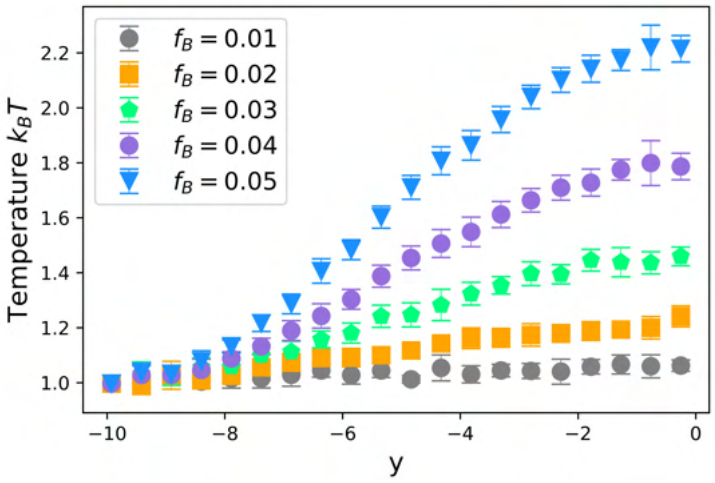

Figure 4.2: Temperature variations for different body forces.

According to Figure 4.2, for body forces f_B above 0.01 the temperature is no longer constant at the value of 1. For this reason, for all the remaining simulations a body force constant and equal to $f_B = 0.01$ will be used.

Another important parameter in the simulations is the time required to reach the steady state. It is important to stop the simulations as soon as the steady state is reached to have a lower computational cost, but care has to be taken to guarantee that a good signal-to-noise is obtained. In Figure 4.3a the velocity profile curves are plotted for time steps ranging from 10,000 up to 300,000. Figure 4.3b shows a clearer visualization on how the maximum velocity varies according to the time step.

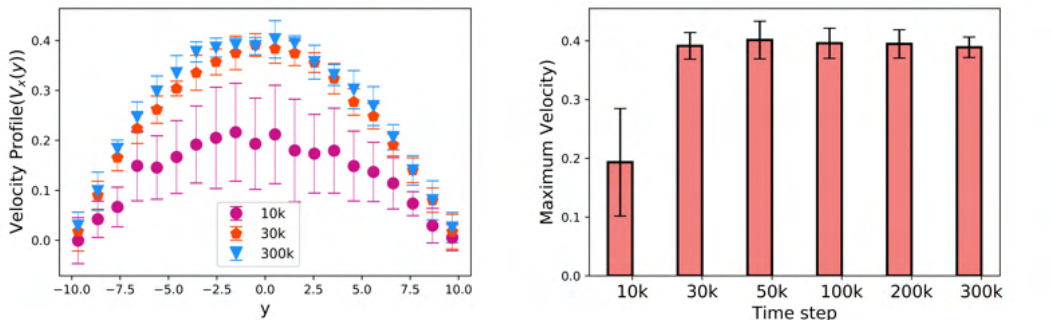

(a) Velocity Profiles (b) Maximum Velocities(middle of the channel

Figure 4.3: Time step required to reach the steady state.

The velocity profile stabilizes around 30,000 time steps. However, some fluctuations are seen and have to be minimized. For this reason, the remaining simulations will be run for 300,000 time steps, when low dispersion of values is seen, as observed in Figure 4.3

Here the phenomena taking place at the wall vicinity is explored. Densities and velocities are studied over a wide range of repulsion interactions a_{ij} and wall densities ρ_w. The fraction of particles inside the wall(wall penetration)

and in the first adjacent layer(depletion) is quantified and their evolution in number as repulsion and wall density increase is tracked. Several simulations varying the two independent variables, wall density and wall-solvent interactions, were performed. Initially it is investigated which of these two parameters is stronger in preventing particles to get close to the wall. The velocity profile results are depicted in Figure 4.4.

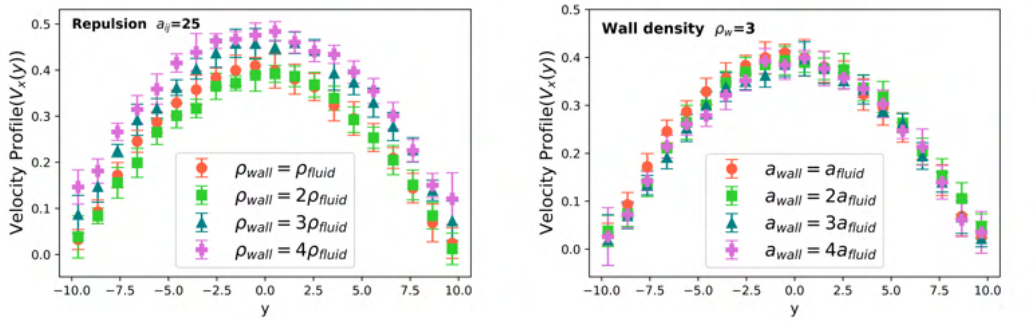

(a) Velocity profiles for a_{ij} fixed at 25 (b) Velocity profile for ρ_w fixed at 3

Figure 4.4: Velocity profiles of the solvent particles. a) Repulsion a_{ij}= 25 and wall density varying 2, 3 and 4 times the solvent density. b) Velocity profiles for the case of wall density constant at ρ_w=3 and repulsion coefficient a_{ij} varying in the same proportion as a).

When the repulsion interaction increases, no significant changes in the velocity profiles can be seen, as illustrated in Figure 4.4b. On the other hand, wall densities 3 and 4 times the fluid density promotes a stronger repulsion of the particles from the wall area. When wall density is 3 or 4 times bigger, large slip at the walls is observed(4.4a).

Density distribution enables the detection of the number of solvent particles present in each layer and therefore, quantify the fraction of particles inside the walls and in the depletion layer. In order to compute the density profile, the simulation domain was divided in 40 layers and the average number of particles detected in each layer per time step was calculated. The densities were averaged over the last 20,000 time steps and particle penetration and depletion were computed according to the expressions:

$$\Phi_w = 100\frac{d_{wall}}{d_{center}} \tag{4-1}$$

$$\Phi_d = 100\frac{d_{deplet}}{d_{center}} \tag{4-2}$$

d_{wall} represents the density of the particles in the first layer (corresponding to the wall) and d_{deplet} is the density at the depletion layer(adjacent layer). d_{center} is the density of the solvent in the middle of the channel. Figure 4.5a introduces the density profiles for the case where the wall density varies and the repulsion interaction is constant at 25, while in Figure 4.5b densities are given for different repulsion values when wall density is equal to 3.

For both cases depicted in Figure 4.17, the density takes the value of around 3 in the middle of the channel and does not fluctuate significantly during all the simulation time. It can be noted that increasing repulsion leads

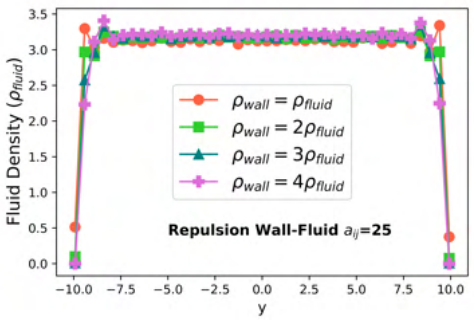

(a) Density Profile for a_{ij} fixed at 25

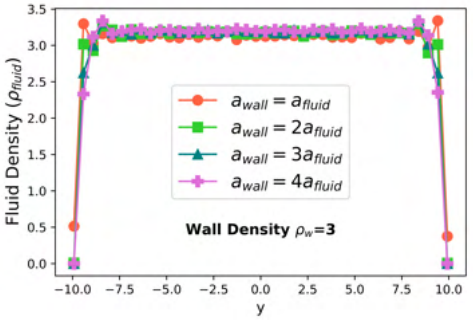

(b) Density Profile for ρ_w fixed at 3

Figure 4.5: Density profiles as a function of the layers of simulation box. a) Repulsion a_{ij} is kept at 25 and wall densities varying 2, 3 and 4 times the solvent density. b) Density profiles when wall density $\rho_w = 3$ and repulsion varies the same proportion as the a) case.

to a decrease in the number of particles inside the wall and in the depletion layer.

At large repulsion solvent particles are excluded from the wall area and migrate towards the center, justifying the increase in density in the middle and a decrease in the wall region. In fact, the density curves are very alike for both scenarios (Figure **??**), suggesting that increasing wall density or repulsive interactions have a similar influence on the final response.

An artifact frequently observed in wall models is the presence of density fluctuations at the wall close vicinity, which has been observed both experimentally(PERRET et al., 2010) and computationally (GUBBIOTTI; CHINAPPI; CASCIOLA, 2019; KASITEROPOULOU; KARAKASIDIS; LIAKOPOULOS, 2011). For the purpose of investigating the presence of density oscillations in our system, the simulation box was divided into bins of 0.2 r_c, except for the wall layers, which were fixed at $0.5r_c$. Figure 4.6 shows the local density evolution plotted as a function of wall distance for all the cases evaluated previously.

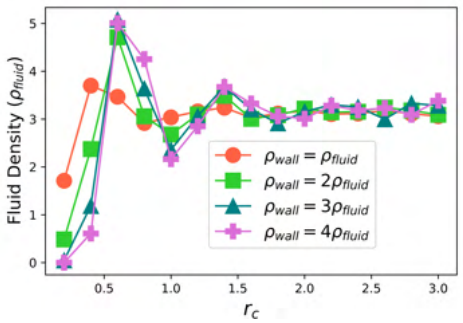

(a) Fluid density for a_{ij}= 25

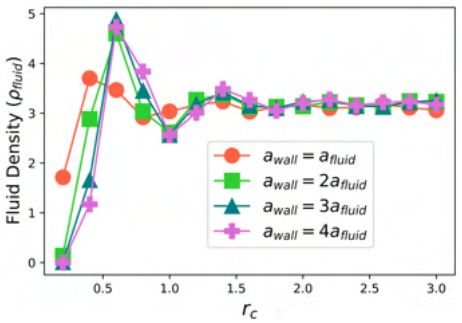

(b) Fluid density for ρ_w= 3

Figure 4.6: Fluid density plotted as function of the distance from the wall, given in r_c units

When particles are at the wall vicinity, the forces are cut by the wall

presence, giving rise to a force imbalance and as a result, the particles are pushed towards the wall. The latter, in response, push them back in the opposite direction due to its artificially imposed repulsive character. That combination of low and high density areas leads to layering and strong density oscillations effects (MEHBOUDI; SAIDI, 2014).

Our results are in partial agreement with previous works (KASITEROPOULOU; KARAKASIDIS; LIAKOPOULOS, 2011; PIVKIN; KARNIADAKIS, 2005) in which stronger density oscillations were observed for larger wall repulsion. In our case, however, for ratios wall/fluid from 2, the oscillations tend to stop increasing, which could be due to a different selection of parameters used in our system.

In order to investigate further density related phenomena, the fraction of particles in the wall and depletion layers is quantified. The results are plotted as a function of the ratio wall/solvent for both interactions and wall density, and are subsequently presented in Figure 4.7.

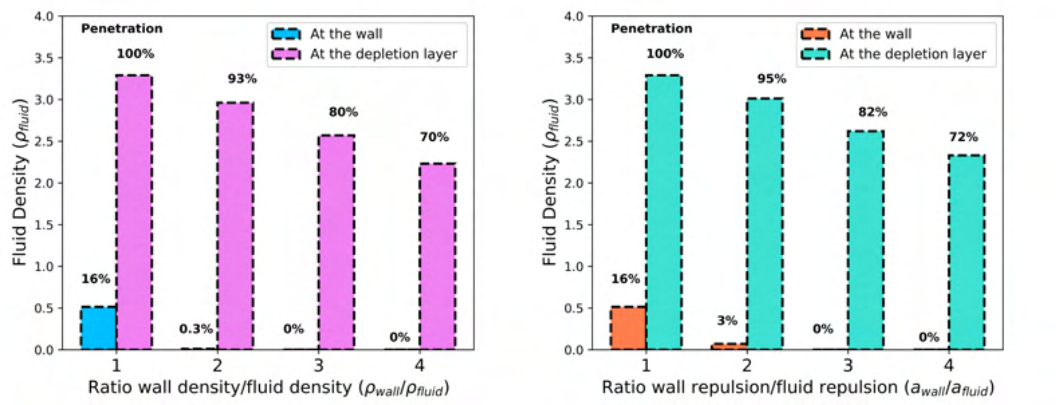

(a) Density and penetration. a_{ij}=25 (b) Density and penetration. $\rho_w = 3$

Figure 4.7: Fluid density at the wall and depletion areas with the respective fraction of particles in each one of these two layers.

Results reveal that increasing wall density is slightly more efficient in keeping particles outside the wall area compared to the case when repulsion is increased.

Next, a quantitative study about particle-wall migration is performed. For that, simulations were run for a broader range of repulsion interactions, going from $a_{ij} = 10$ to $a_{ij} = 100$ and combined with the four wall densities evaluated. The results are shown in Figure 4.8.

The decaying function for the wall case Figure 4.8a is steeper than the case for depletion, which is expected since repulsion becomes weaker further away from the wall. The effect of both wall density and repulsion are additive, which means that for larger wall densities the wall-solvent interaction necessary to reach wall impenetrability is smaller. Depletion is undesirable depending on the application and for those cases the best combination of parameters would be the ones in which there is no wall penetration and depletion minimized. For example the case of $\rho_w = 3$ and $a_{ij} = 55$ where there is only 0.16% of particles in the wall and 95% in the depletion layer.

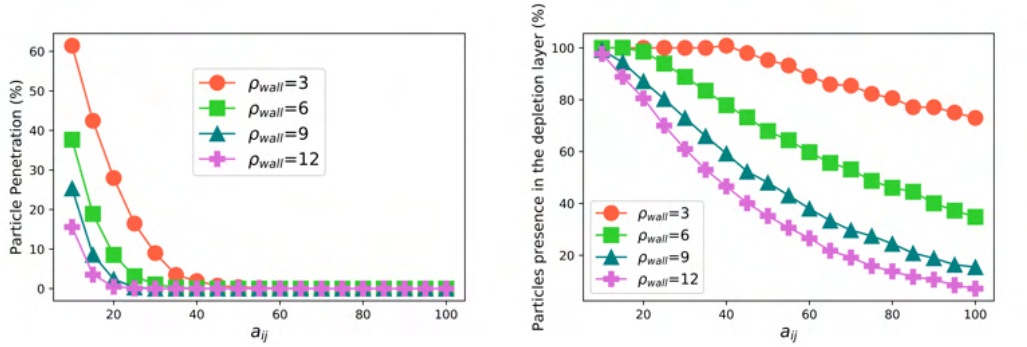

(a) Penetration in the wall (b) Penetration in the depletion layer

Figure 4.8: Fraction of particles in the wall and in the depletion layer. a_{ij} considered from 10 to 100 are combined with the four wall densities evaluated.

4.2
Predicting Particle Penetration in Suspensions: A machine Learning Study

4.2.1
Exploratory and Statistical Data Analysis

As previously stated, solvent particles represented as DPD beads, are, in reality, single points in space with a r_c interaction range. Hence, there is no direct particle parameter that could be affecting particle penetration. Yet, the presence of colloidal particles in the system is likely to influence the way solvent particles move across the channel and migrate towards the walls. In this case, although there is no direct relationship, colloidal particles properties may impact solvent penetration in different levels.

Fig. 4.9 illustrate penetration of colloidal particle at two different body forces, all rigidities and volume fractions evaluated. For simplicity, only colloidal penetration is shown her; a similar behavior for solvent penetration was also observed.

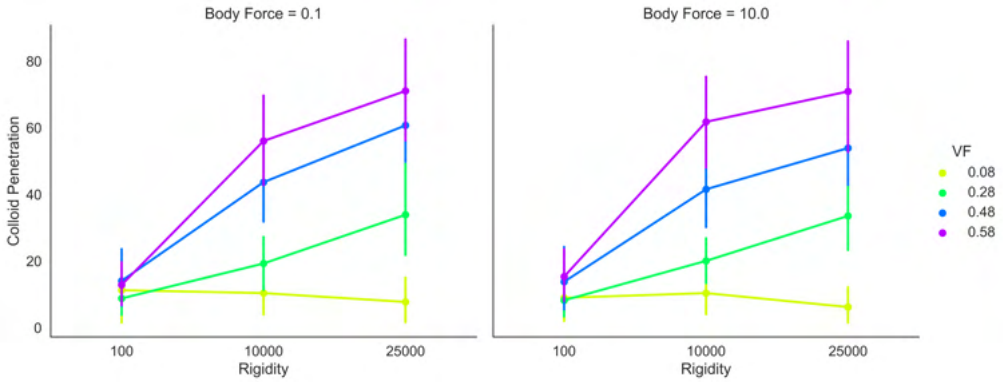

Figure 4.9: Mean colloidal penetration shown for different VF and particle rigidities. The right figure corresponds to a $f_B = 0.1$ and left $f_B = 1$. The data points are averages over all repulsion and confinement ratios for the parameter at interest. That explain the large error bars. For this analysis, only the mean values should be, therefore, considered for comparison.

It can be clearly observed that colloidal penetration is strongly dependent on the VF. Colloidal particles, as opposite to DPD particles have masses and sizes and the force necessary to keep them away from the walls has to be greater than in fluid DPD particles. Particle rigidity also affect penetration, specially evidenced at a stronger volume fraction. Rigid particles are more viscous and the energy necessary to avoid their penetration has to be higher comparative to the soft ones. In terms of body force comparison, it seems that the change in magnitude is not significantly affecting particle penetration.

A second analysis was carried out varying, this time, the repulsion between wall and colloidal particles and the results are displayed in Fig. 4.10. As expected, an increasing in the repulsion(a_{ij}) has a significant effect on particle penetration. Regardless the particle rigidity of body force employed, when a strong interaction is applied a low number of particles will migrate towards the walls. Stronger repulsion combined with small rigidities leads to an nonexistent particle penetration.

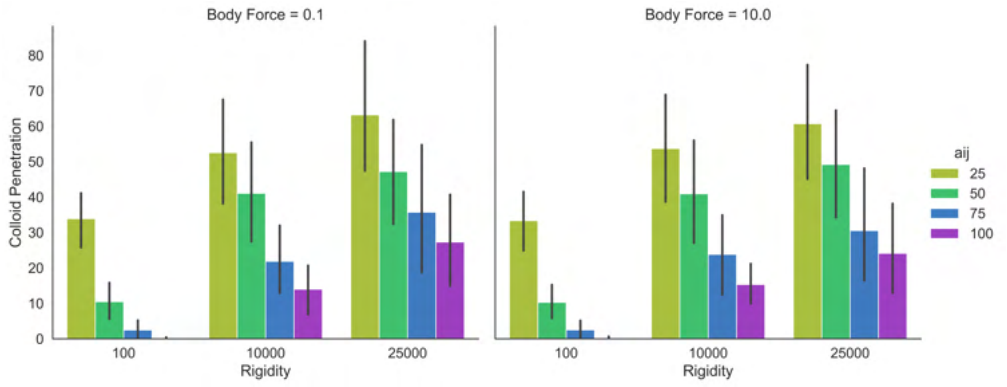

Figure 4.10: Mean colloidal penetration shown for different a_{ij} at different rigidities. The right figure corresponds to a $f_B = 0.1$ and left $f_B = 1$. As in the previous Figure, the data points are averages over all VF and confinement ratios for the parameter at interest, explaining the large error bars. Only the mean values should be considered for comparison.

In order to complement and extend this analyses to all parameters and levels for the two different cases, a correlation analysis can be performed to gain more insights about the relationship between input parameters and final outcomes (penetration).

Correlations and statistical analysis are extremely useful when one wants to investigate associations and dependencies between variables. Spearman correlation [46] represented in Eq. 4-3 is a bivariate analysis based on creating ranks in the variables and measuring the strength of the monotonic relationship between pairs of them. In the Spearman correlation, as opposite to the traditional Pearson correlation, the association does not need to be linear neither normally distributed, as it expresses only the direction of the relationship. The correlations coefficients for all the pairs of variables is illustrated as a heatmap in Fig. 4.11.

$$r_s = 1 - \frac{6 \sum D^2}{n(n^2 - 1)} \tag{4-3}$$

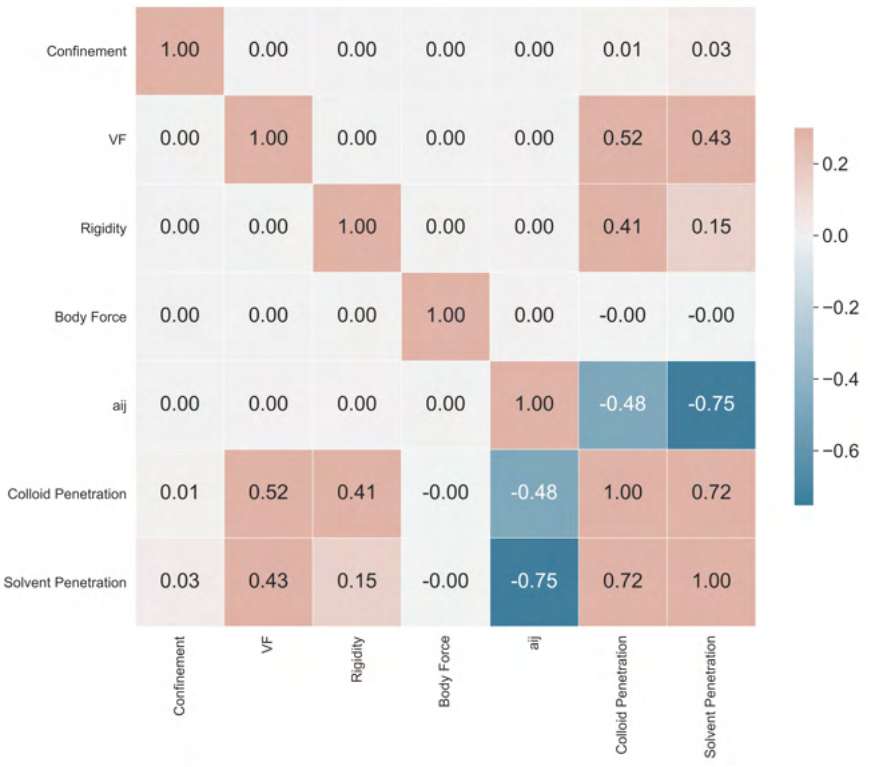

Figure 4.11: Heatmap showing the Spearman correlation coefficients obtained for pairs of variables

Where D^2 is the difference between ranks of the variables and n the total number of observations.

It can be observed that while a moderate negative correlation exists between a_{ij} and colloid penetration in the solvent case it is negatively strong. The closer the coefficient values are to +1 or -1, the stronger the correlation. That means that the higher the a_{ij} the weaker the penetration. Volume fraction is moderately correlated with penetration for both solvent and colloids, being stronger in the colloidal case. Particle rigidity, on the other hand, only correlates moderately with colloidal penetration and does not have a very strong effect in solvent penetration. Confinement and body forces do not show a significant correlation with neither of the response variables.

4.2.2 Machine Learning Modeling

Tuning the parameters to obtain a desired penetration is not a trivial task since several factors may play a role in particle penetration. ML offers a very good alternative to track and predict penetration given a set of initial parameters. It learns the non-linear dependencies between the variables and how they operate together to return the final predictions. Initially the predictions are not accurate but as more data is fed in the model, the performance improves gradually and eventually the model become highly performant. In addition to adding more data, there are alternative techniques to improve a model overall accuracy. One of the most important and popular is hyperparameters tuning, which is based on selecting the best parameters

Metric	Solvent		Colloid	
	Train	*Test*	*Train*	*Test*
MSE	0.05	0.18	0.12	0.34
RMSE	0.22	0.43	0.35	0.35
r^2	0.97	0.92	0.95	0.89

Table 4.1: Model performance obtained for the train and test sets in each estimator

that optimize a given model response. A key parameter in random forest is the number of trees, especially if one considers the computational cost associated in the modeling step. Usually, the higher the number of trees the better the model performance, but when a threshold is reached the addition of more trees has no further influence on the model predictive power.

The results of the training process for both cases with the optimized hyperparameters selection is depicted in Table 4.1. For a better visualization Fig. 4.12 illustrates the predicted versus true values for the train and test sets. The errors found are considerably low for both cases, and the fit of the data to the model is pretty satisfactory. Some data dispersion is seen in the two cases, being more evident in the colloid penetration model, where the performance was slightly worse. r^2 for the training set was above 0.95 and for the test set 0.89, which indicate that the results are valid although a slightly overfitting is taking place. That is not the case for solvent penetration, where not overfitting is observed as the r^2 as well as the errors between train and test sets were not very high.

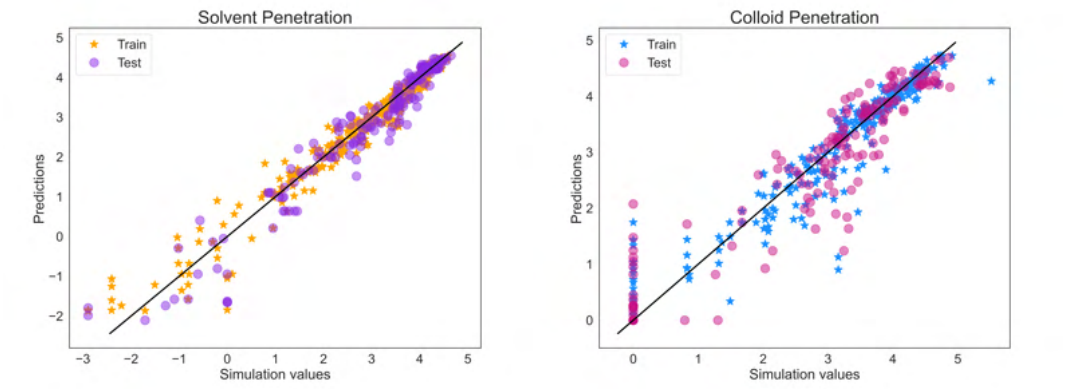

(a) Solvent (b) Colloids

Figure 4.12: Predicted outputs x true values

Tree based methods calculates internally the feature importance, which expresses the magnitude of the contribution of a variable in predicting the output. The main idea behind the concept is that a variable that affects significantly the error when permuted is assumed to be important. Consequently, features that do not influence the error are seen as not relevant for making predictions. RF assigns a score to each feature based on how big the errors in the predictions are. Fig. 4.13 shows the ranking of the top features for solvent and colloids returned by the model.

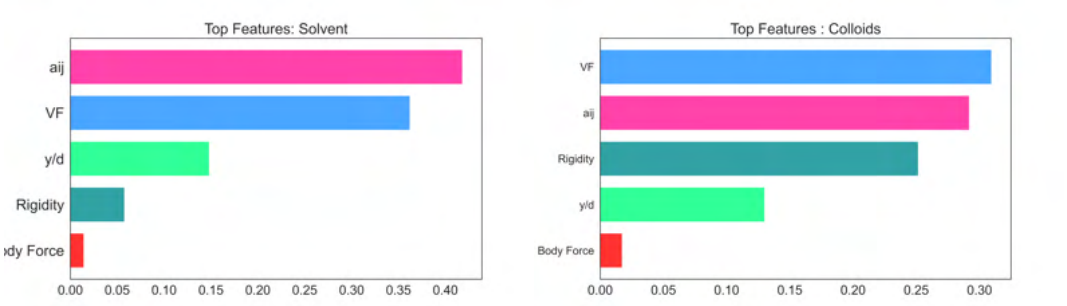

(a) Solvent (b) Colloids

Figure 4.13: Feature importance ranked by Random Forest model. a) Solvent, b) Colloids.

.

In the solvent case, a_{ij} is the most useful attribute in predicting penetration. This result is expected once solvent particles do not have any parameters other than the repulsive interactions that can affect penetration directly. Colloid volume fraction is the second most relevant variable in predicting solvent penetration. By having a rigid core, colloidal particles may push the solvent ones towards the wall leading to an increase in penetration, as previously highlighted. In colloidal penetration, more parameters come to play. The concentration of particles in the system is the most important attribute determining penetration. As more particles are added the repulsive interaction needs to be higher to compensate for the increase in particle number and to prevent their migration inside the wall. VF is followed by a_{ij} and rigidity.

Body force does not seem to be a relevant attribute in predicting penetration, not being the case for confinement. From the correlations analysis previously discussed (Fig. 4.11), it was seen that there is no monotonic relationship between confinement and penetration, and yet, herein it is clear that confinement does play a role in predicting penetration. The effects of confinement in a system depends on many factors, such as particle volume fraction, confinement ratios, particle rigidity, shape, etc (COHEN; MASON; WEITZ, 2004; GALLIER et al., 2016; RAMASWAMY et al., 2017). Particle aggregation might be taking place specially in highly concentrated systems and in some confinement ratios; therefore the agglomerated structures formation will depend on many factors ant those might be affecting indirectly the model predictive power. A more in depth study on the confinement effect on the physics of the system is necessary; this will be addressed in a future work.

4.2.3 Concluding Remarks

Setting up the appropriate parameters in a computational system is a crucial step in the development of a successful simulated system. Particularly, in DPD based models, preventing wall penetration from all the components present in the system is a fundamental step towards reproducing real physical phenomena in confined geometries. The traditional methodologies adopted to prevent DPD penetration are well studied and understood. In the presence of

a second component, such as colloidal particles, additional phenomenological effects might take place that can impact the way particles penetrate the walls. Understanding the factors associated and tune them in order to control penetration is a challenge task due to the complex relationships between the parameters. Statistical analysis and ML represents a very powerful approach to deal with those challenges, providing a deeper understanding of the data and the relationships between the input parameters. With ML it is possible to make penetration predictions based on the selection of numerical values of the input parameters. Using RF, we were able to develop successfully a highly performant predictive model displaying low errors and low overfitting. Additionally, it was possible to understand the most relevant features in predicting outputs. This study showed the enormous potentially of data-driven models and ML tools to systematically study complex systems. In effect, the model developed in this study will be employed to set up properly our wall-solvent and wall-particle interactions in the subsequent works.

4.3
Effect of Particle Rigididy, Flow rate and Confinement in Concentrated Suspensions

4.3.1
Effect of Flow Rate

In a pressure driven flow, a pressure drop is the driven force that promotes the system motion. It can be fairly expressed by means of a body force, which is a force applied to the particles to promote their displacement along the channel. A stronger body force is equivalent to a higher pressure drop. Intuitively, one would expect that the particles motion in a stronger body force condition would lead to a faster flow, which is, in effect, observed, as seen in the velocity profile curves in Figure 4.15. The microstructure evolution of these suspensions, however, does not seem to be significantly affected by the difference in magnitude of the applied forces. Figure 4.14 expresses the evolution in time of the number links per particle and number of clusters from the beginning of the flow stage until the point when it reaches the steady state condition, at 4 million time steps.

It is important to mention that the clustering algorithm used (OLIVEIRA et al., 2020) considers that each individual particle in the system is a cluster and the number decreases as new aggregates are formed. The suspensions evaluated are highly concentrated and their size is relatively big. Therefore at the initial steps of the flow stage the cluster presence is already detected. The number of colloidal particles in the system is 562. If no aggregation was seen the initial number of clusters would be 562, however this number is significantly lower. As time goes by the number of clusters decreases while the number of particle connections increases. That means that additional clusters that were not form on equilibrium are being formed over time when flow is applied. At around 2 million time steps there is a stabilization in microstructure indicating that particles arrangements are no longer changing. In fact, the velocity profile tends to become uniform and the

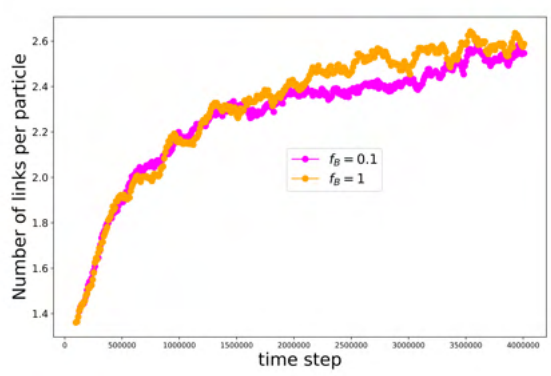

[a]

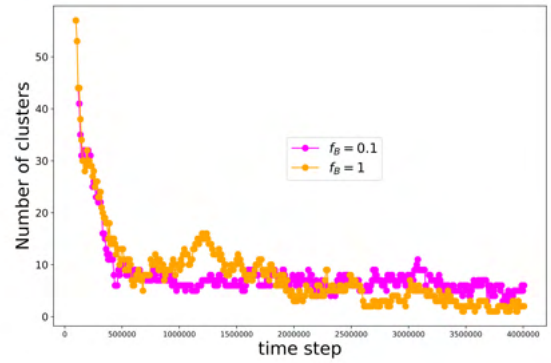

[b]

Figure 4.14: Microstructure evolution of suspensions at y/d = 10, VF = 0.48 and Rigidity=100. a) Number of links normalized by the total number of particles and b) Number clusters

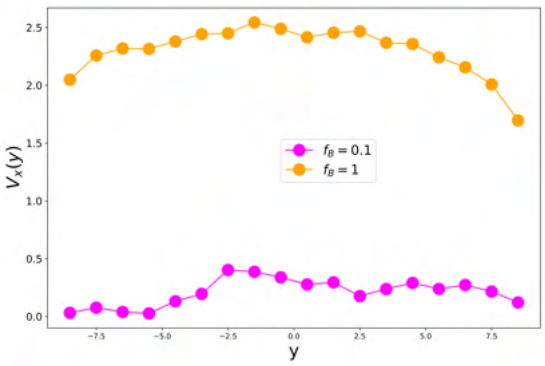

Figure 4.15: Velocity profile comparison between the two body forces evaluated

parabolic shape is merely seen. This velocity profile is characteristic of a plug flow, which is probably a consequence of the clusters that are formed possibly in the middle of the channel, which would decrease the maximum velocity in the center of the box. As one would expect, when a stronger body force is applied the particles have more energy to flow and will displace faster in the channel, as seen in Figure 4.14. Since the kinetics of cluster formations has shown to be independent of body force for the following sections the body force will be kept constant at $f_B = 1$. It is important to mention that a higher body force was not used because we are interested, primarily, in the flow in the laminar regime.

4.3.2 Effect of Concentration

This work focus on two main concentration of particles: VF = 0.48, corresponding to a semi-dense system, and VF = 0.58, relative to a dense one. In the two cases evaluated the trends found for cluster kinetics were similar. In both cases, clusters could be detected in the equilibrium step. In Figure 4.16 it can be seen that the number of clusters decreases rapidly and at time step about 2 million it becomes very small, meaning that a large cluster is likely to be formed. The number of links per particle is higher in the dense case - the number of colloidal particles is higher consequently, there will be more particles to pack resulting in larger aggregates.

In the dense case there is a local concentration peak of particles in the mid plane between the center and the bottom wall as seen in the density profile curve (Figure 4.17a). This local increase of particles density leads to a weaker velocity profile at this point. In the semi-dense suspension, on the other hand, the clusters are distributed all over the channel. At higher volume fraction the dynamics of the system is slowed down, the interactions increase and the free volume available per particle decreases. The later, specially, will cause a decrease in motion since these particles will be more restricted in space and that will lead to a slower velocity profile, as observed in Figure 4.17b.

4.3.3 Effect of Particle Rigidity

Rigidity in our computational system is controlled by the strength of the core force applied between pairs of colloidal particles. Rigid particles are naturally more repulsive and will make the particles approximation less likely; as a consequence, the formation of aggregates will be smaller compared to the system where a weaker force is applied. Even though the repulsion force between the particles is strong, cluster formation is observed when rigid particles are used which is a result of the high suspension volume fraction and potentially the large particle size. By comparing soft and rigid systems, it can observed that rigidity leads to a decrease in the number of links per particle, indicating less connections and likely smaller clusters. The number of clusters is low for lower and intermediate rigidities, suggesting less aggregates. For the highest rigidity case the number of clusters is higher indicating a larger number of individual particles, as seen in Figure 4.18. At around 3.5 million timesteps

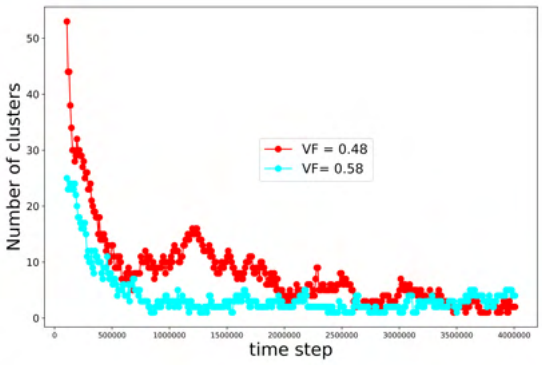

[a]

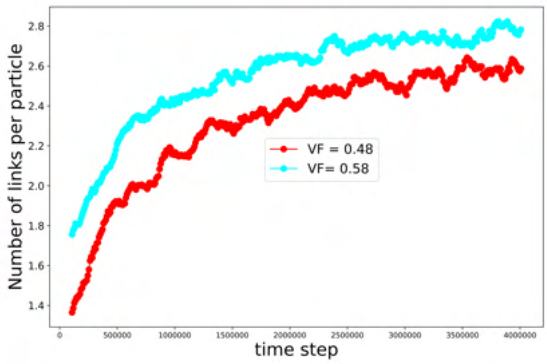

[b]

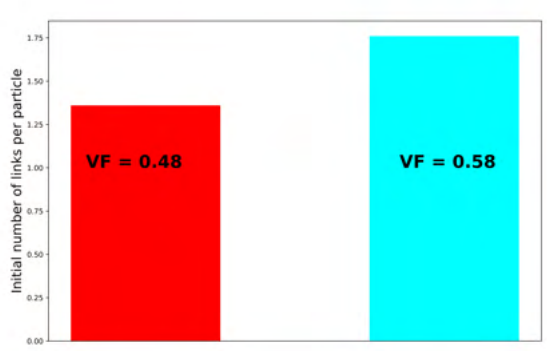

[c]

Figure 4.16: Microstructural changes of suspensions made of soft particles and $f_B = 1$, y/D=10 a) number of clusters, b) number of links per particle c) initial number of links per particle

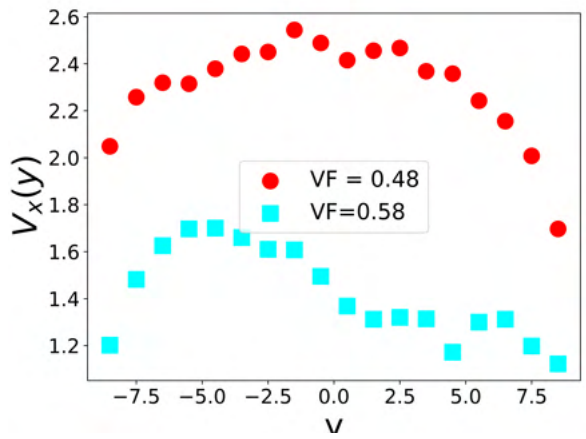

(a) Velocity Profile

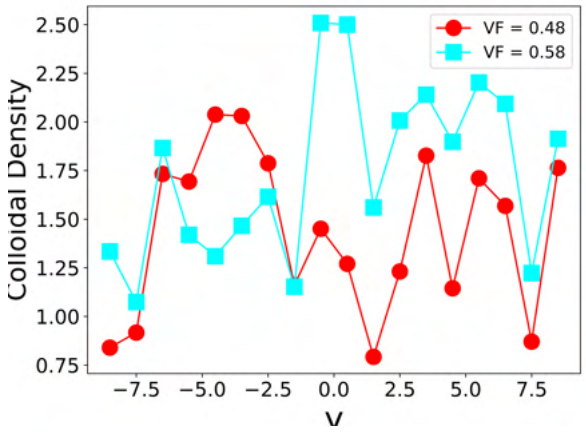

(b) Density Profile

Figure 4.17: Velocity and density profiles for semi-dense and dense suspensions at y/D = 10, soft particles and $f_B = 1$.

there is no more observable changes in the number of clusters and links per particle which suggests that once the giant cluster if formed its microstructure remain unaltered.

Figure 4.19, presents the snapshots for the particles with different rigidities. Although deformation can not be fairly represented in the snapshots some insights can be drawn. Soft particles form a more anisotropic structure as a results of the particles deformability. When rigidity increases the particle distribution is mostly symmetrical in the channel.

Rigid particles are naturally more viscous and have a stronger resistance to flow which will leads to a deceleration in the motion. That can be clearly observed in the velocity profile curves displayed in Figure 4.20. In addition one can note that the profile is not parabolic as a result of the particles presence that breaks up the parabolic symmetry.

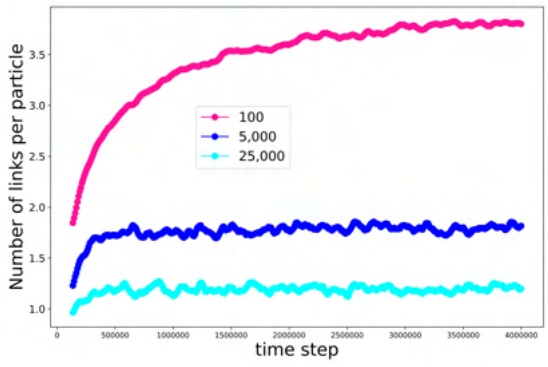

[a]

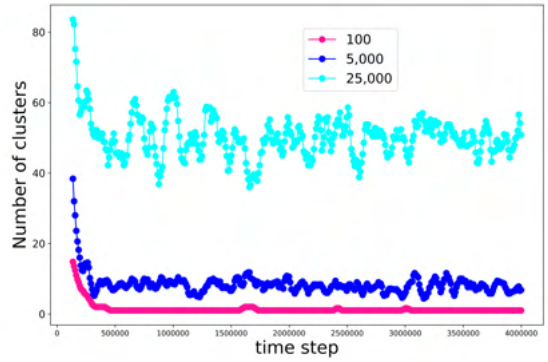

[b]

Figure 4.18: a)Number of clusters and b)number of links normalized by the number of total particles

.

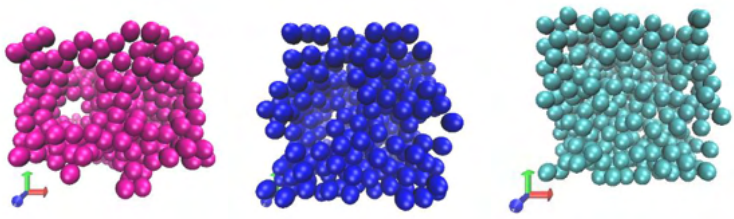

Figure 4.19: Snapshot of the particles at different rigidities. the left image (pink) represents the rigidity or 100, center image 5,000 and the right figure the stiffest particles(rigidigy = 25,000)

.

4.3.4
Effect of Confinement

The effect of walls in suspensions is a topic widely studied and reported in the literature. In concentrated suspensions, the majority of the cases relies on rigid particles. Herein, the effect of seven confinement ratios was evaluated in suspensions made of very for soft particles. Figure 4.21 presents the evolution of the number of links per particle for all range of confinement ratios studied.

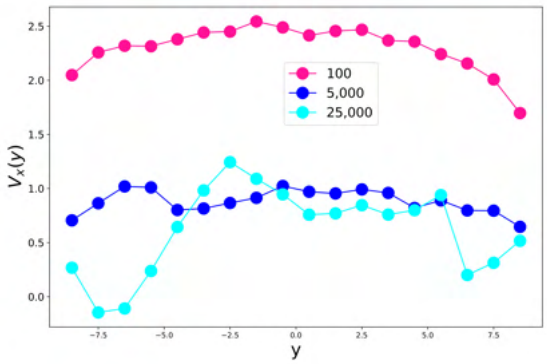

Figure 4.20: Velocity Profiles for all range of the rigidities evaluated

.

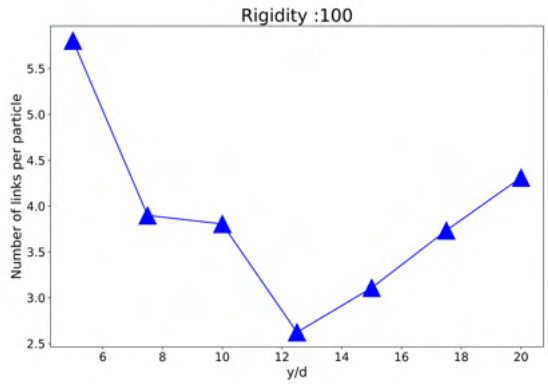

[a]

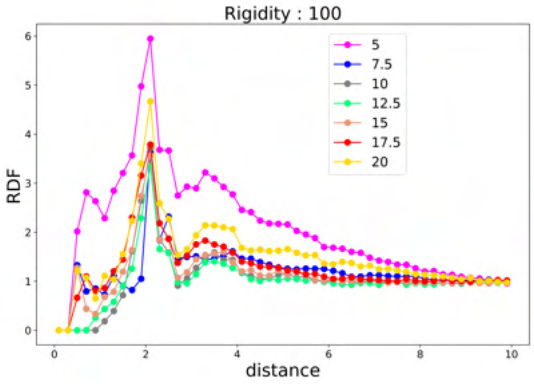

[b]

Figure 4.21: Number or links per particle(a) and radial distribution function(b) for soft particles in all confinement ratios. The values were averaged over the last 100,000 time steps, when no more detected changes changes in the microstructure was detected

In all cases a giant cluster containing all the colloidal particles of the system is detected, and yet, the number of links per particle is different according to the confinement ratio. That is possibly happening due to a difference in the clusters shape and deformability induced by confinement. In our strongest ratio the number of links per particle is the highest one and it decreases until the confinement y/D = 12.5. When confinement is reduced

even more the number of links raises again. The same trend is also observed in the radial distribution function, as displayed in Figure 4.21. The peaks intensity, indicating the number of particles around the reference particle is higher for 5 followed by 20, 7.5 and 15 - that suggests that a more packed structure is seen in those cases. It is interesting to note that for y/d=5 there is an additional peak at distances below 1. Considering that the radius of the particles is one, that would suggests that the particles are highly deformed and that confinement is potentially enhancing that effect as well as it is affecting the hydrodynamic interactions and the contacts number. In fact, the snapshots displayed in Figure 4.22 show a different trend in cluster shape.

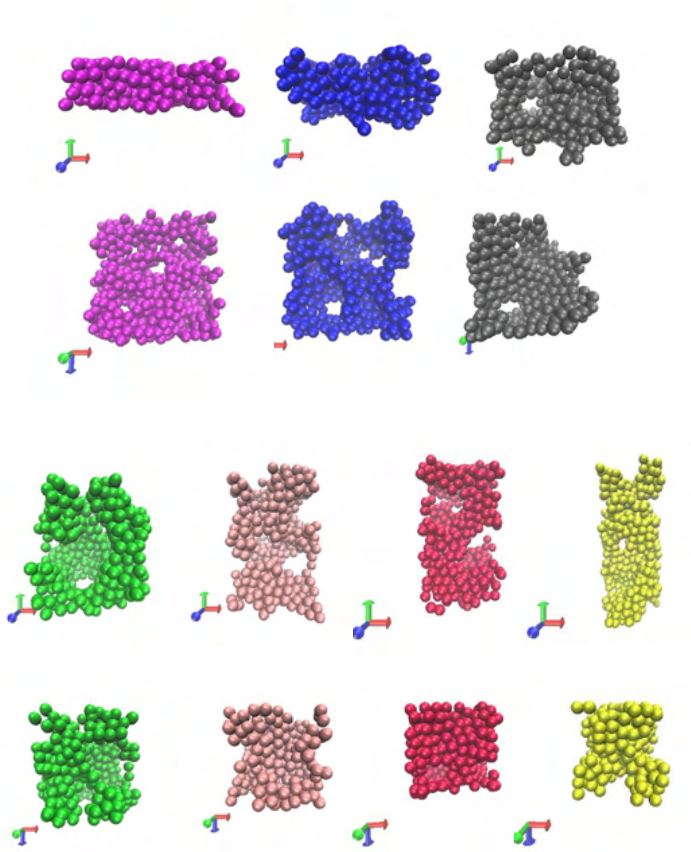

Figure 4.22: Snapshots of the particles at time step 4 million. From left to right, top to bottom the images displayed correspond to, respectively, the confinement ratios 5, 7.5, 10, 12.5, 15, 17.5 and 20

.

The cluster shape is clearly different as one migrate across different confinement ratios. For the extreme ratios (5 and 20) the cluster shape is denser, while for intermediate ratios the cluster forms a percolated network. Our hypothesis is that there is a combined effect of particle rigidity and confinement which alters the hydrodynamic interactions, particle deformation and therefore, the cluster structure. At weak confinement the particles do not deform significantly and the clusters form a packed network, similar to what happens when rigid particles are used. As confinement increases, the

deformability increases and a transition to a percolating network is observed. As a consequence of this cluster structure, the number of particles in contact is smaller and it reaches its minimum at y/d=12.5. Increasing confinement leads the particles to deform even more; the number of connections and the surface area of the particles are higher which enhances the hydrodynamic interactions and as a result, the formation of a packed structure is observed again.

According to the Poiseuillle law, in a broader channel the particles will move faster, as wall effects retarding the motion weaker. In effect, it is observed that our systems obey this condition, as seen in 4.23 which shows that the flow is faster as confinement ratio is weaker. That behavior is seen regardless the particles rigidities.

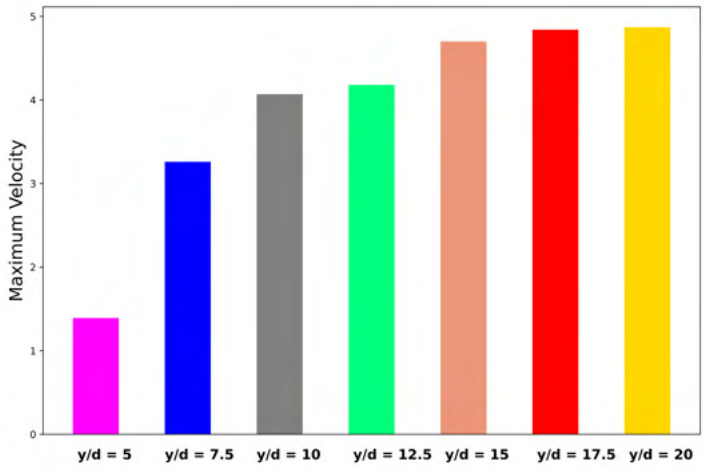

Figure 4.23: Maximum velocity displayed for all rigidities

.

4.3.5 Conclusions

Particle microstructure in suspensions has a fundamental role in the observable physical properties of different materials, which has a primordial importance in many engineering applications. Some particles properties can impact the way particles self-organize in the system which in turn may affect the final macroscopic response. In this work, a systematic study of the effect of flow rate, particle rigidity, volume fraction and confinement on inducing the formation of aggregated structures was carried out. Flow rate was found not to be a relevant factor in cluster formation. Particle rigidity, on the other hand, showed some relevant differences in terms of cluster formation. Although aggregate formation starts on equilibrium in both cases, when rigid particles are used the number of links per particle is significantly higher than when rigid particles are employed. Volume fraction was also found to play a role: more concentrated suspensions leads to more connections per particles and potentially larger clusters. In terms of confinement it could be concluded that the microstructure changes across confinement ratios. For strong and weak

confinement a denser network was detected while intermediate ratios leads to the formation of a percolating network instead.

4.4
Predicting Viscosity and N1 in Suspensions using Machine Learning

4.4.1
Exploratory Data Analysis

Exploratory Data Analysis consist of exploring, understanding, finding patterns in the data and making visualisations using a statistical approach. It enables to gain more insights about the data, understand and capture potential correlations and associations between variables that can lead to smarter, more accurate and optimized decisions.

Rheology The viscosity and first normal stress evolution at different flow rates,for different particle rigidities and volume fraction is expressed in Figure 4.24, and for a cleared visualization the average viscosity values are illustrated in the bar plots in Figures 4.25 and 4.26.

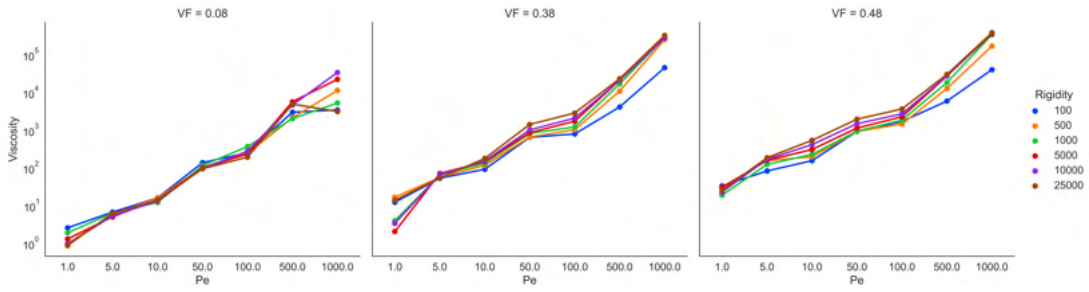

Figure 4.24: Viscosity evolution at three different VF, Pe number and particle rigidity

Increasing the flow strength, i.e. Peclet number, leads to an increase in the flow resistance, therefore, the viscosity. Even when VF=0.08, shear-thickening can be observed at high Pe. Rigid particles for being more viscous tends to generate stronger viscosity, as see in the Figures 4.24. When the volume fraction increases the viscosity is stronger, and at very high Peclet number the curve has an abrupt increase, which suggest that discontinuous regime is reached, even though there is no frictional forces in the system (JAMALI; BRADY, 2019).

It is well known and reported in the literature that suspensions in the shear-thickening regime display negative first normal stresses difference. As it can be evidenced in Fig 4.27, increasing volume fraction, rigidity and Peclet leads to more negatives values, suggesting a stronger shear-thickening behavior.

4.4.1.1
Microstructure

Microstructure is strongly connected to rheology, specially in highly concentrated suspensions. Very commonly, suspensions at strong concentrations and shear rates will display the formation of larger clusters that depending on

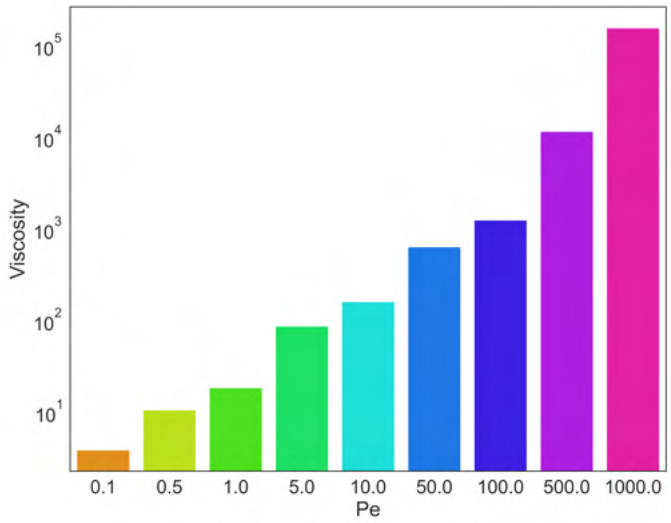

Figure 4.25: Viscosity evolution at different Pe number

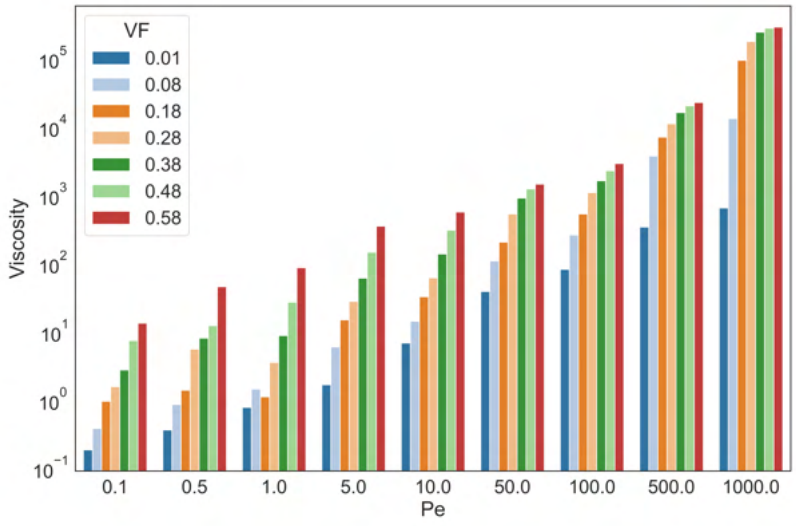

Figure 4.26: Bar plots showing the viscosity changes at all VF and rigidity evaluated and a function of Pe

the conditions will percolate the channel leading to a strong shear-thickening response (BOROMAND et al., 2018).

In this work, the microstrucure algorithm applied is described in (OLIVEIRA et al., 2020). Essentially, it considers that each individual particle is assumed to be a cluster and as aggregates start being formed the number of cluster decreases. If the final stage is composed of a single cluster it means that the number of clusters will be one. The number of links express the number of connections between particles. In general, higher the number of links means more connections and if it comes associated to a decrease in number of clusters it suggests the formation of bigger aggregates.

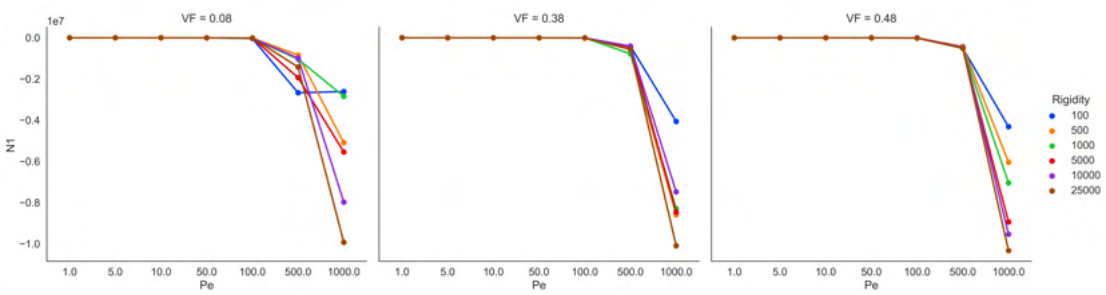

Figure 4.27: N1 evolution at different VF and Pe.

In the next three Figures it is shown the number of clusters(Figure 4.28) and number of links (4.29) when Peclet and rigidity are varied for two volume fraction.

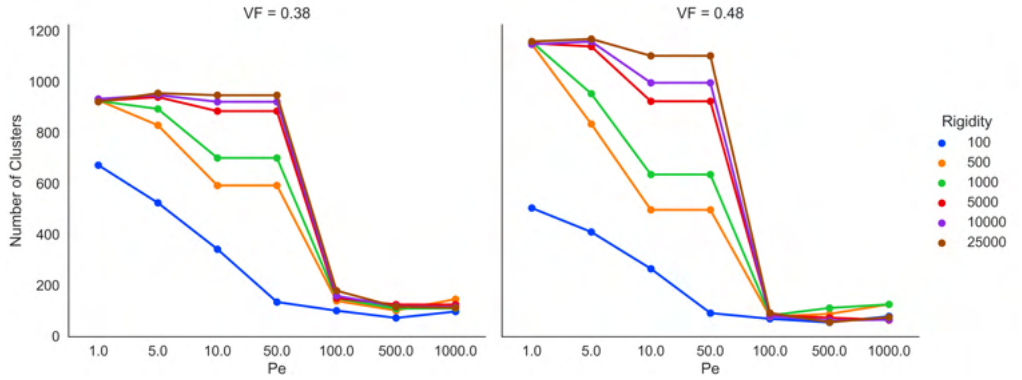

Figure 4.28: Number of clusters at different Pe and particle rigidities for VF=0.38 and VF=0.48.

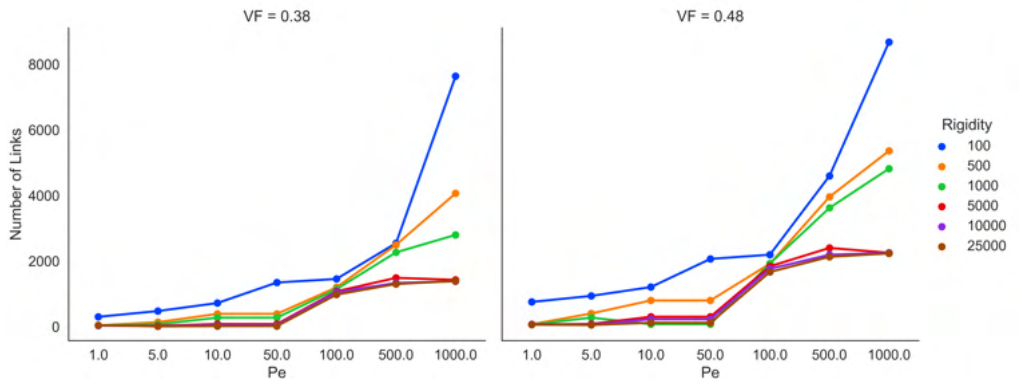

Figure 4.29: Number of links at different Pe and particle rigidities for VF=0.38 and VF=0.48

It can be clearly seen that at moderate and high concentration the number of clusters is small and the number of links is high. Softer particles lead to an even stronger effect. In effect, when particles are extremely soft (blue curves), the number of clusters is smaller than in the other curves for all Pe evaluated. That suggests that the cluster presence can be detected. When Pe $>$ 100 the number of clusters is very small, indicating that at this flow rate

bigger clusters are seen regardless the volume fraction or particle rigidity. The number of links at this point is higher as the the particles are softer, which suggest the formation of larger clusters.

4.4.2 Correlation Analysis

Correlation is a statistical measure of association between variables. The magnitude of this relationship can be expressed in terms of the correlation coefficient, that ranges from -1 to +1. Coefficients closer to -1 or +1 indicates a strong correlation between the variables, while when it is closer to zero it means no relationship. Two of the most important correlation coefficients in statistics are Pearson and Spearman. Person expresses the linear correlation between two variables while Spearman only give insights about the monotonic relationship between them, i.e. if one increase one so does the other, but it doesn't necessary have to be in a linear way as the case of Pearson. In the Figures 4.30 and 4.31 it is shown Pearson and Spearman correlation coefficients for the combination of all variables.

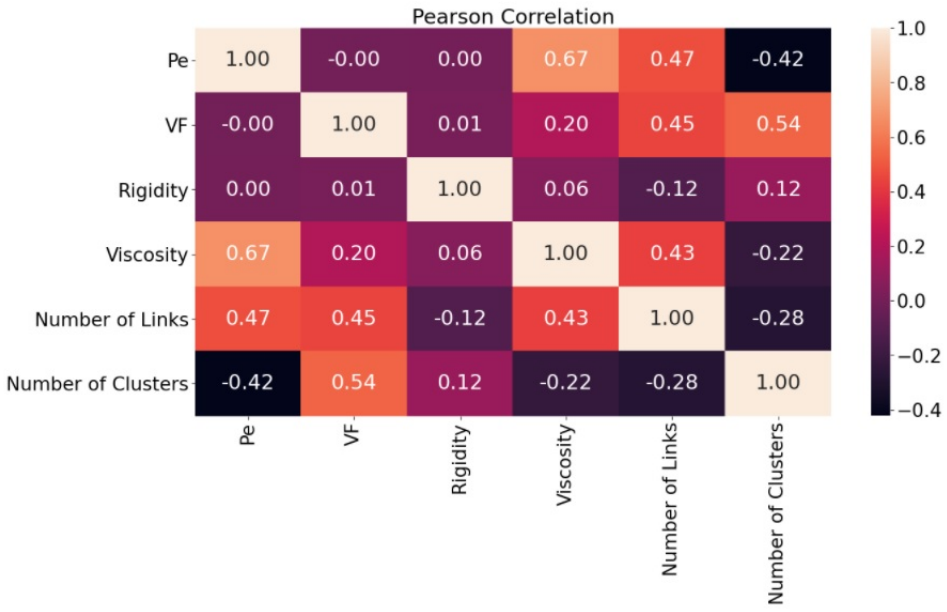

Figure 4.30: Pearson Correlation coefficient

It can be observed that there is a strong positive correlation between viscosity and Pe and viscosity and number of links. That means that the higher the Pe the higher the number of links and viscosity. Analogously, the number of links is also strongly related to volume fraction, meaning that if the concentration increase more links are seen. In Pearson correlation the same trend can be observed, however the coefficient are weaker suggesting that the relationship of those variables is not completely linear. It is worth to highlight that viscosity does not show a correlation with rigidity. A possible reason for that is that larger clusters are seen in softer particles, which are likely to increase the system viscosity. Rigid particles, on the other hand, are less likely to form large clusters, specially at low Pe, but are naturally more viscous than the soft ones. Those two effects would balance the viscosity dependency on

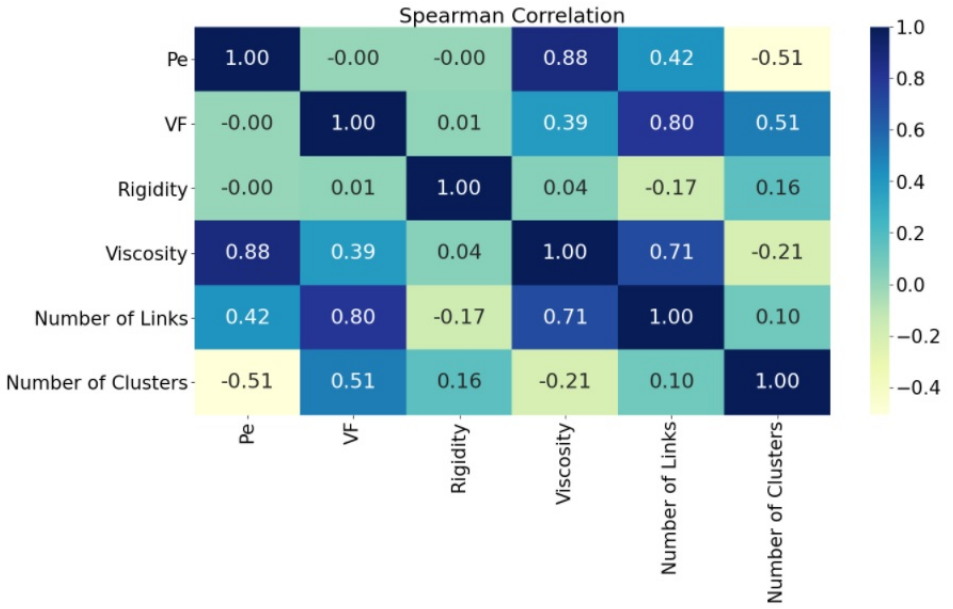

Figure 4.31: Spearman Correlation coefficients

particle rigidity and could explain the non correlation between rigidity and viscosity.

4.4.3 Predictive modeling

In this study the Machine Learning model chosen was Gradient Boosting GB, which is an ensemble and non-parametric ML model. Ensemble models, in general, present higher performances and one of the reasons for it is that they combine individual models and when averaging the results the errors are partially cancelled out. As in the case of Random Forest, GB are built from week learners, in this case decision trees. Decision tress were described in previous chapter and for the sake of simplicity they wont be detailed in this Chapter. The main difference between RF and GB is that in RF the threes are independent and the final prediction is the result of an average of the individual trees. In GB the trees building process takes place sequentially; each tree is built on the errors generated by the previous tree; the learning process is therefore built along the way.

Before training the model it is important to guarantee that the data obey certain requirements. One of the most important ones is to make sure that the data is approximately normally distributed and therefore that the performance results are reliable. There are some strategies used to improve data distribution, one of the most popular ones is applying log transformations. Log transform was applied and the distributions of the target variables can be identified in Fig 4.32.

It is also important to normalize the data since it has varying scales and ranges of values. If normalization is not performed, the model might take into account the absolute values and the difference in scales may lead to inaccurate predictions. All the input variables were normalized. The training set, which corresponds to the set of data used to allow the model to learn, corresponds

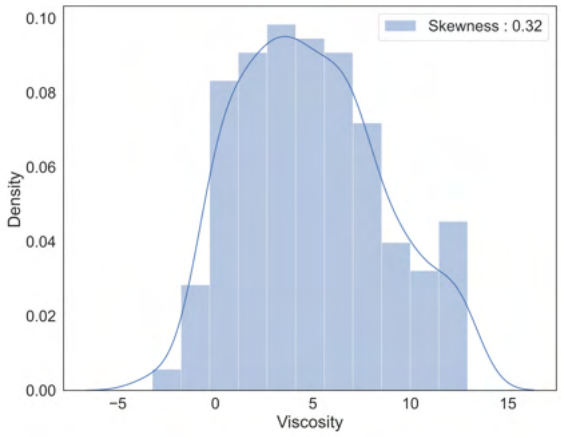

(a) Viscosity

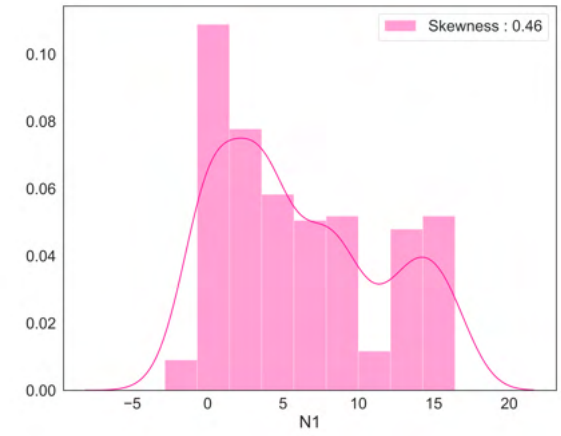

(b) N1

Figure 4.32: Data distribution for the target variables. a) Viscosity and b) N1

to 70% of the simulation data. To evaluate the model performance it was used r^2, RMSE, MAE and MSE as previously described in Chapter 3.

The results of the training process is shown in Figure 4.33 and the Tables 4.2 and 4.3 summarizing the results for Viscosity and N1 is also presented.

The errors obtained were very low and the r^2, which expresses how good is the fit of the data to the model, is very high for both train and test sets in the Viscosity and N1 predictions. That means that the model was able to successfully learn from the data and did not memorize, which can be evidentiated by the low errors obtained in the train and test sets. It other words, overfitting is not taking place here. Tree based methods enable the calculation of the feature importance, which in basically a score that is assign to a feature according to how helpful this variable is in predicting the output. The features importance is displayed in Figure 4.34.

In the two models evaluated the most important feature for making predictions are Peclet number. In the viscosity case, the volume fraction is also playing a role in helping the predictions while for N1 the volume fraction

	Viscosity			
	MSE	**MAE**	**RMSE**	**R2**
Train	0.19	0.27	0.52	0.98
Test	0.23	0.31	0.48	0.97

Table 4.2: Performance metrics for Viscosity

	N1			
	MSE	**MAE**	**RMSE**	**R2**
Train	0.33	0.38	0.62	0.98
Test	0.93	0.62	0.96	0.96

Table 4.3: Performance metrics for N1 Model

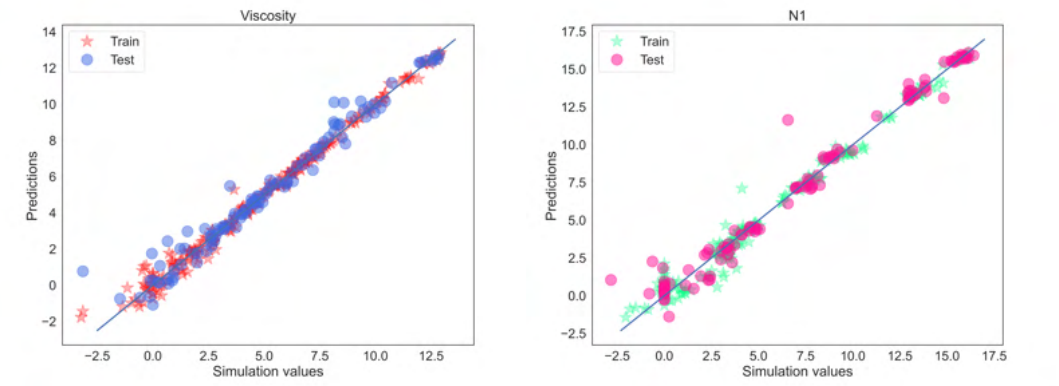

(a) Solvent (b) Colloids

Figure 4.33: Predictions versus ground truth for Viscosity(a) and N_1(b) predictions.

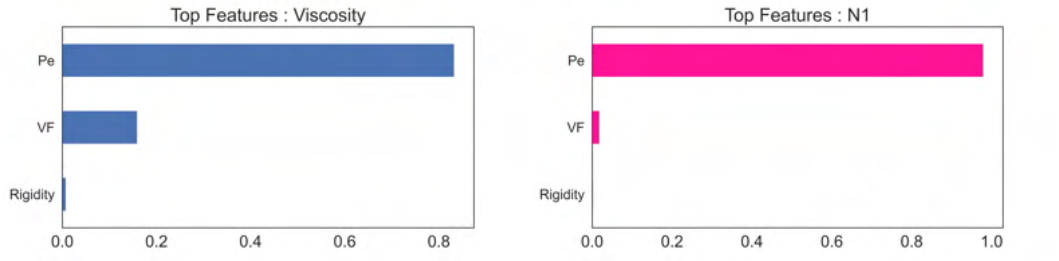

(a) Solvent (b) Colloids

Figure 4.34: Feature importance in making predictions. a) Viscosity and b) N1

contribution is not very relevant. Rigidity in the two cases is not a significant feature for the predictions.

4.4.4 Conclusion

In this chapter, a ML model was proposed to predict viscosity and N1 in suspensions based on VF, Pe and particle rigidity. In exploratory data analysis

some insights and observations about the data could be drawn. Suspensions even at low volume fraction can display shear-thickening if a sufficiently high shear rate is applied. Increasing rigidity, flow rate and volume fraction leads to an increase in viscosity and a more negative first normal stress difference, indicating a stronger shear-thickening response. When soft particles are used, even at very low Pe clusters are already formed, not being the case for the other particle rigidities, in which aggregates start to be formed only at Pe $>$ 1. Correlations analysis enabled to investigate potential relationships between the variables and it was found that rigidity does not have a correlation with viscosity while a strong correlation between Viscosity, Pe and number of links was found. GB was the machine learning algorithm selected to train the data and the predictions on the test set were very accurate. No overfitting was observed, which guarantee that the model was able to effectively learn form the data. The errors obtained were very low for both viscosity and N1 models, which shows that machine learning can successfully be used to maker rheology predictions in suspensions rheology.

5
Conclusion and future work

5.1
Conclusion

In this work, concentrated suspensions were studied using a computational approach. The principal goal of this research was to systematically study the effect of confinement and particle rigidity on the microstructure of highly concentrated suspensions. Before performing the confinement study itself, some additional steps were necessary to guarantee a reliable system, which encompasses the definition of the simulation domain and the right selection of repulsion parameters.

DPD is a very popular approach to study fluids in the mesoscale and it has been extensively used in the modelling of complex fluids. As a particle-based method, in DPD the entire system is made of particles. The fluid ones are commonly expressed as single traditional DPD particles. If one wishes to model solid structures, the most classical approach is to represent the desirable shape by freezing the particles that will behave as a single unit. Although this approach is very compelling, since it enables the modeling arbitrary particle shapes, it has a higher computational cost associated.

Herein we choose to use an alternative approach to represent colloidal particles in which they are built as solid spheres having a hard core and a dissipative coat in a method called Core-Modified Dissipative Particle Dynamics(WHITTLE; TRAVIS, 2010). In CM-DPD, as opposite to traditional DPD, the interactions are surface-to-surface and the DPD forces as replaced by a core force, giving the repulsion nature of the interactions and a lubrication force, expressing the short-range hydrodynamic interactions. In our system, DPD particles represent the solvent, colloidal particles are modelled as core-modified particles and the wall is build by equally spaced DPD particles that are frozen at the edges of the simulation box in accordance to the work of (PIVKIN; KARNIADAKIS, 2005).

The first step in this research was setting the simulation parameters in order to obtain a representative system in which nonphysical phenomena are not taking place. A very important requirement in the development of this system is adjusting wall-solvent interactions; DPD interactions are soft, therefore particles can penetrate each other, which is undesirable at the wall level.

Preventing wall penetration has been highlighted in many previous works. Those were focused mainly on preventing wall penetration while density oscillations at the wall are minimised. Different approaches were used to achieve impenetrability, such as correcting the forces at the wall and modifying the dissipative coefficient. Although many of these works were successful in controlling density oscillations, they are all qualitative studies. A quantitative study to understand deeper the role of interactions and wall density was lacking in the literature and was carried out here, as a first part of the study.

In this study, a large range of interaction parameteres between wall and fluid particles was vary simultaneously for four different wall densities. The initial goal was to understand which one of these two parameters is more effective in preventing wall penetration. It could be seen that although the effects were similar, wall density has shown a slightly stronger effect. The second goal of this study was to quantify penetration and depletion by plotting the decaying functions of penetration when both a_{ij} and wall densities varied. The curve was steeper in depletion than in penetration case and it could be concluded that the effect of wall density and wall interactions combined are additive.

Once established the interaction parameters in the case of a wall-DPD geometry, one could move to a more complex and realistic system, when colloidal particles are incorporated. This study is more challenging because there are more parameters affecting penetration, for example, the concentration of particles, particle rigidity, flow rate and confinement ratio. Understanding and quantifying the magnitude in which those parameters affect penetration is a complex task, since they all might play an individual and collective role. Decouple those effects in a way to develop a mathematical expression encompassing all the parameters would be a solution. However it would required to run a large number of simulations. In addition, some parameters might influence others and decouple them to set interactions would be a very difficult task. In this context, statistics and machine learning appears as a more practical solution to address those problems.

The idea behind ML is that instead of expressing the relationship between dependent and independent variables in a form of a conventional mathematical expression, that could be exhaustive to do, one can feed a model with examples and let the algorithm learns from experience. Machine learning has becoming very popular to tacked specially problems with variables presenting complex and non-linear relationships that are hard to quantify. Herein, ML is a very interesting approach since is enables to make predictions about solvent and particle penetration based on the selection of the parameters.

As a second part of this work, a supervised learning approach was used to train a Random Forest model using around 550 simulations in which particle volume fraction, flow rate, particle rigidity and confinement were varied. Using statistical analysis it could be seen that volume fraction and wall repulsion are strongly correlated to particle penetration for both solvent and colloidal penetration. The performance metrics used were r^2, MSE and RMSE. An $r^2 > 0.92$ was obtained for the training set and for the test set above 0.9. These results suggest that the model is not overffiting and our predictions are valid. Low errors were also obtained for all the cases, meaning that random forest with the proposed parameters can be safely used to make penetration predictions within the range of the input variables.

Once stabilised the ideal range of parameters for the simulations, we could move forward to the confinement study. In this study, seven confinement ratios were varied when two flow rates were applied ($f_B = 0.1$ and $f_B = 1$) in rigid (core coefficient 25,000), moderate (5,000) and soft (100) particles at two particle concentrations(semi dense, VF = 048 and dense, VF=0.58). The main goal of this work was to understand which parameters and in which extension

they affect particle aggregation and microstucture.

It was found that flow rate does not affect the kinetics of cluster formation and that most of clusters are formed at equilibrium regardless the particle rigidity. As particle concentration increases the free volume per particle in the channel decreases, consequently, the cluster formation is facilitated in a denser system. It was also found that when soft particle are used at the end of the simulation all particles belong to a single cluster. However, the number of links per particle was different according to the confinement ratio, which suggest that the way the particles pack and are arranged differs.

In the last part of this work, a machine leaning study was carried out to evaluate if viscosity and first normal stresses can be predicted based on particle volume fraction, Pe and particle rigidity. Using gradient boosting, a non-parametric ML model, we were able to achieve very low errors and very accurate predictions for both Viscosity and N1 models, validating our hypothesis that we can predict rheological properties on suspensions using ML.

5.2 Future Work

In this study, the strategies used to prevent wall penetration consisted on tuning the wall density and interactions between wall and the particles. However, we are aware that it exists other approaches that might be more suitable to control better density oscillations. In order to complement this work, it would be desirable to perform a study testing alternative strategies do prevent density oscillations and evaluate how this implementation would change the results.

To gain computational efficiency, it would be interesting to remove one of the wall of the simulation box and apply regular boundary conditions at the y-direction. This way, all the calculations at the wall, that slow down the code, could be prevented.

In the confinement study, for a more complete work, it would be important to include other colloidal forces, specially frictional ones. Although discontinuous shear thickening have already been observed in frictionless systems (JAMALI; BRADY, 2019), most works in the literature reports the need or a frictional force to observe such phenomenon. Colloidal forces when added require a very low time step to capture all the underlying physics. The code use in this project is single shredded and the computations would take several months if a friction force was added. Although most of the physics we are interested in see can be capture with short-range hydrodynamic forces, adding a long-range hydrodynamic interactions would be interesting to compare, also to make the study and the system more realistic.

Some additional functions to obtain more information about the cluster formation process and microstructure are necessary, as for example, for the calculation of the cluster radius of gyration.

Studies of extensional flows are also important to be carried out in the near future. Many industrial applications involved not only shear flows, but also a combination of both extensional and shear. Therefore, understanding

how confinement affect the flow of suspensions in such situations has a vital importance in the development of new products and technologies.

5.3 Acknowledgement

This study was financed in part by the Coordenação de Aperfeiçoamento de Pessoal de Nível Superior - Brasil (CAPES) - Finance Code 001 - 1910/2016, Conselho Nacional de Desenvolvimento Científico e Tecnológico CNPq 307100/2017-0 and Fundação de Amparo à Pesquisa do Estado do Rio de Janeiro - FAPERJ E-26/202.835/2017. The authors of this work also thank the National Science Foundation financial support through grant CBET 1703919. This work made use of the High Performance Computing Resource in the Core Facility for Advanced Research Computing at Case Western Reserve University.

6
Bibliography

ABU-NADA, E. Simulation of heat transfer enhancement in nanofluids using dissipative particle dynamics. **International Communications in Heat and Mass Transfer**, v. 85, p. 1 – 11, 2017. ISSN 0735-1933. Cited in page 32.

ANDERSON, R. L. et al. Micelle Formation in Alkyl Sulfate Surfactants Using Dissipative Particle Dynamics. **Journal of Chemical Theory and Computation**, American Chemical Society, v. 14, n. 5, p. 2633–2643, 2018. ISSN 15499626. Cited in page 31.

BALL, R. C.; MELROSE, J. R. Lubrication breakdown in hydrodynamic simulations of concentrated colloids. **Advances in Colloid and Interface Science**, v. 59, n. C, p. 19–30, 1995. ISSN 00018686. Cited in page 44.

BARCELOS, E. I. et al. Controlling particle penetration and depletion at the wall using Dissipative Particle Dynamics. **Computer Physics Communications**, v. 258, n. 2, p. 513–526, 2021. ISSN 00104655. Cited 2 times in pages 34 and 48.

BECKER, T.; MUGELE, F. Nanofluidics: Molecularly thin lubricant layers under confinement. **Molecular Simulation**, Taylor Francis, v. 31, n. 6-7, p. 489–494, 2005. Cited in page 32.

BIAN, X. et al. Hydrodynamic shear thickening of particulate suspension under confinement. **Journal of Non-Newtonian Fluid Mechanics**, Elsevier B.V., v. 213, p. 39–49, 2014. ISSN 03770257. Disponível em: <http://dx.doi.org/10.1016/j.jnnfm.2014.09.003>. Cited 5 times in pages 12, 17, 18, 26, and 27.

BISWAS, S. et al. Modeling the formation of layered, amphiphilic gels. **Polymer**, v. 111, p. 214–221, 2017. ISSN 0032-3861. Cited in page 34.

BOEK, E. S.; COVENEY, P. V.; LEKKERKERKER, H. N. Computer simulation of rheological phenomena in dense colloidal suspensions with dissipative particle dynamics. **Journal of Physics Condensed Matter**, v. 8, n. 47, p. 9509–9512, 1996. ISSN 09538984. Cited 2 times in pages 18 and 32.

BOEK, E. S. et al. Simulating the rheology of dense colloidal suspensions using dissipative particle dynamics. **Phys. Rev. E**, American Physical Society, v. 55, p. 3124–3133, Mar 1997. Disponível em: <https://link.aps.org/doi/10.1103/PhysRevE.55.3124>. Cited 2 times in pages 18 and 32.

BOLINTINEANU, D. S. et al. Particle dynamics modeling methods for colloid suspensions. **Computational Particle Mechanics**, v. 1, n. 3, p. 321–356, 2014. ISSN 21964386. Cited in page 29.

BOROMAND, A. et al. A generalized frictional and hydrodynamic model of the dynamics and structure of dense colloidal suspensions. **Journal of Rheology**, v. 62, n. 4, p. 905–918, 2018. ISSN 0148-6055. Cited 7 times in pages 17, 19, 31, 34, 42, 48, and 71.

BOROMAND, A.; JAMALI, S.; MAIA, J. M. Viscosity measurement techniques in Dissipative Particle Dynamics. **Computer Physics Communications**, Elsevier B.V., v. 196, p. 149–160, 2015. ISSN 00104655. Cited 5 times in pages 31, 33, 34, 45, and 47.

BOROMAND, A.; JAMALI, S.; MAIA, J. M. Structural fingerprints of yielding mechanisms in attractive colloidal gels. **Soft Matter**, Royal Society of Chemistry, v. 13, n. 2, p. 458–473, 2017. ISSN 17446848. Cited 3 times in pages 31, 33, and 34.

BRADY, J. F.; BOSSIS, G. Stokesian dynamics. **Annual Review of Fluid Mechanics**, v. 20, n. 1, p. 111–157, 1988. Disponível em: <https://doi.org/10.1146/annurev.fl.20.010188.000551>. Cited in page 22.

BREIMAN, L. Bagging predictors. **Machine Learning**, v. 24, n. 2, p. 123–140, 1996. Cited in page 38.

BREIMAN, L. Random forests. **Machine Learning**, Kluwer Academic Publishers, v. 45, n. 1, p. 5–32, 2001. ISSN 0885-6125. Cited in page 38.

BROWN, E.; JAEGER, H. M. The role of dilation and confining stresses in shear thickening of dense suspensions. **Journal of Rheology**, v. 56, n. 4, p. 875–923, 2012. Disponível em: <https://doi.org/10.1122/1.4709423>. Cited in page 23.

BROWN, E. et al. Shear thickening and jamming in densely packed suspensions of different particle shapes. **Physical Review E - Statistical, Nonlinear, and Soft Matter Physics**, v. 84, n. 3, p. 1–11, 2011. ISSN 15502376. Cited in page 17.

Bybee, M. D. Hydrodynamic simulations of colloidal gels: Microstructure, dynamics, and rheology, PhD Thesis. jan. 2009. Cited in page 29.

CHATTERJEE, A. Modification to Lees-Edwards periodic boundary condition for dissipative particle dynamics simulation with high dissipation rates. **Molecular Simulation**, v. 33, n. 15, p. 1233–1236, 2007. ISSN 08927022. Cited in page 49.

CHATTERJEE, A.; WU, L. M. Predicting rheology of suspensions of spherical and non-spherical particles using dissipative particle dynamics (DPD): Methodology and experimental validation. **Molecular Simulation**, v. 34, n. 3, p. 243–250, 2008. ISSN 08927022. Cited 2 times in pages 18 and 32.

CHEN, S.; YONG, X. Janus Nanoparticles Enable Entropy-Driven Mixing of Bicomponent Hydrogels. **Langmuir**, v. 35, n. 46, p. 14840–14848, 2019. ISSN 15205827. Cited 2 times in pages 36 and 37.

CHEN, Y.-L. Inertia and deformation-driven migration of a soft particle in confined shear and poiseuille flow. **RSC Adv.**, The Royal Society of Chemistry, v. 4, p. 17908–17916, 2014. Disponível em: <http://dx.doi.org/10.1039/C4RA00837E>. Cited 2 times in pages 17 and 28.

COHEN, I.; MASON, T. G.; WEITZ, D. A. Shear-induced configurations of confined colloidal suspensions. **Physical Review Letters**, v. 93, n. 4, p. 046001–1, 2004. ISSN 00319007. Cited in page 60.

COULLIETTE, C.; POZRIKIDIS, C. Motion of an array of drops through a cylindrical tube. **Journal of Fluid Mechanics**, Case Western Reserve University, v. 358, p. 1–28, 1998. ISSN 00221120. Cited in page 28.

COULOMB, A. Favier de et al. Rheology of granular flows across the transition from soft to rigid particles. **Phys. Rev. Fluids**, American Physical Society, v. 2, p. 102301, Oct 2017. Disponível em: <https://link.aps.org/doi/10.1103/PhysRevFluids.2.102301>. Cited in page 17.

COUSSOT, P.; ANCEY, C. Rheophysical classification of concentrated suspensions and granular pastes. **Physical Review E - Statistical Physics, Plasmas, Fluids, and Related Interdisciplinary Topics**, v. 59, n. 4, p. 4445–4457, 1999. ISSN 1063651X. Cited in page 20.

CUDJOE, E. et al. Biomimetic Reversible Heat-Stiffening Polymer Nanocomposites. **ACS Central Science**, v. 3, n. 8, p. 886–894, 2017. ISSN 23747951. Cited in page 31.

CUMMINGS, P. T. et al. Phase transitions in nanoconfined fluids: The evidence from simulation and theory. **AIChE Journal**, v. 56, n. 4, p. 842–848, 2010. Cited in page 32.

DARIAS, J. R. et al. Simulation of suspensions in constricted geometries by dissipative particle dynamics. **Molecular Simulation**, v. 29, n. 6-7, p. 443–449, 2003. ISSN 08927022. Cited in page 18.

DHONT, J. **An Introduction to Dynamics of Colloids**. Elsevier Science, 1996. (ISSN). ISBN 9780080535074. Disponível em: <https://books.google.com/books?id=mmArTF5SJ9oC>. Cited 3 times in pages 12, 20, and 21.

DOYEUX, V. et al. Effective viscosity of two-dimensional suspensions: Confinement effects. **Physical Review Fluids**, v. 1, n. 4, p. 043301, 2016. ISSN 2469-990X. Disponível em: <https://link.aps.org/doi/10.1103/PhysRevFluids.1.043301>. Cited in page 18.

ECKERT, T.; RICHTERING, W. Thermodynamic and hydrodynamic interaction in concentrated microgel suspensions: Hard or soft sphere behavior? **The Journal of Chemical Physics**, v. 129, n. 12, p. 124902, 2008. Disponível em: <https://doi.org/10.1063/1.2978383>. Cited in page 17.

ERAL, H. B. et al. Influence of confinement by smooth and rough walls on particle dynamics in dense hard-sphere suspensions. **Physical Review E - Statistical, Nonlinear, and Soft Matter Physics**, v. 80, n. 6, p. 1–8, 2009. ISSN 15393755. Cited in page 18.

ESPANOL, P.; WARREN, P. Statistical mechanics of dissipative particle dynamics. **Epl**, v. 30, n. 4, p. 191–196, 1995. ISSN 12864854. Cited in page 41.

FAN, X. et al. Simulating flow of DNA suspension using dissipative particle dynamics. **Physics of Fluids**, v. 18, n. 6, 2006. ISSN 10706631. Cited in page 35.

FAN, X. et al. Microchannel flow of a macromolecular suspension. **Physics of Fluids**, v. 15, n. 1, p. 11–21, 2003. ISSN 10706631. Cited in page 35.

FEDOSOV, D. A.; PIVKIN, I. V.; KARNIADAKIS, G. E. Velocity limit in DPD simulations of wall-bounded flows. **Journal of Computational Physics**, v. 227, n. 4, p. 2540–2559, 2008. ISSN 00219991. Cited in page 31.

FEDOSOV, D. A.; PIVKIN, I. V.; KARNIADAKIS, G. E. Velocity limit in DPD simulations of wall-bounded flows. **Journal of Computational Physics**, v. 227, n. 4, p. 2540–2559, 2008. ISSN 00219991. Cited in page 34.

FERNANDEZ, N. et al. Microscopic mechanism for shear thickening of non-brownian suspensions. **Physical Review Letters**, v. 111, n. 10, p. 1–5, 2013. ISSN 00319007. Cited in page 23.

GALLIER, S. et al. Effect of confinement in wall-bounded non-colloidal suspensions. **Journal of Fluid Mechanics**, v. 799, p. 100–127, 2016. ISSN 14697645. Cited 4 times in pages 17, 18, 26, and 60.

GAO, K. et al. Julia language in machine learning: Algorithms, applications, and open issues. **Computer Science Review**, Elsevier Inc., v. 37, p. 100254, 2020. ISSN 15740137. Disponível em: <https://doi.org/10.1016/j.cosrev.2020.100254>. Cited in page 36.

GHOUFI, A.; MALFREYT, P. Coarse grained simulations of the electrolytes at the water-air interface from many body dissipative particle dynamics. **Journal of Chemical Theory and Computation**, v. 8, n. 3, p. 787–791, 2012. ISSN 15499618. Cited 3 times in pages 12, 42, and 49.

GINZBURG, V. V. et al. Modeling the interfacial tension in oil-water-nonionic surfactant mixtures using dissipative particle dynamics and self-consistent field theory. **Journal of Physical Chemistry B**, v. 115, n. 16, p. 4654–4661, 2011. ISSN 15205207. Cited in page 31.

GOMPPER, G. et al. Multi-particle collision dynamics: A particle-based mesoscale simulation approach to the hydrodynamics of complex fluids. **Advances in Polymer Science**, v. 221, p. 1–87, 08 2008. Cited in page 29.

GOONEIE, A.; HUFENUS, R. Polymeric Solvation Shells around Nanotubes: Mesoscopic Simulation of Interfaces in Nanochannels. **Macromolecules**, v. 52, n. 22, p. 8803–8813, 2019. ISSN 15205835. Cited in page 32.

GROOT, R.; RABONE, K. Mesoscopic simulation of cell membrane damage, morphology change and rupture by nonionic surfactants. **Biophysical Journal**, v. 81, n. 2, p. 725 – 736, 2001. ISSN 0006-3495. Disponível em: <http://www.sciencedirect.com/science/article/pii/S0006349501757372>. Cited in page 42.

GROOT, R. D.; WARREN, P. B. Dissipative particle dynamics: Bridging the gap between atomistic and mesoscopic simulation. **Journal of Chemical Physics**, v. 107, n. 11, p. 4423–4435, 1997. ISSN 00219606. Cited 5 times in pages 29, 30, 40, 41, and 45.

GROSS, M.; KRÜGER, T.; VARNIK, F. Rheology of dense suspensions of elastic capsules: Normal stresses, yield stress, jamming and confinement effects. **Soft Matter**, v. 10, n. 24, p. 4360–4372, 2014. ISSN 17446848. Cited in page 18.

GUBBIOTTI, A.; CHINAPPI, M.; CASCIOLA, C. M. Confinement effects on the dynamics of a rigid particle in a nanochannel. **Physical Review E**, American Physical Society, v. 100, n. 5, p. 1–17, 2019. ISSN 24700053. Cited 2 times in pages 32 and 54.

HO, T. K. Random decision forests. In: **Proceedings of the Third International Conference on Document Analysis and Recognition (Volume 1) - Volume 1**. USA: IEEE Computer Society, 1995. (ICDAR '95), p. 278. ISBN 0818671289. Cited in page 38.

HOOGERBRUGGE, P. J.; KOELMAN, J. M. Simulating microscopic hydrodynamic phenomena with dissipative particle dynamics. **Epl**, v. 19, n. 3, p. 155–160, 1992. ISSN 12864854. Cited 3 times in pages 29, 30, and 40.

HSU, C. W.; CHEN, Y.-L. Migration and fractionation of deformable particles in microchannel. **The Journal of Chemical Physics**, v. 133, n. 3, p. 034906, 2010. Cited in page 28.

INOKUCHI, T. et al. Multiscale prediction of functional self-assembled materials using machine learning: High-performance surfactant molecules. **Nanoscale**, Royal Society of Chemistry, v. 10, n. 34, p. 16013–16021, 2018. ISSN 20403372. Disponível em: <http://dx.doi.org/10.1039/c8nr03332c>. Cited 2 times in pages 36 and 37.

INOKUCHI, T.; OKAMOTO, R.; ARAI, N. Predicting molecular ordering in a binary liquid crystal using machine learning. **Liquid Crystals**, Taylor Francis, v. 47, n. 3, p. 438–448, 2020. ISSN 13665855. Disponível em: <https://doi.org/10.1080/02678292.2019.1656293>. Cited 2 times in pages 36 and 37.

IRVING, J. H.; KIRKWOOD, J. G. The statistical mechanical theory of transport processes. iv. the equations of hydrodynamics. **The Journal of Chemical Physics**, v. 18, n. 6, p. 817–829, 1950. Disponível em: <https://doi.org/10.1063/1.1747782>. Cited in page 49.

JAMALI, S. et al. Generalized mapping of multi-body dissipative particle dynamics onto fluid compressibility and the Flory-Huggins theory. **Journal of Chemical Physics**, v. 142, n. 16, 2015. ISSN 00219606. Cited in page 42.

JAMALI, S. et al. Microstructure and rheology of soft to rigid shear-thickening colloidal suspensions. **Journal of Rheology**, v. 59, n. 6, p. 1377–1395, 2015. ISSN 0148-6055. Disponível em: <http://sor.scitation.org/doi/10.1122/1.4931655>. Cited 8 times in pages 12, 17, 19, 24, 31, 33, 34, and 49.

JAMALI, S.; BRADY, J. F. Alternative Frictional Model for Discontinuous Shear Thickening of Dense Suspensions: Hydrodynamics. **Physical Review Letters**, American Physical Society, v. 123, n. 13, p. 138002, 2019. ISSN 0031-9007. Disponível em: <https://doi.org/10.1103/PhysRevLett.123.138002>. Cited 6 times in pages 12, 19, 24, 25, 70, and 80.

JAMALI, S.; YAMANOI, M.; MAIA, J. Bridging the gap between microstructure and macroscopic behavior of monodisperse and bimodal colloidal suspensions. **Soft Matter**, v. 9, n. 5, p. 1506–1515, 2013. ISSN 1744-683X. Cited 9 times in pages 17, 19, 31, 33, 34, 42, 47, 48, and 50.

KASITEROPOULOU, D.; KARAKASIDIS, T. E.; LIAKOPOULOS, A. Dissipative Particle Dynamics investigation of parameters affecting planar nanochannel flows. **Materials Science and Engineering B: Solid-State Materials for Advanced Technology**, Elsevier B.V., v. 176, n. 19, p. 1574–1579, 2011. ISSN 09215107. Cited 3 times in pages 32, 54, and 55.

KHANI, S. et al. Polymer-mediated nanorod self-assembly predicted by dissipative particle dynamics simulations. **Soft Matter**, Royal Society of Chemistry, v. 11, n. 34, p. 6881–6892, 2015. ISSN 17446848. Cited 3 times in pages 31, 33, and 34.

KILIMNIK, A.; MAO, W.; ALEXEEV, A. Inertial migration of deformable capsules in channel flow. **Physics of Fluids**, v. 23, n. 12, 2011. ISSN 10706631. Cited 2 times in pages 17 and 28.

KOELMAN, J. M. V. A.; HOOGERBRUGGE, P. J. Dynamic simulations of hard-sphere suspensions under steady shear. **Europhysics Letters (EPL)**, IOP Publishing, v. 21, n. 3, p. 363–368, jan 1993. Disponível em: <https://doi.org/10.1209%2F0295-5075%2F21%2F3%2F018>. Cited 3 times in pages 12, 32, and 33.

KOH, C. J.; HOOKHAM, P.; LEAL, L. G. An experimental investigation of concentrated suspension flows in a rectangular channel. **Journal of Fluid Mechanics**, Cambridge University Press, v. 266, p. 1–32, 1994. Cited in page 26.

KOMNIK, A.; HARTING, J.; HERRMANN, H. J. Transport phenomena and structuring in shear flow of suspensions near solid walls. **Journal of Statistical Mechanics: Theory and Experiment**, n. 12, 2004. ISSN 17425468. Cited 3 times in pages 18, 31, and 32.

KONG, Y. et al. Simulation of a confined polymer in solution using the dissipative particle dynamics method. **International Journal of Thermophysics**, v. 15, n. 6, p. 1093–1101, 1994. ISSN 0195928X. Cited 4 times in pages 18, 31, 34, and 35.

KUMAR, A.; Henríquez Rivera, R. G.; GRAHAM, M. D. Flow-induced segregation in confined multicomponent suspensions: Effects of particle size and rigidity. **Journal of Fluid Mechanics**, v. 738, p. 423–462, 2014. ISSN 14697645. Cited in page 17.

LAHMAR, F.; ROUSSEAU, B. Influence of the adjustable parameters of the dpd on the global and local dynamics of a polymer melt. **Polymer**, v. 48, n. 12, p. 3584–3592, 2007. ISSN 0032-3861. Cited in page 34.

LEES, A. W.; EDWARDS, S. F. The computer study of transport processes under extreme conditions. **Journal of Physics C: Solid State Physics**, IOP Publishing, v. 5, n. 15, p. 1921–1928, aug 1972. Disponível em: <https://doi.org/10.1088/0022-3719/5/15/006>. Cited in page 49.

LI, Z. et al. A dissipative particle dynamics method for arbitrarily complex geometries. **Journal of Computational Physics**, Elsevier Inc., v. 355, p. 534–547, 2018. ISSN 10902716. Cited 2 times in pages 31 and 34.

LIN, N. Y. et al. Hydrodynamic and Contact Contributions to Continuous Shear Thickening in Colloidal Suspensions. **Physical Review Letters**, v. 115, n. 22, p. 1–5, 2015. ISSN 10797114. Cited in page 23.

LITVINOV, S. et al. Particle-layering effect in wall-bounded dissipative particle dynamics. **Physical Review E - Statistical, Nonlinear, and Soft Matter Physics**, v. 82, n. 6, p. 1–5, 2010. ISSN 15393755. Cited in page 18.

LIU, S. et al. Conformational transitions of polymer brushes for reversibly switching graphene transistors. **Macromolecules**, v. 49, n. 19, p. 7434–7441, 2016. ISSN 15205835. Cited in page 31.

LYON, M. K.; LEAL, L. G. An experimental study of the motion of concentrated suspensions in two-dimensional channel flow. Part 2. Bidisperse systems. **Journal of Fluid Mechanics**, Case Western Reserve University, v. 363, p. 57–77, 1998. ISSN 00221120. Cited in page 18.

MAHMOUDABADBOZCHELOU, M. et al. Data-driven physics-informed constitutive metamodeling of complex fluids: A multifidelity neural network (mfnn) framework. **Journal of Rheology**, v. 65, n. 2, p. 179–198, 2021. Disponível em: <https://doi.org/10.1122/8.0000138>. Cited in page 37.

MAI-DUY, N.; PHAN-THIEN, N.; KHOO, B. C. Investigation of particles size effects in Dissipative Particle Dynamics (DPD) modelling of colloidal suspensions. **Computer Physics Communications**, Elsevier B.V., v. 189, p. 37–46, 2015. ISSN 00104655. Disponível em: <http://dx.doi.org/10.1016/j.cpc.2014.12.003>. Cited 3 times in pages 17, 18, and 33.

MALFREYT, P.; TILDESLEY, D. J. Dissipative particle dynamics simulations of grafted polymer chains between two walls. **Langmuir**, v. 16, n. 10, p. 4732–4740, 2000. ISSN 07437463. Cited in page 35.

MARI, R. et al. Discontinuous shear thickening in brownian suspensions by dynamic simulation. **Proceedings of the National Academy of Sciences**, National Academy of Sciences, v. 112, n. 50, p. 15326–15330, 2015. ISSN 0027-8424. Disponível em: <https://www.pnas.org/content/112/50/15326>. Cited in page 23.

MEHBOUDI, A.; SAIDI, M. S. Physically based wall boundary condition for dissipative particle dynamics. **Microfluidics and Nanofluidics**, v. 17, n. 1, p. 181–198, 2014. ISSN 16134990. Cited 5 times in pages 18, 31, 32, 34, and 55.

MEHRABADI, M.; KU, D. N.; AIDUN, C. K. Effects of shear rate, confinement, and particle parameters on margination in blood flow. **Physical Review E**, v. 93, n. 2, p. 1–11, 2016. ISSN 24700053. Cited 2 times in pages 17 and 28.

MEWIS, J.; WAGNER, N. J. **Colloidal Suspension Rheology**. [S.l.]: Cambridge University Press, 2011. (Cambridge Series in Chemical Engineering). Cited in page 17.

MEWIS J.; WAGNER, N. J. **Colloidal Suspension Rheology**. [S.l.: s.n.]. Cited 5 times in pages 12, 20, 21, 22, and 24.

MITCHELL, T. **Machine Learning**. [S.l.: s.n.], 1997. (McGraw-Hill Series in Computer Science). Cited in page 36.

MURALIDHAR, N. et al. **Physics-guided Design and Learning of Neural Networks for Predicting Drag Force on Particle Suspensions in Moving Fluids**. 2019. Cited in page 37.

MYERS, D. **Surfaces, interfaces, and colloids**. [S.l.: s.n.], 1999. v. 4. 0–471 p. ISBN 0471330604. Cited in page 21.

NARDAI, M. M.; ZIFFERER, G. Simulation of dilute solutions of linear and star-branched polymers by dissipative particle dynamics. **The Journal of Chemical Physics**, v. 131, n. 12, p. 124903, 2009. Cited in page 34.

NOORIAN, H.; TOGHRAIE, D.; AZIMIAN, A. R. Molecular dynamics simulation of Poiseuille flow in a rough nano channel with checker surface roughnesses geometry. **Heat and Mass Transfer/Waerme- und Stoffuebertragung**, v. 50, n. 1, p. 105–113, 2014. ISSN 09477411. Cited in page 32.

NOTT, P. R.; BRADY, J. F. Pressure-driven flow of suspensions: Simulation and theory. **Journal of Fluid Mechanics**, v. 275, n. 6, p. 157–199, 1994. ISSN 14697645. Cited 2 times in pages 25 and 26.

OLIVEIRA, F. C. de et al. Modified clustering algorithm for molecular simulation. **Molecular Simulation**, Taylor Francis, v. 46, n. 18, p. 1453–1466, 2020. Cited 2 times in pages 61 and 71.

PADDING, J. T.; LOUIS, A. A. Hydrodynamic interactions and Brownian forces in colloidal suspensions: Coarse-graining over time and length scales. **Physical Review E - Statistical, Nonlinear, and Soft Matter Physics**, v. 74, n. 3, p. 1–29, 2006. ISSN 15393755. Cited 3 times in pages 12, 29, and 30.

PAIVA, F. et al. Interfacial aggregation of Janus rods in binary polymer blends and their effect on phase separation. **Journal of Chemical Physics**, AIP Publishing, LLC, v. 151, n. 11, 2019. ISSN 00219606. Cited 3 times in pages 31, 33, and 34.

PAIVA, F. L. et al. Dynamic interfacial trapping of janus nanorod aggregates. **Langmuir**, v. 36, n. 15, p. 4184–4193, 2020. PMID: 32200633. Disponível em: <https://doi.org/10.1021/acs.langmuir.9b03604>. Cited 2 times in pages 31 and 34.

PAIVA, F. L. et al. Slip and momentum transfer mechanisms mediated by janus rods at polymer interfaces. **Soft Matter**, The Royal Society of Chemistry, v. 16, p. 6662–6672, 2020. Cited in page 31.

PAKULA, T. A model for dense colloidal systems with deformable, incompressible particles. **The Journal of Chemical Physics**, v. 94, n. 3, p. 2104–2109, 1991. ISSN 00219606. Cited in page 28.

PAN, W.; CASWELL, B.; KARNIADAKIS, G. E. Rheology, microstructure and migration in brownian colloidal suspensions. **Langmuir**, v. 26, n. 1, p. 133–142, 2010. ISSN 07437463. Cited in page 19.

PERRET, E. et al. Molecular liquid under nanometre confinement: Density profiles underlying oscillatory forces. **Journal of Physics Condensed Matter**, v. 22, n. 23, p. 1–8, 2010. ISSN 09538984. Cited 2 times in pages 32 and 54.

PEYLA, P.; VERDIER, C. New confinement effects on the viscosity of suspensions. **EPL**, v. 94, 05 2011. Cited 2 times in pages 17 and 18.

PHAN-THIEN, N.; MAI-DUY, N.; KHOO, B. C. A spring model for suspended particles in dissipative particle dynamics. **Journal of Rheology**, v. 58, n. 4, p. 839–867, 2014. Disponível em: <https://doi.org/10.1122/1.4874679>. Cited 2 times in pages 18 and 33.

PIVKIN, I. V.; KARNIADAKIS, G. E. A new method to impose no-slip boundary conditions in dissipative particle dynamics. **Journal of Computational Physics**, v. 207, n. 1, p. 114–128, 2005. ISSN 00219991. Cited 8 times in pages 18, 31, 34, 45, 46, 48, 55, and 78.

PIVKIN, I. V.; KARNIADAKIS, G. E. Controlling density fluctuations in wall-bounded dissipative particle dynamics systems. **Physical Review Letters**, v. 96, n. 20, p. 1–4, 2006. ISSN 00319007. Cited 4 times in pages 18, 31, 34, and 46.

PRYAMITSYN, V.; GANESAN, V. A coarse-grained explicit solvent simulation of rheology of colloidal suspensions. **Journal of Chemical Physics**, v. 122, n. 10, 2005. ISSN 00219606. Cited 2 times in pages 19 and 33.

RAISSI, M.; PERDIKARIS, P.; KARNIADAKIS, G. E. Physics-informed neural networks : A deep learning framework for solving forward and inverse problems involving nonlinear partial differential equations. **Journal of Computational Physics**, Elsevier Inc., v. 378, p. 686–707, 2019. ISSN 0021-9991. Disponível em: <https://doi.org/10.1016/j.jcp.2018.10.045>. Cited in page 37.

RAMASWAMY, M. et al. How confinement-induced structures alter the contribution of hydrodynamic and short-ranged repulsion forces to the viscosity of colloidal suspensions. **Physical Review X**, v. 7, n. 4, p. 1–14, 2017. ISSN 21603308. Cited 4 times in pages 17, 18, 27, and 60.

RANJITH, S. K.; PATNAIK, B.; VEDANTAM, S. No-slip boundary condition in finite-size dissipative particle dynamics. **Journal of Computational Physics**, v. 232, n. 1, p. 174–188, 2013. ISSN 0021-9991. Disponível em: <https://www.sciencedirect.com/science/article/pii/S0021999112004317>. Cited in page 34.

REVENGA, M. et al. Boundary Models in DPD. **International Journal of Modern Physics C**, v. 09, n. 8, p. 1319–1328, 1998. ISSN 0129-1831. Cited in page 34.

RUSSEL, W. B. Review of the Role of Colloidal Forces in the Rheology of Suspensions. **Journal of Rheology**, v. 24, n. 3, p. 287–317, 1980. ISSN 0148-6055. Cited in page 20.

SCHLIJPER, A. G.; HOOGERBRUGGE, P. J.; MANKE, C. W. Computer simulation of dilute polymer solutions with the dissipative particle dynamics method. **Journal of Rheology**, v. 39, n. 3, p. 567–579, 1995. Disponível em: <https://doi.org/10.1122/1.550713>. Cited 2 times in pages 32 and 34.

SETO, R. et al. Discontinuous shear thickening of frictional hard-sphere suspensions. **Physical Review Letters**, v. 111, n. 21, p. 1–5, 2013. ISSN 00319007. Cited in page 23.

SILBERT, L. E.; MELROSE, J. R.; BALL, R. C. Colloidal microdynamics: Pair-drag simulations of model-concentrated aggregated systems. **Phys. Rev. E**, American Physical Society, v. 56, p. 7067–7077, Dec 1997. Disponível em: <https://link.aps.org/doi/10.1103/PhysRevE.56.7067>. Cited 2 times in pages 13 and 44.

SMIATEK, J.; SCHMID, F. Mesoscopic simulations of electroosmotic flow and electrophoresis in nanochannels. **Computer Physics Communications**, v. 182, n. 9, p. 1941 – 1944, 2011. ISSN 0010-4655. Computer Physics Communications Special Edition for Conference on Computational Physics Trondheim, Norway, June 23-26, 2010. Cited in page 32.

SPENLEY, N. A. Scaling laws for polymers in dissipative particle dynamics. **Europhysics Letters (EPL)**, IOP Publishing, v. 49, n. 4, p. 534–540, feb 2000. Cited in page 34.

Van Der Sman, R. G. Simulations of confined suspension flow at multiple length scales. **Soft Matter**, v. 5, n. 22, p. 4376–4387, 2009. ISSN 17446848. Cited 4 times in pages 18, 20, 29, and 30.

VISSER, D.; HOEFSLOOT, H.; IEDEMA, P. Comprehensive boundary method for solid walls in dissipative particle dynamics. **Journal of Computational Physics**, v. 205, n. 2, p. 626–639, 2005. ISSN 0021-9991. Disponível em: <https://www.sciencedirect.com/science/article/pii/S0021999104004838>. Cited in page 34.

WANG, M.; JAMALI, S.; BRADY, J. F. A hydrodynamic model for discontinuous shear-thickening in dense suspensions. **Journal of Rheology**, v. 64, n. 2, p. 379–394, 2020. Cited 2 times in pages 33 and 34.

WANG, Y.; OUYANG, J.; WANG, X. Machine learning of lubrication correction based on gpr for the coupled dpd–dem simulation of colloidal suspensions. **Soft Matter**, The Royal Society of Chemistry, p. –, 2021. Cited in page 36.

WANG, Y.; OUYANG, J.; WANG, X. Machine learning of lubrication correction based on GPR for the coupled DPD–DEM simulation of colloidal suspensions. **Soft Matter**, Royal Society of Chemistry, p. 10–12, 2021. ISSN 1744-683X. Cited in page 37.

WHITTLE, M.; TRAVIS, K. P. Dynamic simulations of colloids by core-modified dissipative particle dynamics. **Journal of Chemical Physics**, v. 132, n. 12, 2010. ISSN 00219606. Cited 5 times in pages 19, 33, 35, 42, and 78.

WILLEMSEN, S.; HOEFSLOOT, H.; IEDEMA, P. No-slip boundary condition in dissipative particle dynamics. **International Journal of Modern Physics C**, v. 11, n. 5, p. 881–890, 2000. ISSN 01291831. Cited 2 times in pages 18 and 31.

YAMANOI, M.; POZO, O.; MAIA, J. M. Linear and non-linear dynamics of entangled linear polymer melts by modified tunable coarse-grained level Dissipative Particle Dynamics. **Journal of Chemical Physics**, v. 135, n. 4, 2011. ISSN 00219606. Cited in page 31.

YEO, K.; MAXEY, M. R. Dynamics of concentrated suspensions of non-colloidal particles in Couette flow. **Journal of Fluid Mechanics**, v. 649, p. 205–231, 2010. ISSN 14697645. Cited in page 26.

YEO, K.; MAXEY, M. R. Ordering transition of non-Brownian suspensions in confined steady shear flow. **Physical Review E - Statistical, Nonlinear, and Soft Matter Physics**, v. 81, n. 5, p. 1–8, 2010. ISSN 15393755. Cited in page 26.

YONG, X. et al. Harnessing interfacially-active nanorods to regenerate severed polymer gels. **Nano Letters**, v. 13, n. 12, p. 6269–6274, 2013. Cited in page 34.

ZHANG, D.; SHANGGUAN, Q.; WANG, Y. An easy-to-use boundary condition in dissipative particle dynamics system. **Computers and Fluids**, Elsevier Ltd, v. 166, p. 117–122, 2018. ISSN 00457930. Cited 2 times in pages 31 and 34.

ZHAO, L. et al. Active- and transfer-learning applied to microscale-macroscale coupling to simulate viscoelastic flows. **Journal of Computational Physics**, Elsevier Inc., v. 427, p. 110069, 2021. ISSN 10902716. Cited in page 36.

ZHAO, T. et al. Dissipative particle dynamics simulation of dilute polymer solutions—Inertial effects and hydrodynamic interactions. **Journal of Rheology**, v. 58, n. 4, p. 1039–1058, 2014. ISSN 0148-6055. Cited 2 times in pages 31 and 34.